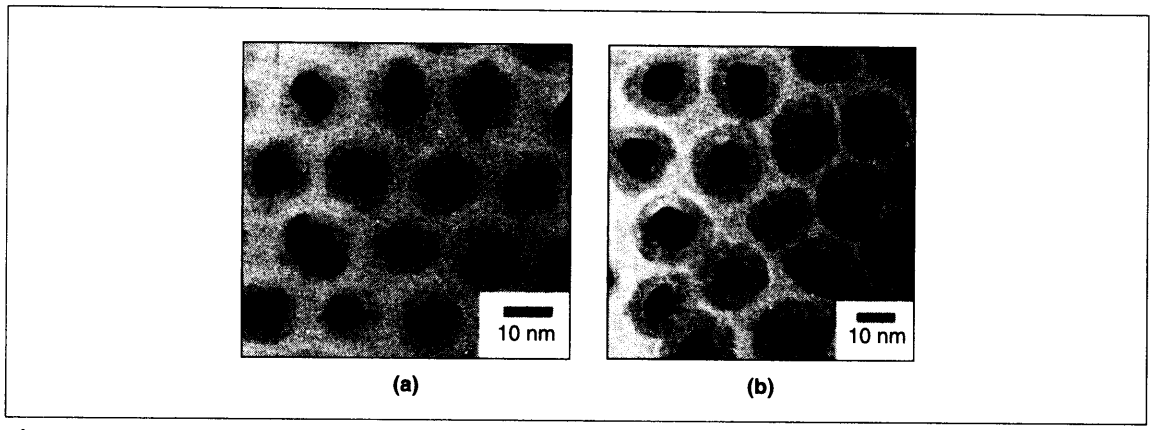

Fig. 9.3: *TEM image of Pt-maghemite core-shell nanoparticles having different shell thickness made with different shell-forming precursors. The shell thicknesses are 3.5 nm and 5.4 nm, respectively (left to right). Reprinted with permission from Teng, et al., (Ref. 7) Copyright (2003) American Chemical Society.*

Mayya, *et al.*, (Ref. 11) demonstrated the coating of Au nanoparticles with titania by using a facile approach based on the complexation of a negatively charged titanium (IV) bis (ammonium lactate) dihydroxide with poly (dimethyldiallyl ammonium hydroxide). This method has an advantage over other reported methods in the fact that in it controlled hydrolysis and condensation reactions of titanium (IV) bis (ammonium lactate) dihydroxide are possible, thereby enabling controlled coating of the nanocore. Reverse micelle and sol–gel techniques are also employed in the synthesis of metal–metal oxide core-shell nanoparticles. The inorganic coatings around the nanoparticles modify the optical properties of the systems in addition to stabilizing them against coalescence. Core-shell geometry allows shell functionalization too (Ref. 12) for better re-dispersibility and ease of handling using appropriate organic monolayers. Figure 9.4 depicts the high-resolution TEM image of a stearate functionalized Ag@ZrO_2 core-shell nanoparticle. The distinct core-shell geometry is visible from the image, though the organic monolayer build-up around the ZrO_2 shell is not clearly seen.

The inorganics-coated particles can catalyze redox reactions on their surface, which will be discussed in detail in Section 9.5.3. Heat dissipation from Au@SiO_2 core-shell nanoparticles in both water and ethanol were studied by Liz-Marzan, *et al.*, (Ref. 13) using time-resolved spectroscopy. The characteristic time constant for heat dissipation depends on the thickness of the silica shell and the solvent. Chen, *et al.*, (Ref. 14) have done the synthesis and characterization of Au@SiO_2 core-shell nanoparticles by incorporating a mercaptosilane at the core-shell interface. The highest degree of functional group organization at the core-shell interface was achieved using this methodology which involves exploiting the strong interaction between thiols and gold. Recently Wang, *et al.*, (Ref. 15) synthesized Au-SiO_2 inverse opals by colloidal crystal templating. Inverse opals represent an excellent class of materials for the manipulation of the flow of light when their lattice parameter is comparable to the wavelength of electromagnetic waves. Inverse opals are highly ordered 3D macroporous structures that can exhibit a bandgap at optical wavelengths.

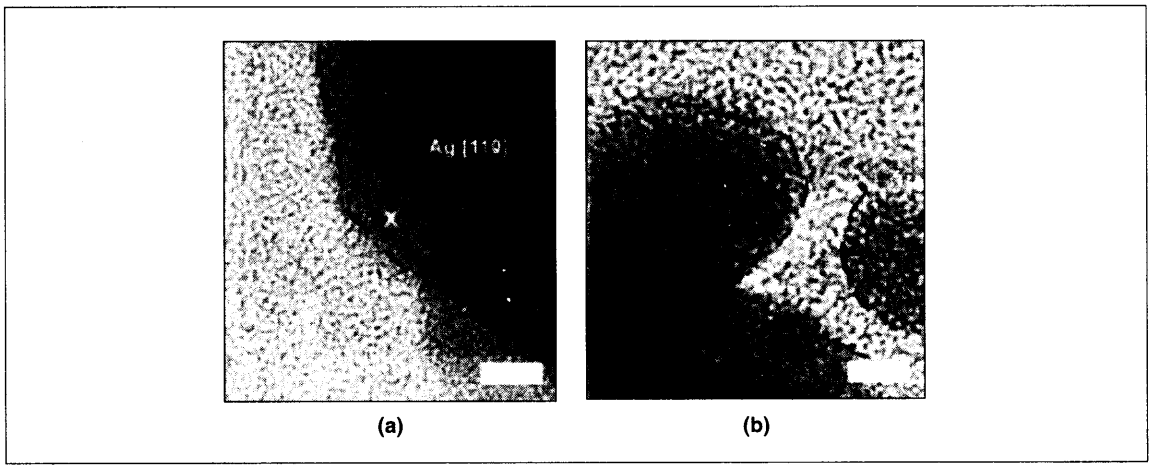

Fig. 9.4: *HRTEM images of Ag@ZrO $_2$ core-shell nanoparticles functionalized with a stearate monolayer. From Nair et. al. (Ref. 12). Reproduced by permission of the Royal Society of Chemistry.*

Figure 9.5 shows the transmission electron micrographs of Au@SiO_2 inverse opals described above. Images a, b and c have different shell thicknesses. Hodak, *et al.*, (Ref. 16) proved that the frequency of the breathing modes of core-shell nanoparticles strongly depend on the thickness of the shell. They found that a visible or near-UV pulse could be used to selectively excite small metal spheres, which coherently excites the acoustic vibrational modes as the photon energy is absorbed by the particles before any significant heat transfer to the dielectric shell. A theoretical model of the acoustic breathing modes of core-shell nanoparticles has recently been proposed by Sader, *et al.* (Ref. 17).

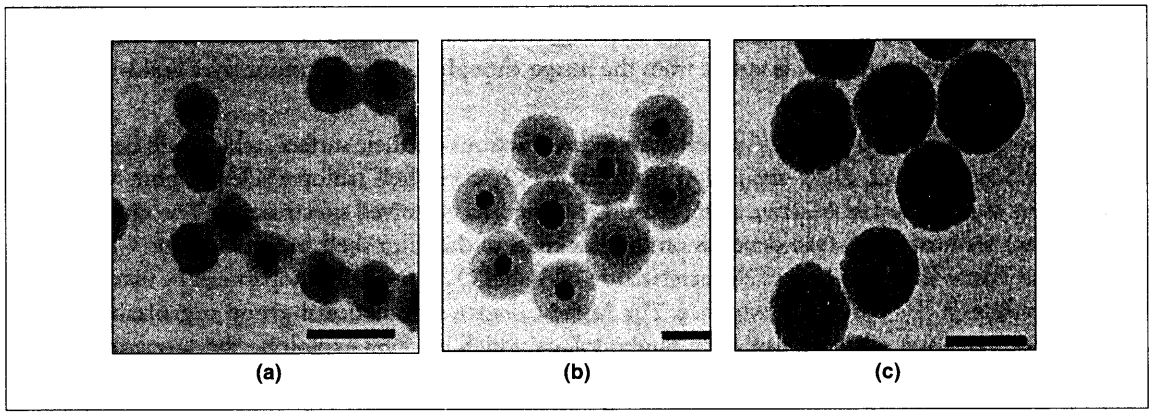

Fig. 9.5: *TEM images of Gold-silica inverse opals. The core dimension is ~15 nm and the silica shells are around 8, 18 and 28 nm, respectively. Scale bars are 50 nm in all cases. Reprinted from Ref. 15. Copyright (2002) Wiley-VCH.*

9.2.2 Bimetallic Core-shell Nanoparticles

Various bimetallic core-shell nanoparticles have been synthesized in the recent past because of their renewed interest in catalysis. Henglein (Ref. 18) synthesized core-shell alloys of Au-Pt through the simultaneous reduction of chloroauric acid and chloroplatinic acid. The TEM images of the Au@Pt core-shell nanoparticles (image on the right) are shown in Fig. 9.6, produced by the coating of Pt on Au nanoparticles (image on the left). Yonezawa, *et al.*, (Ref. 19) reported the synthesis of Au core-Pt shell type nanoparticles through a single-step procedure. Schmid, *et al.* (Ref. 20) also reported the synthesis of the Au core-Pt shell nanoparticle by the simultaneous reduction of $PtCl_6^{2-}$ in an aqueous gold sol. γ-irradiation based synthesis and linear optical characterization of Ag/Cd, Ag/Pb and Ag/In core-shell nanoparticles were reported as early as 1980 by Henglein (Ref. 21). Mulvaney, *et al.* (Ref. 22) and Kreibig, *et al.* (Ref. 23) synthesized Ag core-Au shell nanosystems. Link, *et al.* (Ref. 24) synthesized Ag-Au alloy core-shell nanoparticles of 17–25 nm size. The synthesis of Au core-Ag shell nanoparticles and their optical characteristics like linear extinction and resonant hyper-Rayleigh scattering studies, were carried out by Kim, *et al.* (Ref. 25).

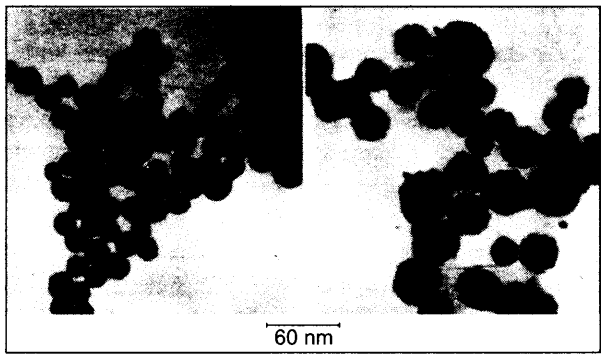

Fig. 9.6: *TEM images of Au nanoparticles (left) coated with Pt (right) in the ratio 1:2. Reprinted with permission from Henglin. (Ref. 18) Copyright (2000) American Chemical Society.*

Sobal, *et al.* (Ref. 26) showed that Ag core-Co shell exhibit optical behavior distinct from that of individual components. The presence of a noble metal also protects the Co shell against oxidation. The synthesis of Pt core-Co shell nanocrystals was also reported by Sobal, *et al.* (Ref. 27) by thermal decomposition of cobalt carbonyl in the presence of nanosized Pt dispersion. The thickness of the Co shell can be controlled by varying the amount of cobalt carbonyl. These types of systems are ideal for probing induced polarization of Pt at the core-shell interface. There are also several reports about the synthesis of various other core-shell nanoparticles in literature. A novel low temperature synthetic protocol for Cu@Au core-shell nanoparticles was developed by Cai, *et al.* (Ref. 28). These are extremely useful systems for the electrochemical DNA hybridization detection assay. The use of core-shell alloy nanoparticles

combines the easy surface modification properties of Au with the good voltammetric response of Cu. The oxidative peak current of Cu colloid is much more than that of Au of the same size and quantity. Also, one layer of Au coated on the Cu core is sufficient for protecting Cu from oxidative degradation and can also provide an active surface for the immobilization of oligonucleotides.

The synthesis of dumb-bell shaped Au–Ag core-shell nanorods by seed-mediated growth under alkaline conditions was reported by Huang and Matijevic (Ref. 29). The method uses gold nanorods as seeds in the presence of Ag and ascorbate ions. The Ag ions that are being reduced by ascorbate ions become deposited on the surface of the Au nanorods to form dumb bell shaped Au–Ag core-shell nanorods. Recently, the synthesis of Au–Ag core-shell nanoparticles using tyrosine as a pH dependent reducing agent was reported by Sastry, *et al.* (Ref. 30).

9.2.3 Semiconductor Core-shell Nanoparticles

Semiconductor nanocrystals exhibit interesting size-dependent optical properties because of the confinement of electronic wavefunctions. Control of their surface is the key to highly luminescent nanocrystals. This is because of the presence of a large number of surface defects arising from nonstochiometry, unsaturated bonds, etc. Core-shell type composite quantum dots exhibit novel properties which make them attractive for chemists. Overcoating the nanocrystallites with higher band gap inorganic materials has been shown to increase the photoluminescence quantum yield due to the passivation of surface non-radiative recombination sites. Also, particles passivated with inorganic composite materials are much more reliable and robust than their corresponding organic analogues. The synthesis and characterization of strongly luminescent CdSe–ZnS core-shell nanocrystals were reported by Hines and Guyot-Sionnest (Ref. 31). Layered and composite semiconductor nanocrystals have been widely studied by several groups. Epitaxially grown CdSe/CdS core-shell nanocrystals with high luminescence properties and photostabilities were reported by Alivisatos, *et al.* (Ref. 32). Similarly the synthesis and characterization of highly luminescent CdSe–ZnS core-shell quantum dots were reported by Bawendi, *et al.* (Ref. 33). One pot synthesis of highly luminescent CdSe/CdS core-shell nanocrystals *via* organometallic and greener chemical approaches was reported by Weller, *et al.* (Ref. 34). Molecular nanocluster analogues of CdSe/ZnSe and CdTe/ZnTe core-shell nanoparticles were reported by DeGroot, *et al.* (Ref. 35). The off-resonance optical non-linearities of Au@CdS core-shell nanoparticles, embedded in $BaTiO_3$ thin films, were reported by Yang, *et al.* (Ref. 36). Semiconductor nanocrystallites are studied extensively because of their large third order non-linearities and ultra-fast non-linear optical response.

9.2.4 Polymer-coated Core-shell Nanoparticles

Polymer-coated core-shell nanoparticles have interesting applications ranging from catalysis to industry in making additives, paints and pigments and a host of other materials. The synthetic methodologies adopted for polymer capping of nanoparticles are of two main classes, namely: (a) polymerization at the nanoparticle surface, (b) adsorption of pre-formed polymer onto the nanoparticle cores. The monomer adsorption onto nanoparticles followed by polymerization (Refs 28, 34, 36–39) heterocoagulation-polymerization

(Ref. 40) and emulsion polymerization (Refs 41–44) are the most commonly adopted methods for the polymerization leading to core-shell nanostructures. Polymerization can be catalyzed by an initiator or by colloidal particles themselves. Huang and Matijevic (Ref. 29) reported the synthesis of silica particles coated with polydivinyl benzene layers by a pre-treatment method. Using similar approaches, poly (vinylbenzyl chloride), copolymers of polydivinyl benzene-poly (vinylbenzyl chloride) and double shells of polydivinyl benzene and poly (vinylbenzyl chloride) were also synthesized. Polymer coating of the particles allowed cores incorporating dyes to be retained on the nanocores as the polymer shells are permeable to small inorganic ions. Polymerization can also be achieved in the presence of catalytically active cores.This approach was utilized in the synthesis of poly (pyrrole) coated nanoparticles of catalytically-active cores like Fe_2O_3/ceria. Hematite (α-Fe_2O_3), silica-modified hematite and cerium (IV) oxide were coated with polypyrrole by using exactly the same procedures. Polypyrrole-coated α-Fe_2O_3 and CeO_2 are electrically conductive core-shell nanosystems. Uniform coatings can be achieved by this method as is shown in Fig. 9.7. Figure 9.7 shows the core-shell nanoparticles of SiO_2-polypyrrole with distinct and robust polypyrrole shell around SiO_2 core.

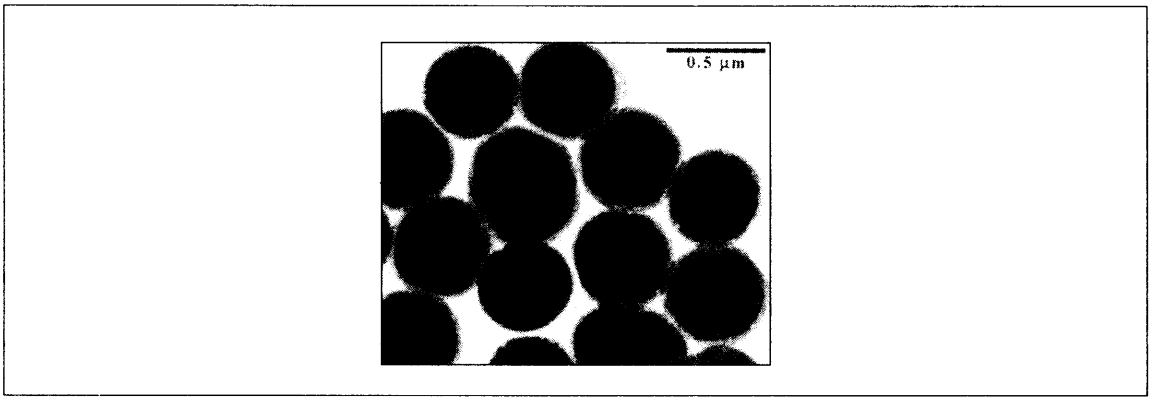

Fig. 9.7: *TEM of polypyrrole coated SiO_2 core-shell nanoparticles. Reproduced from Ref. 29, Copyright 1995 Materials Research Society, also published in F. Caruso, Adv. Mater., 2001, 13, 11. Copyright (2001) Wiley-VCH.*

The thickness of the polymer coating can be controlled by varying the contact time with the core. The polymer thickness is also dependent on the type of core employed and the nature of the polymer (Ref. 29). An excellent strategy for the synthesis of polymer coated nanoparticles was developed by Feldheim, *et al.* (Ref. 40). This is followed by trapping and aligning the particles in the pores of the membrane by vacuum filtration followed by polymerization of the monomer inside the pores. Au nanoparticles can be coated with polypyrrole by this method and the corresponding TEM images are shown in Fig. 9.8.The increased shell thickness of the polymer shell as a result of change in the monomer is evident from the figure on the right. The attractive feature of this methodology is that it facilitates controlling the thickness and composition of the polymer coating. Usually in almost all these polymerization reactions, the thickness of the coating depends on the polymerization time. Another widely used method for the polymer coating is the heterocoagulation of small particles with larger ones, followed by heating.

Polystyrene core coated with a uniform layer of polybutylmethacrylate is prepared by this method. Emulsion polymerization is another widely accepted strategy for the synthesis of polymer-capped core-shell nanoparticles.

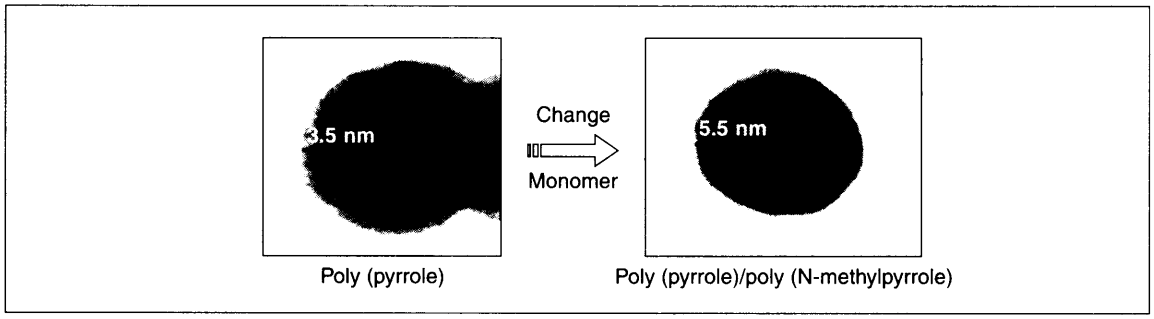

Fig. 9.8: *TEM of polypyrrole-capped Au nanoparticles (left) and with further increase in shell thickness by polymerization with poly (N-methylpyrrole). Reprinted with permission from Marinakos, et al. (Ref. 40) Copyright (1999) American Chemical Society.*

Sub nanometer- and micrometer-sized organic and inorganic particles can be coated with polymer by this method. The polymerization of styrene and/or methacrylic acid in emulsions of oleic acid resulted in the formation of a uniform polymer layer around the metal core. Unlike the uncoated particles, the polymer-coated particles can be easily centrifuged and re-dispersed. They usually exhibit strong resistance to etching. Polymer-coated nanoparticles are very easy to modify in the form of thin films by using self-assembly techniques. Layer by layer (LbL) templating strategy is commonly used for the same. Here a polymer solution (having an opposite charge to that on the particles) in excess to that required for saturation adsorption, was added to the colloidal dispersion. The polymer is adsorbing to the nanoparticles by electrostatic interactions. The LbL assembly of the polystyrene capped Au nanoparticles is shown in Fig. 9.9.

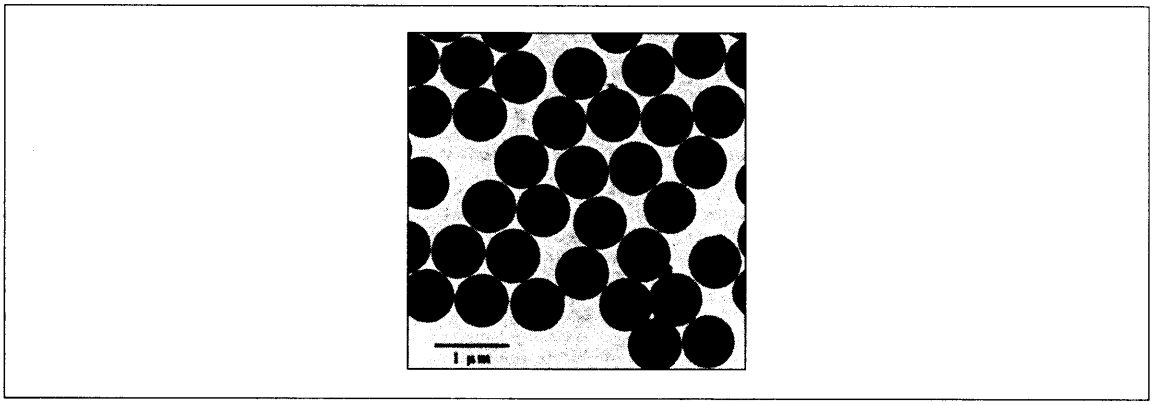

Fig. 9.9: *TEM of LbL assembled polystyrene-capped Au nanoparticles. Reproduced from F. Caruso, Adv. Mater., 2001, 13, 11. Copyright (2001) Wiley-VCH.*

9.3 Characterization

9.3.1 X-ray Diffraction (XRD)

Powder X-ray diffraction is one of the powerful techniques for the characterization of core-shell nanoparticles. In the case of materials where the core and the shell are crystalline, diffraction patterns from the prominent lattice planes can be seen in the diffractograms. A representative powder XRD pattern (Ref. 7) of Pt/Fe_2O_3 core-shell particles is shown in Fig. 9.10. The X-ray diffraction peaks at 2θ = 39.8°, 46.3°, 67.5° and 81.3° can be assigned to (111), (200), (220) and (311) planes of cubic phase of Pt particles. The Fe_2O_3 features are not seen because of the strong scattering from Pt nanoparticles. The XRD patterns of $Ag@ZrO_2$ and $Ag@TiO_2$ core-shell nanoparticles reveal the diffractions from the crystalline core and the shell, however (Ref. 6).

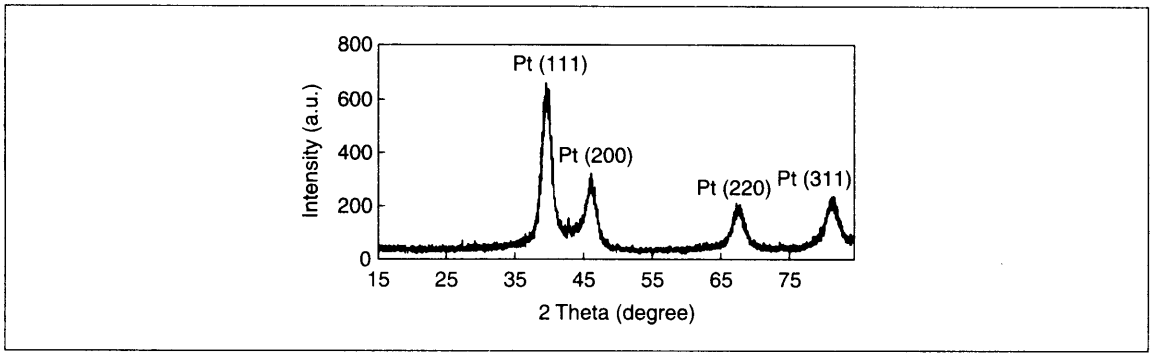

Fig. 9.10: *Powder XRD pattern of Pt@Fe $_2O_3$ core-shell nanoparticles. Reprinted with permission from Teng, et al. (Ref. 7) Copyright (2003) American Chemical Society.*

9.3.2 Optical Spectroscopy

Optical spectroscopy or absorption spectroscopy is another very important tool used for the characterization of nanomaterials. All the nanostructured materials exhibit unique and complex optical properties. We will confine ourselves to metal nanoparticles here. The most striking phenomenon encountered in these structures is the electromagnetic resonances resulting from the collective oscillations of conduction band electrons called plasmons. Plasmon modes vary depending on the geometry and are studied especially in noble metals like silver, gold and copper. The electrons in these metals originate from the completely filled *d* bands, which are relatively close to the Fermi energy. Since the diameter of the nanoparticle is of the order of the penetration depth of electromagnetic waves in metals, the excitation light is able to penetrate the particles. The field inside the particle shifts the conduction electrons collectively with respect to the fixed positive charge of the lattice ions. The electrons build-up a charge on the surface at one side of the

particle. The attraction of this negative charge and positive charge of the remaining lattice ions on the opposite side results in a restoring force. If the frequency of the excitation light field is in resonance with the eigen frequency of this collective oscillation, even a small exciting field leads to strong oscillation. The resonance frequency mainly depends on the restoring force. This force, in turn, depends on the separation of the surface charges, i.e. the particle size, and the polarizability of the medium between and around the charges, which, in turn, depends on the embedding medium and the polarizability of the core electrons of the metal particle. The alternating surface charges effectively form an oscillating dipole, which radiates electromagnetic waves. The core-shell nanoparticles of noble metals and most of semiconductor nanoparticles are characterized by surface plasmon resonance, which results in strong absorption characteristics in the visible or UV region. The absorption characteristics are tunable depending on the nature and thickness of the shell material, which is described in detail in Section 9.4.2.

9.3.3 Zeta Potential

Due to dipolar characteristics and ionic attributes, the colloidal particles (including nanoparticles) suspended in solvents are electrically charged. For example, the surface groups of a colloid may be ionized (COO^-, NH_4^+, etc.). This leads to a net electric charge at the surface, which causes the accumulation of opposite charges (counter ions) around them. This, in turn, results in an electrical double layer. The ion (with positive or negative charge) with a set of counter ions form a fixed part of the double layer. The diffuse or mobile part of the double layer consists of ions of different polarities, which extends into the liquid phase. This double layer may also be considered to have two parts, an inner region which includes ions bound relatively strongly to the surface, and a diffuse region in which the ion distribution is determined by balance of electrostatic forces and random thermal motion. When an electric field is applied, the particles are attracted towards electrodes depending upon their polarity. The potential at which the fixed part of the double layer along with a part of the mobile layer move towards an electrode, is called Zeta potential or electrokinetic potential. It can also be defined as the potential at the shear plane of the particle when it moves in the medium.

The zeta potential depends on a number of parameters like surface charges, ions adsorbed at the interface and the nature and composition of the surrounding medium. The net charge in a specific medium depends on the particle charge and counter ions. The zeta potential is an index of interaction between the particles.

Zeta potential is calculated according to, Smoluchowski's Formula.

$\zeta = 4\pi\eta/\varepsilon \times U \times 300 \times 300 \times 1000$,

where ζ = zeta potential in mV, ε = dielectric constant of the medium, η = viscosity of solution, U = electrophoretic mobility ($v/V/L$), v = speed of the particles in the electric field in cm/s, V = applied voltage and L = distance of the electrode.

The measure of zeta potential throws light on the stability of colloidal/nanoparticle solutions. If all the particles in a suspension have large negative or positive zeta values, then they will repel each other and there will not be any tendency to flocculate. However, if the particles have low zeta potential values, then there is no force to prevent the particles from coagulating. The threshold of stability of colloidal/nanoparticle

solution in terms of the zeta potential is ± 30mV. The greater the zeta potential, the greater will be the stability. The value of the zeta potential is largely affected by pH.

The zeta potential is traditionally measured by using the 'micro electrophoresis' method, which needs extreme dilutions and hence stringent sample handling requirements. Microelectrophoresis is a technique based on light scattering by particles. In the case of nanoparticle solutions, however, the microelectrophoresis is not ideal due to the Doppler broadening of the scattered light from the fine particles. Modern methods used for zeta potential measurements are based on electro-acoustic methods based on electrokinetic properties. In this method, the application of a high frequency electric field sets in motion the eletrophoretic movements of the particles. This generates an alternating acoustic wave due to the density difference between particles and the medium. The velocity of the particles is measured by using laser Doppler electrophoresis. The velocity of these particles or mobility is converted into the zeta potential using Henry's equation:

$U = 2\varepsilon z f(\mathrm{ka})/3\eta$, where ε = dielectric constant, z = zeta potential, η = viscosity and f (ka) = Henry's function. Zeta potential measurements in aqueous media and moderate electrolyte concentration generally employ f (ka) value of 1.5 (Smoluchowski approximation). f (ka) value is generally taken as 1 for the measurements of zeta potentials of small particles in non-aqueous media (Huckel approximation). The zeta potential measurement by microelectrophoresis is a passive technique as it does not alter the chemical properties of the systems.

9.4 Properties

9.4.1 Electrochemistry

The shells in core-shell nanoparticles are porous and hence permit electron transport through them. Ag@ZrO_2 shows a characteristic anodic peak at 0.310 V and a cathodic peak at 0.120 V in the solution phase containing 0.1 M tetrabutyl ammonium hexafluorophosphate (TBAHFP)/CH_3CN on the Pt electrode surface (Ref. 45). The redox couple is centered at $E_{1/2}$ = 0.215 V vs. Ag/AgCl with a peak separation of 0.190 V at 25 °C for the anodic curve (trace a in Fig. 9.11 A). The sharp and symmetrical anodic peak at 0.310 V with FWHM (full width-half maximum) of 60 mV suggests one electron transfer of silver nanoclusters. The quasi-reversible peaks corresponding to the oxidation and reduction of Ag clusters can be represented as:

$$Ag_n \rightarrow Ag_n^+ + e.$$

In the case of Au, the peak was observed at $E_{p1/2}$ = 320 mV (Ref. 45). The electron transport is sensitive to the shell matrix. With the adsorption of long chain fatty acids like stearic acid on the shell matrix of ZrO_2, electron transport through the shell is hindered. Traces (a-f) in Fig. 9.11 (A and B) show a decrease in the peak current of Ag@ZrO_2 and Au@ZrO_2, respectively (Ref. 6) with an increase in the stearic acid concentration. Similar trends occur with the adsorption of dyes on shell surfaces as well. The porosity of core-shell nanoparticles was extensively investigated by using cyclic voltammetry and absorption

spectroscopy. Small molecules (whose sizes are equivalent to or less than the pore diameter of the shells) which react/interact with the metal cores, penetrate through the shell. The subsequent changes in the metal core caused by these interactions were manifested in the absorption as well as redox characteristics of the core (Ref. 45). Electro chemistry of core-shell particles has been investigated by Koktysh, *et al.* (Ref. 46) also.

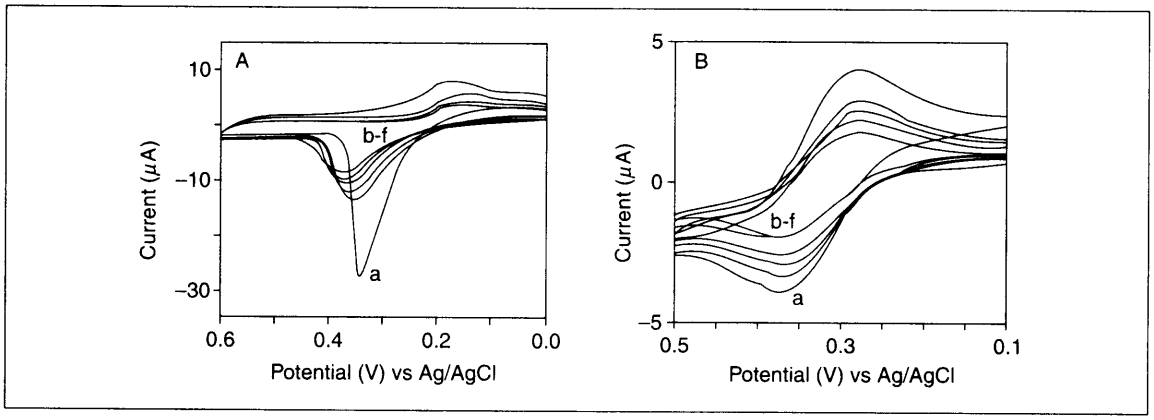

Fig. 9.11: *Cyclic voltammetry responses of core-shell nanosystems. Reprinted from Tom, et al. (Ref. 6). Copyright (2003) American Chemical Society.*

9.4.2 Optical Properties

Optical properties of nanoparticles

The optical properties of nanoparticles have been extensively investigated in recent years. When an electromagnetic wave passes through a metal particle, the electronic and vibrational states get excited. The optical interaction induces a dipole moment that oscillates coherently at the frequency of the incident wave. The frequency of this oscillation depends on the electron density, its effective mass, the shape and size of the charge undergoing oscillation. There can be other influences such as those due to other electrons in the system. The restoring force arises from the displacement of the electron cloud relative to the nuclei, which results in the oscillation of the electron cloud relative to the nuclear framework. The collective oscillation of the free conduction electrons is called 'plasmon resonance' or 'dipole plasmon resonance' of the particle, and is schematically depicted in Fig. 9.12 (Ref. 47). In this resonance, the total electron cloud moves with the applied field. There can be higher modes of plasmon resonance as well. In the quandrupole mode, half the electron cloud is parallel while the other half is anti-parallel to the applied field.

The dipole plasmon frequency is related to the dielectric constant of the metal. The frequency dependent dielectric constant of a bulk metal $\varepsilon(w)$ is measurable. In the discussion, in order to simplify matters, we consider a spherical particle whose diameter is much smaller than the wavelength of the electromagnetic radiation. As can be understood from Fig. 9.12, under such conditions, the electric field of light felt by the particles can be regarded as a constant. This reduces the interaction to be treated by electrostatics, rather

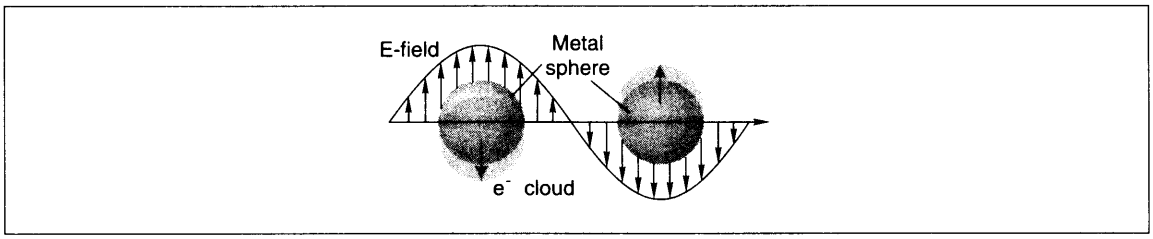

Fig. 9.12: *Surface plasmon resonance in metal nanoparticles in an electromagnetic field. The displacement of the conduction band electrons relative to the nuclei can be seen. Reprinted with permission from Kelly, et al. (Ref. 47) Copyright (2003) American Chemical Society.*

than electrodynamics. This treatment is referred to as the quasi-static approximation—'quasi' because we consider the wavelength dependent dielectric constant. In electrostatic theory when the incident electric filed of the radiation interacts with the electrons, we get a net field due to the applied field and its induced field. This field in reality is a radiating one and contributes to extinction and Rayleigh scattering by the particle. The strength of extinction and scattering can be given in terms of their efficiencies.

Extinction efficiency, $Q_{Ext} = 4\ x\ Img_d$

Scattering efficiency, $Q_{scat} = (8/3)\ x^4\ |g_d|^2$

Where $x = 2\pi R\varepsilon_m/\lambda$, $g_d = (\varepsilon_c - \varepsilon_m)/(\varepsilon_c + 2\varepsilon_m)$, ε_c and ε_m are the dielectric constants of the metal and the medium, respectively, R is the particle radius. Dielectric functions are complex quantities and Im refers to the imaginary part.

The efficiency = cross section/area (πR^2).

In particles of diameter, less than 10 nm light scattering does not make a significant contribution.

$$Q_{Ext} \sim Q_{Abs} = [4(2\pi R\varepsilon_0^{1/2})/Im[(\varepsilon_c - \varepsilon_m)/(\varepsilon_c + 2\varepsilon_m)]$$

When $\varepsilon_c = -2\varepsilon_m$, we get the resonance condition when Q_{Abs} goes to a maximum. Since the dielectric function is a complex quantity this equation can be given in terms of the real and imaginary parts of the metals dielectric function, ε' and ε'', respectively. There are two distinct size regimes of the particles; in both the plasmon resonance depends on size. For particles larger than 10 nm in diameter, the dielectric function itself is independent of size. The shape and size dependence of plasmon resonance in this regime is due to the dependence of electrodynamics on size and shape. This is called the extrinsic size regime. In the intrinsic regime, for particles less than 10 nm in diameter, the dielectric function itself changes with size.

For metals, the absorption characteristics depend, to a large extent, on the conduction band electrons. The spatial confinement of the free conduction band electrons results in plasmon excitations that are restricted to a small range of frequencies, usually in the UV-visible region. Bulk metals absorb very strongly in the IR or near IR region, but colloidal metals are transparent.

Assuming the metal to have a simple dielectric function, $\varepsilon_c' = \varepsilon_\infty - \lambda^2/\lambda_p^2$ where ε' refer to the real part (and ε'', the imaginary part) of the dielectric function. Then the peak position of the absorption obeys the equation, $\lambda_{peak}^2 = \lambda_p^2(\varepsilon_\infty + 2\varepsilon_m)$, where ε_∞ is the high frequency value of the dielectric

function of the metal and λ_p is the bulk plasma wavelength of the metal. (The bulk plasma wavelength of the metal is given by $\lambda_p^2 = 4\pi^2 c^2 m\varepsilon_0/Ne^2$, where N is the electron concentration, 'm' is the effective mass of the conduction band electrons and ε_0 is the vacuum permittivity.) ε_∞ is determined by all the transitions within the metal at UV and higher frequencies. It is clear from the equation that the peak maximum depends on ε_m (solvent dielectric constant) and changes in λ_p. The most important parameter which governs λ_p is N. Variations in electron charge density will alter the plasma frequency and results in shifts in peak maximum. Similarly the particles in the media of varying refractive index can also alter the absorption maxima.

A dispersion diagram showing the conditions of surface plasmon resonance as a function of wavelength of the incident light is shown in Fig. 9.13. The figure shows a plot of the real part of the dielectric function for two metals with two different values of λ_p, determined by $\varepsilon_c' = \varepsilon_\infty - \lambda^2/\lambda_p^2$, keeping a constant value of 1 for ε_∞. The variation of the dielectric function is shown by the curve for the two metals. When the dielectric constant of the medium is ε_{m1}, we get resonance at point A for metal 1, but at point B for metal 2. For the medium with dielectric constant, ε_{m2} the points are C and D. Also if the alloying of the metals 1 and 2 is assumed, the alloy tends to have a dielectric function intermediate between that of 1 and 2, and therefore, the plasmon band of the alloy will peak between that of 1 and 2 depending on the total electron concentration.

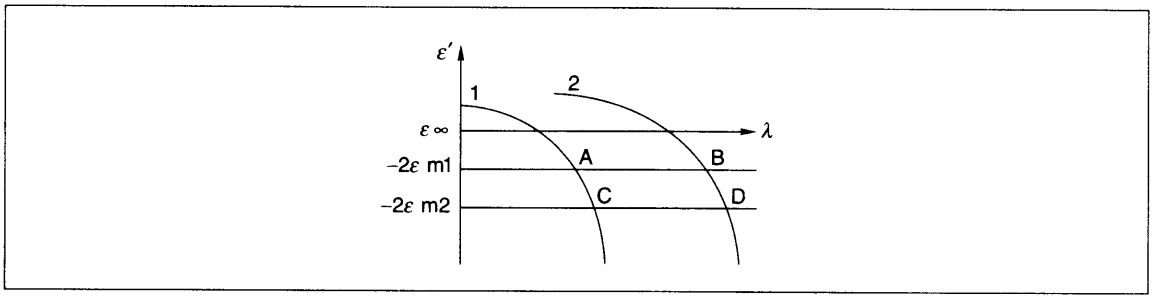

Fig. 9.13: *Dispersion diagram showing the conditions of surface plasmon resonance absorption as a function of the wavelength of the incident light. Reproduced from Mulvany, et al. (Ref. 8). Reproduced by permission of the Royal Society of Chemistry.*

Optical properties of core-shell nanoparticles

The optical characteristics of core-shell nanoparticles can be explained on the basis of the modified Mie's theory (Ref. 48), which considers the scattering of light from spheres coated with a homogeneous layer of uniform thickness. The absorbing medium of this layer has dielectric properties that are different from those of the core and the surrounding medium. The electromagnetic radiations scattered from the core-shell geometry can be described in the same form as that scattered from a homogeneous sphere by considering the influence of the radial variation of scattering coefficients on the extinction cross section. For the nanometer-sized objects of core-shell nanoparticles considered here, the particles may be described as dipole oscillators. The extinction efficiency can be calculated as:

$$Q_{ext} = 4x\ Im\left[\frac{(\varepsilon_s - \varepsilon_m)(\varepsilon_c + 2\varepsilon_s) + (1-g)(\varepsilon_c - \varepsilon_s)(\varepsilon_m + 2\varepsilon_s)}{(\varepsilon_s + 2\varepsilon_s)(\varepsilon_c + 2\varepsilon_s) + (1-g)(\varepsilon_s - 2\varepsilon_m)(\varepsilon_c - \varepsilon_s)}\right]$$ where the subscript 'c' refers to the core and 's' to the shell layer. The radius R refers to the coated particle radius and 'g' is the volume fraction of the shell layer. In the above expression, ε_c is a complex function, while ε_s and ε_m are real. The existence of shell layer modifies the surface plasmon resonance condition and the surface plasmon resonance occurs when the denominator of the above equation is zero, i.e. $\varepsilon_c' = -2\varepsilon_s\ [\varepsilon_s g + \varepsilon_m(3-g)]/[\varepsilon_s(3-2g) + 2\varepsilon_m g]$. For thin shells, $g \ll 1$ the condition of surface plasmon resonance becomes: $\varepsilon_c' = -2\varepsilon_m\ [2g(\varepsilon_s - \varepsilon_m)/3]$. This gets reduced to the usual resonance condition for small spheres without coating as $g \to 0$. Taking the metal to have a simple dielectric function, $\varepsilon_c' = \varepsilon_\infty - \lambda^2/\lambda_p^2$, where λ_p is the metal's bulk plasma wavelength, the peak position can be determined by:

$$\lambda_{peak}^2/\lambda_p^2 = \varepsilon_\infty + 2\varepsilon_m + [2g(\varepsilon_s - \varepsilon_m)/3].$$

A plot of λ_{peak}^2 vs. ε_m will now have a slope less than 2. Compare this with the case of isolated particles (without shell). Physically this is due to the fact that the shell layer is also polarizable by light and sets up a dipole. This would cause a red shift or it may act to reduce the core polarization thereby giving a blue shift as compared to the bare nanoparticle plasmon resonance. In the limit of very thick shells, $g \to 1$ the surface plasmon band becomes insensitive to the medium. The resonace is similar to a core immersed in a solvent made of the shell material. This becomes apparent when we consider the decreasing core volume fraction f. Since $f = 1-g$ and $f \ll 1$, the resonance condition can be written as,

$\varepsilon_c' = -2\varepsilon_m\ [\varepsilon_s(1-f) + \varepsilon_m(2+f)/\varepsilon_s(1+f) + 2\varepsilon_m(1-f)]$. For small f,

$\varepsilon_c' = -2\varepsilon_m\ [(\varepsilon_s + 2\varepsilon_m) + f(\varepsilon_m - \varepsilon_s)/(\varepsilon_s + 2\varepsilon_m)]$. As $f \to 0$, the surface plasmon resonance shifts towards a limiting value of $\varepsilon_c = -2\varepsilon_s$, similar to the case where the shell is the medium for the particles. The surface plasmon resonance peak position becomes:

$\lambda_{peak}^2/\lambda_p^2 = \varepsilon_\infty + 2\varepsilon_s\ [(\varepsilon_s + 2\varepsilon_m) + f(\varepsilon_m - \varepsilon_s)/(\varepsilon_s + 2\varepsilon_m)]$. Taking values of $\varepsilon_s = 2.25$, and $\varepsilon_m = 1.7$ to 3, and with $f = 0.05$, a plot of λ_{peak}^2 vs. ε_m will have a slope of less than 0.1, i.e. the surface plasmon mode will show no sensitivity to the solvent refractive index. The degree of scattering by the shell layer can be controlled by altering the refractive index of the solvent. This means that even if the particles are grown to micron size by silica deposition, the sol can still exhibit the optical properties of the nanoparticle cores. Figure 9.14 (top) shows the changes in the optical absorption spectra of $Au@SiO_2$ nanoparticles as a function of the increasing shell thicknesses of the SiO_2 shell. An increase in the background of the absorption and shift in the absorption maximum accompanied by broadening due to strong scattering are evident from the traces. Figure 9.14 (bottom) shows the absorption characteristics of $Au@TiO_2$ (a) and $Ag@ZrO_2$ (b) nanoparticles. Figure 9.14(a) shows the absorption spectral characteristics as a function of the increase in core dimension while Fig. 9.14(b) shows the corresponding changes as a function of shell thicknesses.

The color of the core-shell solutions of nanoparticles changes by varying the shell thickness, as shown in Fig. 9.15 (Plate 5). The transmitted and reflected colors of thin films of $Au@SiO_2$ colloids as a function of silica shell thicknesses are shown in the Fig. 9.15 (Plate 5) (Ref. 49).

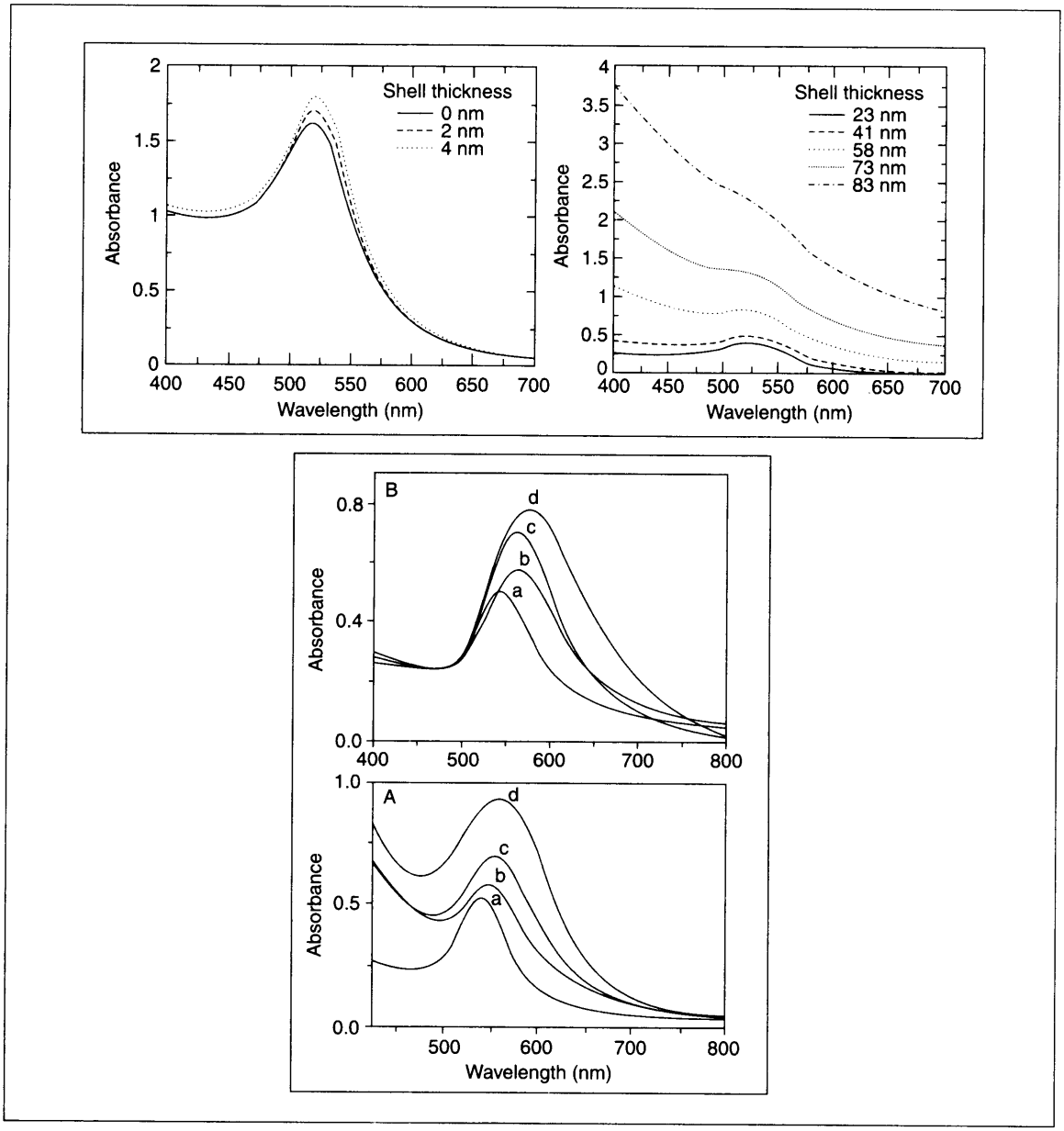

Fig. 9.14: *The absorption spectra of Au@SiO$_2$ colloids as a function of solvent refractive index (top figures) and Ag@TiO$_2$ (bottom (A)) and Ag@ZrO$_2$ (bottom (B)) as a function of increasing core dimension, a–d (A) and increasing shell thickness, a–d (B). Reprinted with permission from Liz-Marzan, et al. (Ref. 2) (top) and Tom, et al. (Ref. 6) (bottom). Copyright (1996 and 2003, respectively) American Chemical Society.*

9.4.3 Optical Non-linearity

There is a considerable interest in the role of non-linear optical materials in manipulating optical signals in optical communication and optical signal processing applications. Organic non-linear optical materials can be used for high density data storage, phase conjugation, holography, and spatial light modulation. Among the non-linear optical applications, optical limiting has been the most promising. Optical limiters have a transmission that varies with the incident intensity of light. Transmission is high at normal light intensities, but low for intense beams. The intensity-dependent transmission can limit the transmitted light intensity so that it is always below some threshold, and hence the name 'optical limiting'. This is useful in protecting elements that are sensitive to the sudden high intensity light, such as optical elements, sensors, the human eye and other sensitive devices. A non-linear absorption wherein the material's absorbance increases with the intensity of the incident light is obviously useful for good optical limiting. One mechanism that has been particularly useful for optical limiting is two-photon absorption and is shown by most of the materials. A simple energy level diagram where this can occur is shown in Fig. 9.16, depicting the 'reverse saturable absorption (RSA)' or excited state absorption (Refs 50–52).

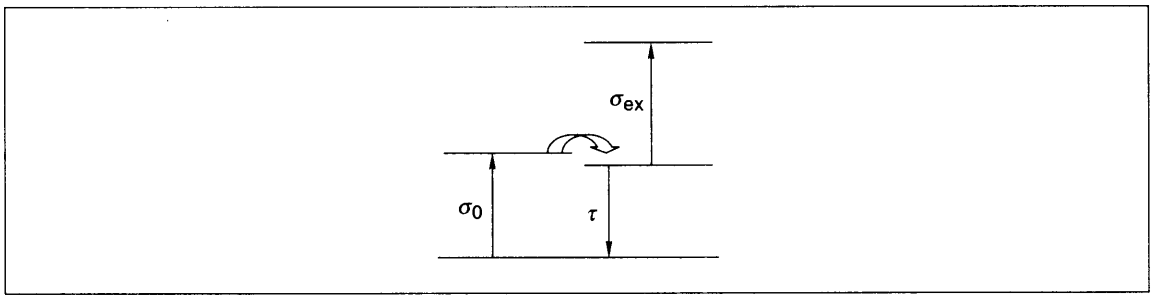

Fig. 9.16: *Schematic of two-photon absorption mechanism of optical limiting.*

In case when the incident light intensity is sufficiently high to allow a significant population to accumulate in the excited state and if the material has an excited state absorption cross section, σ_{ex} which is larger than the ground state absorption cross section, σ_o, the effective absorption coefficient of the material increases. The excited state may relax and subsequent absorption may occur from another state. In order to achieve largest non-linear absorption, both a large excited state absorption cross section and a long excited state life-time, τ are required, else the excited state population will not be high to increase net absorption. This sequential two-photon absorption is also called a large, positive non-linear absorption. A large σ_{ex} and a large difference between the ground and excited state absorption cross sections are essential for this to occur. The non-linear response should possess a low threshold value and remain large over a range of fluences before the non-linearity saturates. A high saturation fluence normally requires a high concentration of the non-linear material in the optical beam. Since no communication from the sensor or from any other device is required for the optical limiting devices to become active, they provide a type of 'smart' protection. Increased speed is particularly important for applications wherein the sensor may be exposed to sudden bursts of high intensity light. Optical limiting devices are used, for example, to

protect optical sensors used in conjunction with pulsed laser systems. The most important difficulty with the usage of common optical limiters is their low damage threshold, that is, the materials themselves get damaged under the impact of high intensity laser pulses. Studies have shown that protected nanoparticles of silver, gold and Pd are good optical limiters in the nanosecond regime. They give materials with a high damage threshold when incorporated into polymer matrices. The utility of the core-shell nanoparticles in optical limiting is given in Section 9.5.6.

9.5 Applications

9.5.1 Biological Applications

Magnetic core-shell nanoparticles are used in clinical applications and biotechnology, as the shells can be made biocompatible. Such core-shell particles find use in hyperthermia as immunoassays. They also find extensive uses in the transportation of drugs to the sites of diseases, and function as magnetic carriers for the identification and isolation of blood cells and antibodies. Further they are used in imaging for the magnetic mapping of organs, tissue repair, detoxification of biological fluids, drug delivery and in cell separation. The biomedical applications of polymeric core-shell nanoparticles of poly(ethylene oxide-β-ε-caprolactone) (PEO-β-PCL) diblock copolymer have been demonstrated by Gan, *et al.* (Ref. 53). The engineering of polymeric materials at the nanometer scale holds great promise in various biological applications. Shell cross-linked nanoparticles consisting of a polyisoprene (PI) core and poly (acrylic acid-co-acrylamide) shell have been used in drug delivery (Ref. 54). Functionalized internal surface of the nanocage, obtained by the dissolution of the polystyrene cage by ozonolysis, which uses masked fluorescent compounds, has biomedical applications. The masked compound, conjugated to the nanocage becomes fluorescent, when treated with aminopeptidase. Core-shell nanoparticles serve as intriguing building blocks for designing chemically and biologically active materials for analytical applications. Nanostructured thin films of gold nanoparticles and molecular linkers of different binding properties, namely 1,9-nonanedithiol and 11-mercaptoundecanoic acid, act as vapor sensors since the vapor accumulation at the interface changes the electrical conductance. Shell cross-linked nanoparticles possessing novel surface functionalities are ideal candidates for probing multivalent contacts with bacterial moieties and cell membranes. Shell cross-linked nanoparticles, when developed as multifunctional delivery and sequestration vessels, find utility in the treatment of bacterial infections. Amphiphilic block copolymers, consisting of poly(γ-benzyl L-glutamate) (PBLG) as the hydrophobic part and poly(ethylene oxide) (PEO) [or poly(N-isopropylacrylamide) (PNIPAAm)] as the hydrophilic one, can self-assemble in water to form nanoparticles which show a slow release of hydrophobic drugs from these polymeric nanoparticles. The entrapment of proteins in biodegradable nanospheres of amphiphilic di-block copolymers obtained by the ring opening polymerization, have been widely investigated as sustained release formulations for proteins and anti-cancer drugs. Monodisperse core-shell maghemite nanoparticles protected with a thin layer of divinyl benzene cross-linked polystyrene molecules are used in biological applications. The formation of core-shell type nanoparticles of linear polymer–dendrimer block copolymer–plasmid DNA complexes are

used in gene delivery applications *in vitro*.The super paramagnetic magnetite-silica core-shell nanoparticles find extensive uses in biology because of the presence of the inert silica shell (Ref. 55).The development of a novel biological reporter system based on the surface enhanced Raman scattering properties of silica-gold core-shell nanoparticles, was reported by Jensen, *et al.* (Ref. 56).The SERS activity of the nanostructures can be tuned by changing the dielectric constant and size of both the core and the shell.

9.5.2 Magnetism of Core-shell Nanoparticles

The magnetism of core-shell nanoparticles can be tuned by varying the shell thickness. The $Fe_{58}Pt_{42}$/Fe_3O_4 core-shell nanoparticles are ferromagnetic at low temperatures, but super-paramagnetic at room temperature. Such materials find applications in ultra high density magnetic storage media, biological labeling and detection and drug delivery.The bimetallic core-shell nanoparticles exhibit new properties of the core-shell magnetic systems which are often distinct from those of the corresponding monometallic properties. Fe–Pt, Pt–Co and Pt_3–Co alloy core-shell systems show high magnetic anisotropy and chemical stability. Bimetallic colloids of this type are expected to reveal interesting magnetic behavior like an induced polarization at the bimetallic interface or a giant magnetoresistance effect.The super paramagnetism of γ-Fe_2O_3 nanoparticles has been utilized in making facile recyclable catalysts in Suzuki cross-coupling reactions (Ref. 57).

Core-shell type magnetic nanosystems are also of great interest from the technological point of view. Magnetic nanoparticles are used in various areas such as bearing, seals, lubricants, heat carriers, printing, recording and polishing media. One of the rapidly emerging applications of magnetic nanoparticles is in biologically labeled areas including MRI, drug delivery, rapid biological separations and therapy. The synthesis of magnetic nanoparticles is also generating interest for the purpose of research. Polymeric shells have some unique advantages because of the flexibility in the control of chemical compositions and functions of the polymers. Magnetic nanoparticles are being tested as contrast-enhancing agents for cancer imaging and therapy. Aqueous magnetic fluids composed of small magnetic particles, covered with biocompatible functionalized shells, find use in biology as mentioned in Section 9.5.1.

9.5.3 Catalysis

Catalysis by core-shell nanoparticles is a very important, active and emerging area, which can have a tremendous impact in the chemical industry, pharmaceutical products and the fuel sector. More than 90 per cent of all industrial processes are catalytically controlled. Enhancement in specific catalytic activity and selectivity coupled with a reduction in the cost of catalysts would benefit the industrial sector in a big way. Catalysis of core-shell particles can either be due to the core or due to the shell.

The specific features which were seen to enhance the utility of the nanoparticles in the catalytic industry were their large surface-to-volume ratio and the specific binding sites on them (Ref. 58). Nanosized gold has high catalytic activity in the oxidation and reduction of hydrocarbons. Monolayer-encapsulated Au and alloy core-shell nanoparticles are model building blocks for devising nanostructured catalysts.

Tremendous variation can be achieved in the catalytic activity by changing the composition of the core, size, shape and surface properties.

Catalysis by shell includes asymmetric catalysis and mediated electrotransfer. In catalysis by nanoparticle cores, three types of nanoparticles are of relevance. These are: (a) nanoparticles supported on oxides including core-shell nanoparticles or polymers, (b) nanoparticles encapsulated in dendrimers and (c) nanoparticles encapsulated in alkane thiolate monolayers. Nanosized Au supported on oxide surfaces showed a high degree of catalytic activity as compared to bulk gold, which is a poor catalyst. A typical example is the oxidation of CO. It is observed that the catalytic activity of Au is high when its size is around 5 nm. Partial electron transfer from the Au clusters' surface is believed to play an important role in the activation of nano gold clusters as catalysts. A decrease in the mean coordination number and the ready mobility of Au atoms on the surface could lead to greater chemisorptivity, larger coverage of O_2 and a stronger interaction with the support to create special gold sites near the support. The oxidation of CO was considered to occur preferentially on the peripheral edges between Au nanoparticles and oxide support. However, the exceptionally high catalytic activity of the nanosized gold in the restricted size range is still a puzzle for chemists. The porosity of the shells facilitates size-selective accessibility of molecules to the metal cores.

It is well known that nanoparticles incorporated in the dendrimer cavities exhibit remarkable catalytic activity and selectivity towards hydrogenation and C–C coupling reactions like Suzuki, Heck, and Sonogashira reactions. Such nanoparticles are prepared by trapping the metal ions within the dendrimer cavities followed by a chemical reduction to yield metal nanoparticles of desired size range, usually 1–5 nm (Ref. 59). Nanoparticle encapsulation in dendrimer cavities possess advantages like uniformity in structure, protection against agglomeration, and the access of only small molecules to the nanoparticles' surface.

In order to exploit core-shell nanoparticle-based catalysis, the most important issue that must be addressed is the surface passivation of nanoparticles. This can be enhanced by place exchange, interparticle linking, size processing, electrochemical, thermal and photochemical annealing.

9.5.4 Sensing

The most important challenge in the filed of chemical/biological sensors is the rational design of materials with high sensitivity and selectivity. Nanostructured materials provide challenging opportunities for addressing problems because of their new and unique interparticle spatial and chemical properties that can be fine-tuned with various parameters. The sensing properties are highly dependent on several design parameters such as particle size, interparticle distances and the dielectric constant of the surrounding medium. Sensors in the field of biology are in great demand now because of their potential uses in detecting the mutations of genes. Biosensor technologies for DNA are also in great demand because of the sensitivity and selectivity they offer. The construction of nanoarrays on the basis of design parameters facilitates real-world sensing applications like detection of toxic gases, explosives and toxins. Alternative layer-by-layer assemblies of core-shell nanostructured materials have found interesting new applications in sensors and actuators on a wide scale. Dye-embedded core-shell nanoparticles with surface Raman

enhancement are excellent spectroscopic tags for detection protocols. These core-shell nanoparticles have a metallic core as an optical enhancer, a reporter molecule as a spectroscopic tag, and an inert shell for stabilization and conjugation. These find better applications in the sensing of biological warfare agents. Core-shell nanoparticles having a metallic core and an organic monolayer shell in ionic liquids have interesting applications such as optical sensors for anions, which work on the basis of aggregation-induced color changes. Thin films/membranes of pre-engineered gold nanoparticles derivatized with thiolate shells with carboxylate endings and a polymer, poly(2-hydroxyethyl methacrylate), are novel systems for chemical/biological sensing applications. Core-shell nanomaterials with gold/alloy/semiconductor nanocrystal cores and functional polymer shells, in solution state and thin films, have been studied as model systems for chemical and electrochemical sensing. Systems with the above-mentioned metal cores with thiols, thioethers, carboxylic acids, polymeric matrix, etc. as monolayers are excellent materials for the sensing of nitro aromatics and for the electrochemical detection of metal ions and biologically relevant molecules. The sensitivity, selectivity, detection limit and response time depend on a number of parameters like electronic conductivity, interfacial mass flux, binding specificity of the ligand and catalytic properties of the nano-framework. Such systems involve inter-core or inter-shell covalent linkages or non-covalent hydrogen bonding. The responses of material to volatile organic compounds, toxic gases and explosive vapors have been discussed by Han, *et al.* (Ref. 60). Organic-inorganic network assembly comprising gold nanoparticle core and organic linkers such as 1, 9-nonanedithiol and 1, 5-pentadithiol is responsive towards organic vapors and their nature of response depends on the chain length of the linker. These are chemically sensitive interfacial materials. Core-shell nanoparticle arrays cross-linked by the molecular receptor species act as sensing interfaces. Layered metal and semiconductor nanoparticle systems cross-linked by nucleic acids find extensive uses in the optical, electronic and photoelectrochemical detection of DNA. Similarly, nanoparticles incorporated in hydrogel matrixes yield new composite materials with novel sensing properties.

Bacteria, viruses and other micro-organisms responsible for diseases are also detectable via their unique and specific nucleic acid sequences. Metal nanoparticles are excellent candidates for the purpose because of their unique optical and electrical properties. Mirkin, *et al.* (Ref. 61) used hybridization-induced optical changes of oligonucleic acids-modified gold nanoparticles for devising DNA sensors. The electrochemical stripping detection of DNA by gold nanoparticles and further enhancement in signal amplification with silver have been reported by Cai, *et al.* (Ref. 28) and Wang, *et al.* (Ref. 15), respectively. The detection of glucose (as a sensor for blood glucose) with metal core-polymer shell system in an aqueous solution using surface-enhanced Raman scattering was reported by El Khoury, *et al.* (Ref. 62).

9.5.5 Chemical Reactivity

The chemical reactivity of core-shell nanoparticles is fascinating because they are excellent substrates for the conduct of C–C coupling reactions. Also, their specific chemistry leads to the metal core getting leached away by suitable molecules and thereby results in oxide shells or oxide nanobubbles (see Chapter 10) (Ref. 63). The synthesis, characterization and use of highly crystalline γ-Fe_2O_3 nanoparticles capped with a very thin polymer shell of polystyrene for the loading of Pd catalyst to facilitate Suzuki cross-coupling reactions was recently demonstrated by Stevens, *et al.* (Ref. 57). The most important aspect of the above

method is that the catalyst can be recovered to the extent of 97 per cent by a permanent low-field magnet since the catalyst-loaded substrate is magnetic. Dendrimer-encapsulated Pd core-shell nanoparticles are used as catalysts for the Stille coupling reactions of aryl halides and organostannanes. The nanoparticle Pd catalyst brings about catalysis at room temperature very efficiently even with 0.10 per cent Pd incorporation. Core-shell nanoparticles of Pd embedded into aluminum hydroxide act as dual catalysts for alkene hydrogenation and aerobic alcohol oxidation. The construction of core-shell nanoassemblies on gold nanostructures via Sonagashira coupling reactions was reported by Xue, *et al.* (Ref. 64) Suzuki coupling reactions using colloidal Pt nanocrystals with polyvinyl pyrrolidone(PVP) capping were recently investigated by El-Sayed, *et al.* (Ref. 65). There is a marked difference in the catalysis of tetrahedral PVP-Pt nanoparticles versus spherical PVP-Pt nanoparticles towards Suzuki reactions. The effect of molecular mass of the capping agent on the reactivity and the shape transformation of Pd nanoparticles during catalysis was also investigated in detail by the authors. Polyethylene glycol-capped Pd catalyst is an ideal catalyst for Heck coupling reactions. The utility of core-shell nanoparticles of gold stabilized by poly (N-vinyl-2-pyrrolidone) shows a high efficiency in catalyzing C–C bond formation in the aerobic homocoupling of aryl boronic acid in water.

The reactions between core-shell nanoparticles and reactive molecules present an entirely different chemistry leading to new systems. The most widely studied core-shell nanosystems in this category are $Ag@TiO_2$, $Au@TiO_2$, $Ag@ZrO_2$, $Au@ZrO_2$ and $Au@SiO_2$, respectively. The oxide shells in the above core-shell nanoparticles are porous and therefore, allow ionic and molecular transport through the shell. The dissolution of the core in $Ag@TiO_2$ by NH_3 resulting in TiO_2 nanoshells is shown in Fig. 9.17(b). The core-shell geometry of $Ag@TiO_2$ nanoparticles is shown in Fig. 9.17(a). Reactions of $Ag@ZrO_2$ and $Au@ZrO_2$ core-shell nanoparticles with halocarbons also result in the selective leaching of the metal core to give oxide nanobubbles of ZrO_2 (Ref. 63). The time-dependent reaction between $Ag@ZrO_2$ core-shell nanoparticles with CCl_4 and benzylchloride results in nanobubbles (see Chapter 10). The surface

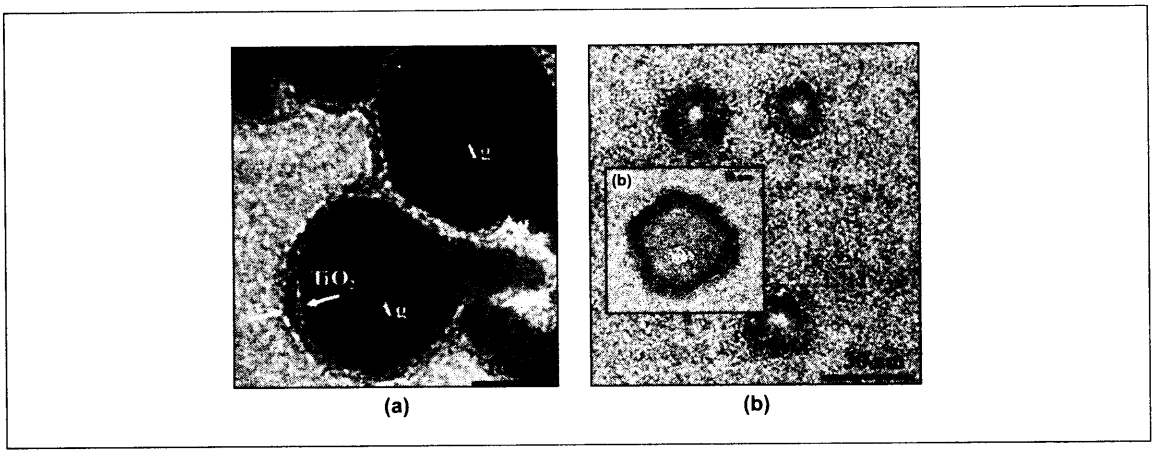

Fig. 9.17: *TEM images of $Ag@TiO_2$ core-shell nanoparticles (a) and the TiO_2 nanoshells formed from the same after leaching the core with NH_3. The inset of Fig. 9.17. (b) shows an expanded view of a TiO_2 shell. Reprinted from Ref. 46. Copyright (2002) Wiley-VCH.*

plasmon resonance of the Ag nanoparticles steadily decreases in intensity with the addition of the halocarbon, signifying the conversion of the Ag nanoparticles into silver halide. The dissolution of the metal core was also evident from cyclic voltammetry measurements. With the addition of the halocarbon, both the anodic and cathodic peak current intensity decrease and finally become flat. The decrease in peak current occurs because of the removal of the electro-active Ag nanoparticles in the form of AgCl from the system by the degradation of the halocarbon. The reactivity difference between CCl_4 and benzylchloride towards $Ag@ZrO_2$ is also evident from the absorption spectra. The ZrO_2 nanobubbles resulting from the reaction of CCl_4 with $Ag@ZrO_2$ core-shell nanoparticles can be seen in TEM images. Various types of carbonaceous materials were seen in the above reactions. The chemistry works with a series of other halocarbons like benzylchloride, $CHBr_3$, CH_2Cl_2, $CHCl_3$ and CCl_2F_2. The halocarbon reaction between $Au@SiO_2$ core-shell nanoparticles and CCl_4 results in carbon onions within SiO_2 nanoshells (Ref. 66). Increasing the shell thickness results in a decrease in the core-removal kinetics.

9.5.6 Optical Limiting

Optical sensors are important, for the light-sensitive devices that are used in the detection of light. However, they may be susceptible to damage if exposed to a high intensity of light, especially as in the case of a laser. Therefore, a proper protective device is essential for protecting the sensor at high light intensities. Nanomaterials constitute one of the best optical limiters discovered so far. The optical limiting characteristics of bare nanoparticles of silver and gold have been studied in detail by Mostafavi, *et al.* (Ref. 67). The optical limiting mechanisms of carbon nanotubes, carbon nanoparticles and carbon black suspensions have already been studied in detail. The biggest problem with bare nanoparticles is that they are prone to laser-induced damage at higher laser fluences. Therefore, the relevance of core-shell nanomaterials for this purpose has been considered as an alternative. The presence of inert shells around the core of nanoparticle protects them from higher laser powers as illustrated in Fig. 9.18. The optical limiting characteristics of thiol protected Au, Ag and Au/Ag alloy core-shell nanosystems have been investigated in detail. The core-shell nanomaterials are very good optical limiters and a comparative study of their optical limiting characteristics was attempted by Anija, *et al.* (Ref. 68). The most prominent mechanism observed in the case of core-shell nanoparticles for optical limiting is non-linear scattering, like in the case of bare metal nanoparticles or carbon nanotubes or carbon black suspensions. The optical limiting characteristics, as revealed by *Z*-scan experiments, of $Au@ZrO_2$ and $Au@TiO_2$ core-shell nanomaterials are shown in Fig. 9.19. The inset of the figure shows the Z-scan curve of $Ag@ZrO_2$. The z-scan technique is a method

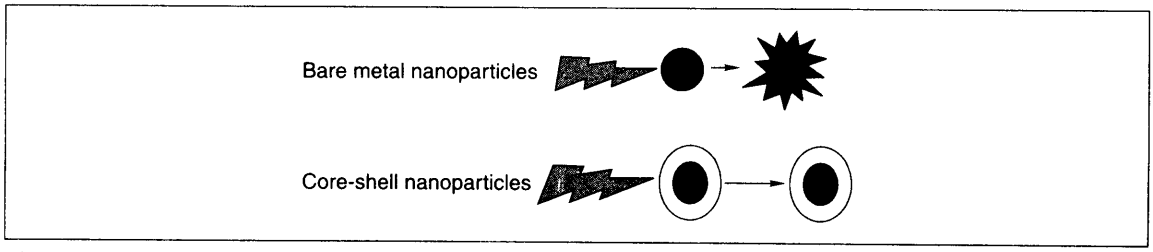

Fig. 9.18: *Schematic showing the stability of core-shell nanoparticles with intense laser fluences.*

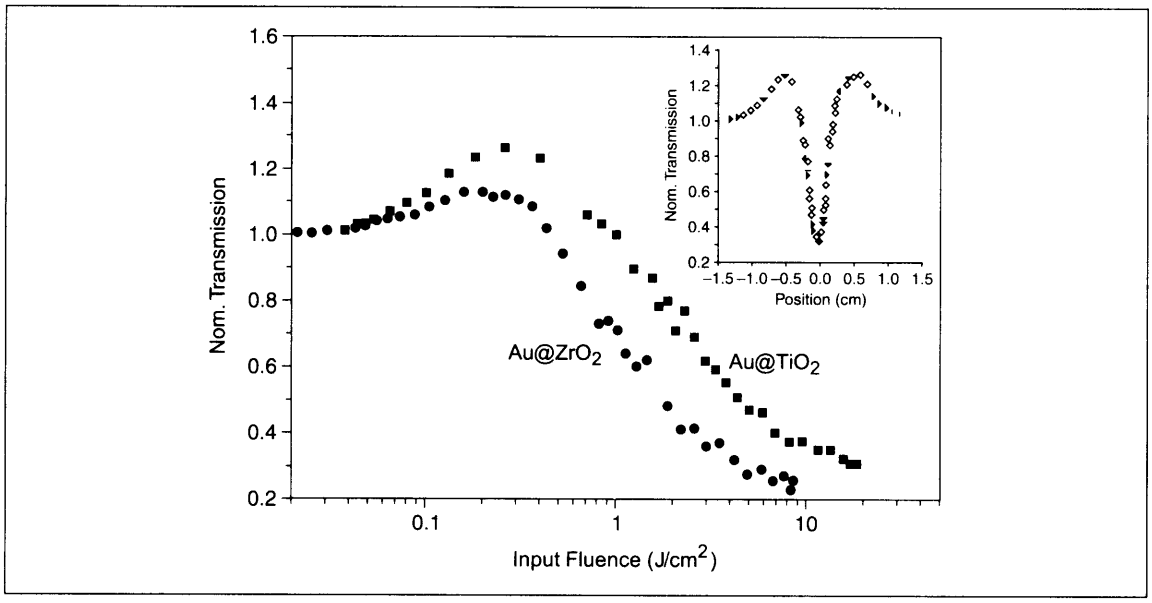

Fig. 9.19: *Optical limiting responses of Au@TiO$_2$ and Au@ZrO$_2$ core-shell nanoparticles using the Z-scan technique. Inset shows the Z-scan curve of Ag@ZrO$_2$ system. Reprinted with permission from Tom, et al. (Ref. 6). Copyright (2003) American Chemical Society.*

by which the sample is scanned along an axis (z-axis) while the laser is focused on it by a lens. At $z = 0$ the light intensity falling on the sample is a maximum. The intensity of the transmitted light is measured, which shows a minimum at $z = 0$, when light intensity is maximum. The optical limiting response of Au–Ag alloy systems with varying mole fractions of Au and Ag has also been investigated in detail by Nair, *et al.* (Ref. 69). The core-shell nanosystems incorporated into polymer matrices signify new approaches to help increase the limiting performance and damage threshold of optical limiting materials (Ref. 70). In the case of oxide-protected nanoclusters, no signs of damage were seen with laser pulses of fluences up to 20 J/cm^2 and intensities up to 2.8 GW/cm^2. However, the exact mechanism of energy transport, i.e. how the electrons communicate with the insulator shell, is not completely understood. Plasmon damping and electron-phonon scattering at the interface, however, may be important in these cases and more studies are being carried out to understand the electron transport mechanism in detail.

Review Questions

1. What are the principal core-shell systems?
2. How do we understand the optical properties of core-shell systems starting from the core?
3. What are intrinsic and extrinsic size regimes?
4. What are the essential aspects of Mie theory?

5. What are the principal applications of core-shell systems?
6. Why are they important in biology in contrast to simple particles?
7. Why core-shell particles are important in optical limiting applications?

References

1. Davies, R., G.A. Schurr, P. Meenan, R.D. Nelson, H.E. Bergna, C.A.S. Bervett and R.H. Goldbaum, *Adv. Mater.*, **10** (1998), p. 1264.
2. Liz-Marzan, L.M., M. Giersig and P. Mulvaney, *Langmuir*, **12** (1996), p. 4329.
3. Hofman-Caris, C.H.M., *New. J. Chem.*, **18** (1994), p. 1087.
4. Liz-Marzan, L.M., M. Giersig and P. Mulvaney, *Chem. Commun*, (1996), p. 731.
5. Pastoriza-Santos, I., D.S. Koktysh, A.A. Mamedov, M. Giersig, N.A. Kotov and L.M. Liz-Marzan, *Langmuir*, **16** (2000), p. 2731.
6. Tom, R.T., A.S. Nair, N. Singh, M. Aslam, C.L. Nagendra, R. Philip, K. Vijayamohanan and T. Pradeep, *Langmuir*, **19** (2003), p. 3439.
7. Teng, X., D. Black, N.J. Watkins, Y. Gao and H. Yang, *Nano Lett.*, **3** (2003), p. 261.
8. Mulvaney, P., L.M. Liz-Marzan, M. Giersig and T. Ung, *J. Mater. Chem.*, **10** 2000, p. 1259.
9. Liz-Marzan, L.M., M. Giersig and P. Mulvaney, *Langmuir*, **12** (1996), p. 4329.
10. Konya, Z., J. Zhu, A. Szegedi, I. Kiricsi, P. Alivisatos and G.A. Somorjai, *Chem. Commun.*, (2003), p. 314.
11. Mayya, K.S., D.I. Gittins and F. Caruso, *Chem. Mater.*, **13** (2001), p. 3833.
12. Nair, A.S., T. Pradeep and I. MacLaren, *J. Mater. Chem.*, **14** (2004), p. 857.
13. Hu, M., X. Wang, G.V. Hartland, V. Salgueirino-Maceira and L.M. Liz-Marzan, *Chem. Phys. Lett.*, **372** (2003), p. 767.
14. Chen, M.M.M. and A. Katz, *Langmuir*, **18** (2002), p. 8566.
15. Wang, D., V. Salgueirino-Maceira, L.M. Liz-Marzan and F. Caruso, *Adv. Mater.*, **14** (2002), p. 908.
16. Hodak, J.H., A. Henglein and G.V. Hartland, *J. Chem. Phys.*, **111** (1991), p. 8613.
17. Sader, J.E., G.V. Hartland and L.M. Liz-Marzan, *J. Phys. Chem. B*, **106** (2002), p. 1399.
18. Henglein, A., *J. Phys. Chem. B*, **104** (2000), p. 2201.
19. Yonezawa, T. and N. Toshima, *J. Mol. Catal.*, **83** (1993), p. 167.
20. Schmid, G., A. Lehnert, J.-O. Malm and J.-O. Bovin, *Angew. Chem. Int. Ed. Engl.*, **30** (1991), p. 874.
21. Henglein, A., *J. Phys. Chem.*, **83** (1979), p. 2209.
22. Mulvaney P., M. Giersig and A. Henglein, *J. Phys. Chem.*, **97** (1993), p. 7061.
23. Sinzig, J., U. Radtke, M. Quinten and U. Kreibig, *Zeitschrift Fur Physik D-Atoms Molecules and Clusters*, **26** (1993), p. 242.

24. Link, S., C. Burda, Z.L. Wang and M.A. El-Sayed, *J. Chem. Phys.*, **111** (1999), p. 1255.
25. Y. Kim, R.C. Johnson, J. Li, J.T. Hupp and G.C. Schatz, *Chem. Phys. Lett.*, **352** (2002), p. 421.
26. Sobal, N.M., M. Hilgendorff, H. Mohwald, M. Giersig, M. Spasova, T. Radetic and M. Farle, *Nano Lett.*, 2 (2002), p. 621.
27. Sobal, N.S., U. Ebels, H. Mohwald and M. Giersig, *J. Phys. Chem. B*, **107** (2003), p. 7351.
28. Cai, H., N. Zhu, Y. Jiang, P. He and Y. Fang, *Biosensors and Bioelectronics*, **18** (2003), p. 1311.
29. Huang, C.L. and E. Matijevic, *J. Mater. Res.*, **10** (1995), p. 1327.
30. Sastry, M., A. Swamy, S. Mandal and P. R. Selvakannan, *J. Mater. Chem.*, **15** (2005), p. 3161.
31. Hines, M.A. and P. Guyot-Sionnest, *J. Phys. Chem.*, **100** (1996), p. 468.
32. Peng, X., M.C. Schlamp, A.V. Kadavanich and A.P. Alivisatos, *J. Am. Chem. Soc.*, **119** (1997), p. 7019.
33. Dabbousi, B.O., J. Rodriguez-Viejo, F.V. Mikulec, J.R. Heine, H. Mattoussi, R. Ober, K.F. Jensen and M.G. Bawendi, *J. Phys. Chem. B*, **101** (1997), p. 9463.
34. Mekis, I., D.V. Talapin, A. Kornowski, M. Haase and H. Weller, *J. Phys. Chem. B*, **107** (2003), p. 7454.
35. DeGroot, M.W., N.J. Taylor and J.F. Corrigan, *J. Mater. Chem.*, **14** (2004), p. 654.
36. Yang, Y., J.I. Shi, H. Chen, S. Dai and Y. Liu, *Chem. Phys. Lett.*, **370** (2003), p. 1.
37. Sprycha, R., H.T. Oyama, A. Zelenev and E. Matijevic, *Colloid Polym. Sci.*, **273** (1995), p. 693.
38. Marinakos, S.M., L.C. Brousseau, A. Jones and D.L. Feldheim, *Chem. Mater.*, **10** (1998), p. 1214.
39. Marinakos S.M., D.A. Shultz and D.L. Feldheim, *Adv. Mater.*, **11** (1999), p. 34.
40. Marinakos, S.M., J.P. Novak, L.C. Brousseau, A.B. House, E.M. Edeki, J.C. Feldhaus and D.L. Feldheim, *J. Am. Chem. Soc.*, **121** (1999), p. 8518.
41. Ottewill, R.H., A.B. Schofield, J.A. Waters and N.S.J. Williams, *Colloid Polym. Sci.*, **275** (1997), p. 274.
42. Hergeth, W.D., U.J. Steinau, H.J. Bittrich, K. Schmutzler and S. Wartewig, *Prog. Colloid Polym. Sci.*, **85** (1991), p. 82.
43. van Herk, A.M., *NATO ASI ser. E*, **335** (1997), p. 435.
44. Quaroni, L. and G. Chumanov, *J. Am. Chem. Soc.*, **121** (1999), p. 10642.
45. Nair, A.S., R.T. Tom, V. Suryanarayanan and T. Pradeep, *J. Mater. Chem.*, **13** (2003), p. 297.
46. Koktysh, D.S., X. Liang, B.-G. Yun, I. Pastoriza-Santos, R.L. Matts, M. Giersig, C. Serra-Rodriguez, L.M. Liz-Marzan and N.A. Kotov, *Adv. Funct. Mater.*, **12** (2002), p. 255.
47. Kelly, K.L., E. Coronado, L.L. Zhao and G. C. Schatz, *J. Phys. Chem. B*, **107** (2003), p. 668.
48. Mie, G., *Ann. Phys.*, **25** (1908), p. 377.
49. Ung, T., L.M. Liz-Marzan and P. Mulvaney, *J. Phys. Chem. B*, **105** (2001), p. 3441.
50. Pittman, M., P. Plaza, M.M. Martin and Y.H. Meyer, *Opt. Commun.*, **158** (1998), p. 201.
51. Chen, P.L., I.V. Tomov, A.S. Dvornikov, M. Nakashima, J.F. Roach, D.M. Alabran and P.M. Rentzepis, *J. Phys. Chem.*, **100** (1996), p. 17507.

52. Philip, R., G. Ravindra Kumar, N. Sandhyarani and T. Pradeep, *Phys. Rev. B*, **62** (2001), p. 13160.
53. Gan, Z.H., T.F. Jim, M. Li, Z. Yuer, S.G. Wang and C. Wu, *Macromolecules*, **32** (1999), p. 590.
54. Liu, J.Q., and K.L. Wooley, *Abstr. Paper Amer. Chem. Soc.*, **221** (2001), U 439.
55. Sun, Y.K., L. Duan, Z.R. Guo, D.M. Yun, M. Ma, L. Xu, Y. Zhang and N. Gu, *J. Mag. Mag. Mater.*, **285** (2005), p. 65.
56. Jensen, T., L.A. Kelley, A. Lazarides and G.C. Schatz, *J. Cluster Sci.*, **10** (1999), p. 295.
57. Stevens, P.D., J. Fan, H.M.R. Gardimalla, M. Yen and Y. Gao, *Org. Lett.*, **7** (2005), p. 2085.
58. Templeton, A.C., M.J. Hostetler, E.K. Warmoth, S. Chen, C.M. Hartshom, Y.M. Krishnamurthy, M.D.E. Forbes and R.W. Murray, *J. Am. Chem. Soc.*, **120** (1998), p. 4845.
59. Zhao, M.Q. and R.M. Cooks, *Adv. Mater.*, **11** (1999), p. 217.
60. Han, L., J.M. Kneller, D.R. Daniel, S.R. Kowaleski, F.L. Kirk, J. Luo and C-J. Zhong, *Mater. Res. Soc. Symp. Proc.*, **710** (2002), DD 6.4.1.
61. Mirkin, C.A.; R.L. Letsinger, R.C. Mucic and J.J. Storhoff, *Nature*, **382** (1996), p. 607.
62. http://www.ohiolink.edu/etd/view.cgi?arkon1123637252
63. Nair, A.S., R.T. Tom, V.S. Suryanarayanan and T. Pradeep, *J. Mater. Chem.*, **13** (2003), p. 297.
64. Xue, C., G. Arumugam, K. Palaniappan, S.A. Hackney, H. Liu and J. Liu, *Chem. Commun.*, (2005), p. 1055.
65. Narayanan, R. and M.A. El-Sayed, *Langmuir*, **21** (2005), p. 2027.
66. Rosemary, M.J., I. MacLaren and T. Pradeep, *Carbon*, **42** (2004), p. 2352.
67. Francois, L., M. Mostafavi and J. Belloni, *J. Phys. Chem. B*, **104** (2000), p. 6133.
68. Anija, M., J. Thomas, N. Singh, A.S. Nair, R.T. Tom, T. Pradeep and R. Philip, *Chem. Phys. Lett.*, **380** (2003), p. 223.
69. Nair, A.S., V. Suryanarayanan, T. Pradeep, J. Thomas, M. Anija and R. Philip, *Mater. Sci. Engg. B*, **117** (2005), p. 173.
70. Porel, S., S. Singh, S.S. Harsha, D.N. Rao and T. P. Radhakrishnan, *Chem. Mater.*, **17** (2005), p. 9.

Additional Reading

1. Link, S. and M.A. El-Sayed, *Ann. Rev. Phys. Chem.*, **54** (2003), p. 331.
2. Hanack, M., T. Schneider, M. Barthel, J.S. Shirk, S.R. Flom and R.G.S. Pong, *Coord. Chem. Rev.*, (2001), pp. 219–221, 235.
3. Bond, G.C. and D.T. Thomson, *Catal. Rev.*, **41** (1999), p. 319.
4. Kolmakov, A. and M. Moskovits, *Ann. Rev. Mater. Res.*, **34** (2004), p. 151.
5. Kreibig, U. and M. Vollmer, *Optical Properties of Metal Clusters*, (1993) Springer, Berlin.
6. Rao, C.N.R., A. Muller and A.K. Cheetham (eds) (2004), *The Chemistry of Nanomaterials: Synthesis, Properties and Applications*, Wiley–VCH, Weinheim.

Chapter 10

NANOSHELLS

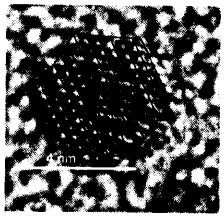

Nanoshells are important from the point of view of cancer therapy and spectroscopic applications. As we have seen, their method of synthesis is quite simple and includes one-step and two-step approaches. Silica nanoshells are used mainly in the field of molecular encapsulation while metal nanoshells are used for cancer therapy. Principal tools for their characterization are absorption spectroscopy, fluorescence spectroscopy and transmission electron microscopy. Even though intense research is taking place in this area, many questions remain unanswered regarding the biodegradability of these shells. The questions that need to be answered are, what the byproducts of these materials will be and what changes they are likely to create in the body.

Learning Objectives

- What are the various nanocavity systems?
- How do we study them?
- What are their properties?
- Are there any immediate applications for them?

10.1 Introduction

Nanoparticles are stabilized by different types of ligands such as organic molecules, polymers, surfactants, etc. The advantage of this kind of stabilization is that both the properties of the metal (or other) core as well as the stabilizing ligand can be made use of, in addition to the hybrid properties (properties due to both the core and the shell). Nanoparticles, whose surface is passivated by a shell with its own distinct properties other than the core, are called *core-shell particles*. Depending upon the use, this shell can also be made of metals, oxides, etc. Such coatings not only stabilize colloidal dispersions but also allow modification and tailoring of the particle properties (e.g. optical, magnetic, catalytic, etc.). Oxide-protected nanoparticles are found to be more stable even in extreme conditions such as exposure to intense lasers, which normally degrades materials. The shell makes the metal nanoparticle inert to chemical reagents. Nano-sized objects which have only the shell and are devoid of the core, are called nanoshells. They are also called by other names such as nanocapsules and nanobubbles.

There are some other types of nanoshells which are made of metals such as gold, silver, etc. and have a dielectric core. Nanoparticles of metallic, semiconducting, and magnetic materials have recently generated interest in terms of research because of their potential uses in optoelectronics, reprography, catalysis, chemical and biological sensing, etc. Among the metallic particles, the study of colloidal gold particles particularly stands out. It is one of the most widely studied systems, scientific interest in which can be traced back to the time of Faraday (see Chapter 1). This nanostructure has a unique optical property in that by changing the relative sizes of the core and the shell, its surface plasmon resonance can be tuned in a broad spectrum of wavelength (see Chapter 9). Halas and co-workers (Ref. 1) have developed a procedure to make gold nanoshells on silica treated with (aminopropyl) triethoxysilane. They have also tuned the properties of this system in such a way that it has been used for biological imaging and the therapy of cancer cells. There are reports of gold shells with polystyrene cores (Ref. 2). These gold nanoparticle-decorated silica cores can be modified for further stability by using self-assembled monolayers of alkane thiols. Other kinds of nanospheres are formed by the deposition of silica on biological systems such as liposomes.

The nanoshells which are obtained in the case of oxide nanoshells have diameters in the range of 10–20 nm. However, this is a variable and can be changed depending upon the required size. In the case of metal nanoshells like gold with silica shell, the thickness of the shell can be up to around 20 nm. It has been found that these nanoshells are highly porous in nature. One of the main uses of these hollow silica shells is in the form of containers of drugs. The outer surface of these shells can be used for attaching antibodies so that the silica shell-antibody complex can be used to bind to a specific antigen in fluid systems.

This chapter deals with different types of nanoshells, principally nanoshells of silica and gold. The applications of these nanoshells in different fields are also discussed. In the case of nanoshells made of silica, encapsulation of different analyte molecules has been done. Different kinds of methods used for the synthesis of coreshell particles as well as nanoshells are listed and the different techniques used for their characterization are discussed in this chapter.

10.2 Types of Nanoshells

It is possible to obtain nanoshells by a variety of methods. Given an application and size, one can select a method of synthesis. But most of these methods have the disadvantage of non-uniform coating which limits their applications. Hence it is very important to decide on the method of synthesis as it is difficult to obtain controlled and uniform coating. The preferred method involves surface precipitation of inorganic molecular precursors on particles and removal of the core by thermal or chemical means. However, the method used also depends on the type of the shell.

The two principal methods available for the synthesis of oxide-protected core shell particles, are 'layer-by-layer precipitation' of the inorganic precursor from solution and 'one-pot synthesis' carried out in the presence of several chemical ingredients. The multi-step synthesis involves making the core particle first and then covering it by using the shell forming precursor (e.g. TiO_2, SiO_2) and one-pot synthesis

entails reduction of the metal in the presence of the shell-forming precursor, typically an organometallic species. In some other cases, dielectric substances such as silica or polymers are covered with gold or silver, thereby forming metal-coated particles. Nanoshells are obtained when the core of these particles is removed by chemical or physical means.

Most of the nanoshells are made of oxides, which include silica, zirconia and titania and oxides of a few other metals. As mentioned earlier, their method of synthesis varies from one another. Silica nanoshells, which are formed by two-step synthesis, are mainly used for studies related to the encapsulation of molecules, which may be dyes or drugs. While the titania shell is used for sensing purposes, new materials can also be formed from it.

For synthesizing metal nanoshells, first the dielectric material was made followed by the adsorption of the small metal nanoparticle over it, that was synthesized separately. Gold nanoshell is especially important in bio-imaging because gold is biocompatible. Another type of silica shell system with a liposome core, which is useful for drug delivery has also been reported. This is also highly biocompatible and biodegradable. These nanoshells can basically be divided into groups: (a) those that are formed from the oxide core shell particles, with a hollow core, and (b) those having a dielectric core and a metallic shell. Both these shells have applications in the fields of drug delivery, sensing and catalysis as also in the study of the micro-environment in which they are placed.

10.2.1 Oxide Nanoshells

This group includes silica, titania and zirconia nanoshells. The unique feature of this group is that they have a hollow core and a covering made of oxide. Their main applications are in the fields of encapsulation of molecules and in spectroscopy.

Hollow silica nanoshells

Silica has certain advantages when used as a protecting agent. It is chemically inert and therefore, does not affect the reactions which are taking place with the core. Also, since it is optically transparent, the spectroscopy of the system can be easily investigated. Most of the silica nanoshell systems are found to be useful in the study of the photochemistry of molecules, mainly fluorophores.

In the typical synthesis of silica-covered gold and silver core-shell particles (Refs 3, 4), organic molecules were used first to stabilize the metal nanoparticles. These ligands have the dual role and are used also as the primers for the growth of shells on the core. This means that the first layer of oxide is grown with the help of these molecular linkers. First, gold and silver silica colloids are prepared. 3-aminopropyltrimethoxysilane (APS) is used as the primer (and stabilizer) to make the gold surface vitreophilic and it also allows the formation of a thin layer of silica. The silica layer is formed by the hydrolysis of the methoxy groups. After this, another precursor of silica, i.e. sodium silicate solution is added at the appropriate pH to get a thicker layer of shell followed by the Stöber process (Ref. 5), which is a method to make larger particles of silica. This process is achieved by transferring the particles to an alcohol medium and creating the silica monomer

in-situ by adding tetraethoxy silane, which leads to a slow homogeneous growth of silica around the particles. The reactions involved in the Stöber process are,

$$Si(OC_2H_5)_4 + 4H_2O \rightarrow Si(OH)_4 + 4C_2H_5OH$$

$$Si(OH)_4 \rightarrow \text{(in presence of } NH_3 \text{ and alcohol) } SiO_2 + 2H_2O$$

Hydrolysis of the tetraethoxysilane as well as the condensation of silica are base catalyzed events. This also provides the particles with a negative charge, thereby stabilizing the surface. It is possible to get a silica shell covered gold and silver core shell particles by using this method. Since standard methods of synthesis of gold and silver particles having a definite size are available in literature, it is possible to obtain core shell particles with a fixed core size.

Nanoshells can be obtained from these coreshell particles through the removal of the core material. It is important to use a suitable procedure for removing the core without disturbing the shell structure. The most common methods involve the use of cyanide ion in the case of gold and ammonia in the case of silver. Another method using halocarbons, mainly CCl_4 and benzyl chloride, is also found to be useful for making nanoshells.

In order to obtain nanoshells from $Au@SiO_2$, sodium cyanide solution was added to it and the core of the particle was dissolved. The dissolution of the core was monitored by using absorption spectroscopy from the disappearance of the surface plasmon peak of the gold nanoparticle (see Chapter 8). In the case of $Ag@SiO_2$, ammonia solution was used to remove the core.

The reactions can be represented as follows:

$$4Au + 8NaCN + 2H_2O + O_2 \rightarrow 4NaOH + 4NaAu(CN)_2$$

$$4Ag + 8CN^- + O_2 + 2H_2O \rightarrow 4Ag(CN)_2^- + 4OH^-$$

$$4Ag + 8NH_3 + O_2 + 2H_2O \rightarrow 4Ag(NH_3)_2 + 4OH^-$$

Zirconia nanoshells

Zirconia nanoshells also constitute an important class of materials that can be made of core-shell particles of silver and gold. Even though there are no reports of any specific application of this material nor has any study of molecular encapsulation been carried out, this material is important, especially form the point of view of catalysis and sensing. The shells are made (Ref. 6) from core-shell particles synthesized by two-step or one-step routes.

Synthesis of core-shell particles

1. Two-step synthesis: The first step is the synthesis of the core-shell particles. Silver nanoclusters are made first as in the case of monolayer protected clusters (Chapter 8). The monolayer made has a carboxyl functionality. The method used is called the Brust method (see Chapter 8). In a standard synthesis, 0.01g of the as prepared cluster is dispersed in a toluene-methanol mixture. To this mixture, zirconylchloride octahydrate is added in a 1:10 (weight) ratio. This solution is equilibrated and then 5 ml of diethylamine

is added slowly over a period of 15 minutes. Fifty ml of water is then added. The solution is stirred for over 24 hours. The mixture is centrifuged, washed with plenty of methanol and air dried. The powder obtained is zirconia coated nanoparticles and the shell thickness is several nanometers (Ref. 7).

2. One pot synthesis: In this method of making core-shell nanoparticles, the method adopted is the reduction of noble metals by dimethylformamide in the presence of oxide forming precursors. It is possible to make silver- and gold-covered zirconia as well as titania in this manner. A typical procedure is as follows: A solution containing equimolar (19.9 mM) amounts of titanium isopropoxide (or zirconium (IV) propoxide) and acetylacetone (a complexation agent for metal ions, to increase the stability of the alkoxide used) in 2-propanol is prepared. A clear solution is formed upon mild sonication. Another solution of 8.80 mM $AgNO_3$ (or $HAuCl_4.3H_2O$) and 13.88M H_2O in DMF is prepared. A 40 mL sample of the first solution and 20 mL of the second solution are mixed and stirred for about ten minutes. The mixture is transferred to a heating mantle and refluxed for 45 minutes. The solution becomes pink in the case of Au and green-black in the case of Ag. The color change is abrupt in the case of Au and more gradual in the case of Ag. Further refluxing of the solution results in the formation of a precipitate, which can be dispersed by sonication. The colloidal material is precipitated by the addition of toluene. The precipitate is washed repeatedly with toluene and re-dispersed in 2-propanol. The cleaning procedure is important for obtaining well-defined absorption spectra and electrochemical properties. This one-pot synthesis can be used to make coreshell particles, especially in the case of zirconia, titania, etc. (Refs 6, 8).

Formation of nanoshells from core-shell particles prepared by one pot synthesis

The core shell particles which are synthesized by the above methods are subjected to different reactions which result in nanoshells. Fo. getting nanshells, 4 ml of the core-shell particle dispersion was mixed with 1 ml each of CCl_4 or benzyl chloride separately. The reaction took place a period of several hours and the solution turned colorless. Silver ions were leached out and precipitated as AgCl during the reaction.

Titania nanoshells

Titania nanoshells can also be prepared by the dissolution of the cores of $Ag@TiO_2$ nanoparticles by using ammonia solution (Ref. 8). Ammonia complexes with the surface silver atoms, oxidizing the silver metal to silver ion complexes which diffuses from the interior of the core-shell particle through the pores in the titania shell. The shells have diameters of 10–30 nm and thicknesses of 3–5 nm. The diameter of the channels in the titania shells were comparable to the thickness of the electrical double layer (0.3–30 nm). The permeation of ions through these channels can be tuned by parameters such as pH and ionic strength. This has applications in the biomedical field (Ref. 8).

Zinc oxide nanoshell having silica core

Almost the same method that was used for the synthesis of zinc oxide covered silica (Ref. 9) which is photoluminescent. Simultaneous introduction of triethanolamine and $Zn(Ac)_2$ into the SiO_2 ethanol–water dispersion yields this composite. About 0.2 g of SiO_2 was dispersed in 30 mL ethanol–water (2:3 in

volume) mixture and heated to 90 °C. After 10 minutes, 1.6 M triethanolamine and 0.02 mol/L $Zn(Ac)_2$ were dropped simultaneously through latex tubes into the previous mixture at a constant flow rate. The mixture was stirred for 1 h at 90 °C. The resulting white powders were recovered by centrifugation, washed repeatedly with water, and dried in vacuum. Finally, the powders were sintered at 700 °C for 3 hours.

10.2.2 Metal Nanoshells

Metal nanoshells are different from oxide nanoshells in their structure, which has a dielectric core made of silica. The main advantage of such a system is that the optical properties can be tuned by changing the thickness of the shell. Among this group, gold nanoshells find application in the field of cancer therapy.

Gold nanoshells

The novelty of this material is that its properties can be tuned to scatter or adsorb light over a broad spectral range including the near IR, a wavelength region that provides maximal penetration of light through the tissue. This property offers the opportunity to design nanoshells which can be used for diagnostic and therapeutic applications and also can be used to monitor different analytes such as immunoglobulin in blood, saline, etc. This system is found to have sensitivity in the subnanogram per mL range within 10–30 min. Gold nanoshells have many advantages over silica nanoshells. Apart from the fact that their optical properties, especially absorption, can be tuned as a function of the thickness of the gold layer, they have large optical cross section as compared to the conventional near-IR (NIR) dyes, such as

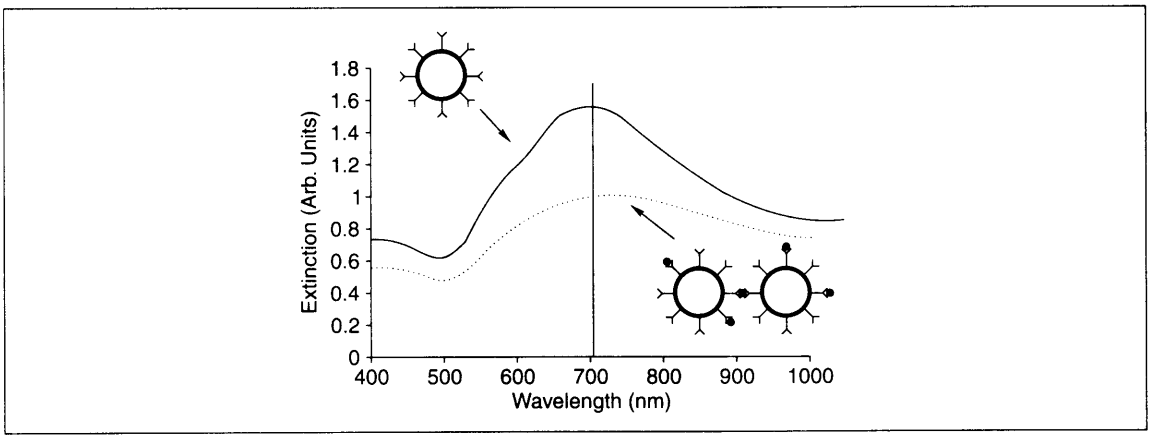

Fig. 10.1: *UV-vis spectrum of dispersed nanoshells fabricated with a 96-nm-diameter core and 22-nm-thick gold shell (—); spectrum of nanoshells/antibody conjugates following addition of analyte (- - -). Extinction reduction upon aggregation in the presence of analyte was monitored at 720 nm, as indicated. Reprinted with permission from Hirsch, et al. (Ref. 1), Copyright (2003), American Chemical Society.*

indocyanine green. They also show improved photostability. Another advantage is that the gold surface can be used to anchor different molecules, especially proteins and other biomolecules. The gold surface is generally considered to be biocompatible. It can be modified according to the type of anchoring needed by using molecules like polyethylene glycol. Alkanethiols can be used for functionalization to facilitate increased solubility in the organic media, see Fig. 10.2 (Plate 6).

Synthesis of gold nanoshell having silica as the core

Method I Nanoshells with extinction maximum at ~800 nm were synthesized as follows (Ref. 10). Using the Stöber method, 120 nm diameter silica nanoparticles were made first. The surface of these particles were functionalized using (aminopropyl) triethoxysilane (APTES). Small gold colloid was grown as per the method of Duff and Baiker (Ref. 11) and these were adsorbed on aminated silica nanoparticles. More gold was reduced into these nucleation sites using potassium carbonate and formaldehyde.

Method II The original method is due to Sun and Xia (Ref. 9). Ag nanoparticles were prepared by injecting $NaBH_4$ (50 mM, 2 mL) into 0.2 mM, 100 mL aqueous solution of $AgNO_3$, in the presence of sodium citrate (0.5 mM). The Ag colloid formed was kept at 70 °C for 2 hours. $HAuCl_4$ (0.1 M, 0.68 mL) was added to 100 mL of the Ag colloid. A series of color changes from yellow to red to dark blue were observed during the course of the replacement reaction (Refs 12, 13). After 1 hour of stirring, the particles were purified by gradient centrifugation, washed using aqueous sodium citrate (0.3 mM), re-dispersed in 5 mL of sodium citrate (0.3 mM), and finally kept at 4 °C.

Silver nanoshell

In another method, the seed growth approach was used to prepare to silver nanoshells on silica nanoparticles (Ref. 14). In this case also, the optical properties could be changed by changing the thickness of the shell. Since its Mie resonance occurs at energies distinct from any bulk interband transition, a silver colloid is expected to have a stronger and sharper plasmon resonance than gold. Another advantage of a silver colloid is that the plasmon resonance of a solid silver nanoparticle appears at a shorter wavelength than that of gold.

Fig. 10.3: *High-resolution TEM photograph of an individual Au nanoshell. Reprinted with permission from Hao, et al. (Ref. 12), Copyright (2004), American Chemical Society.*

Preparation of a silver nanoshell on a silica sphere

Scheme 1 shows the typical strategy used to prepare a silver nanoshell (Ref. 14). First, the silica sphere core is treated with an amine terminated surface silanizing agent (step I, see Fig. 10.4). The resultant terminal amine groups act as attachment points for small colloidal silver particles, which is used for the growth of a silver nanoshell overlayer (step II). This was followed by the growth of silver particles (using the standard sodium citrate route, step III). By repeating step III, the thickness of the silver shell can be tailored, as expected. Reduction of silver ions can also be done by other reducing agents such as $NaBH_4$.

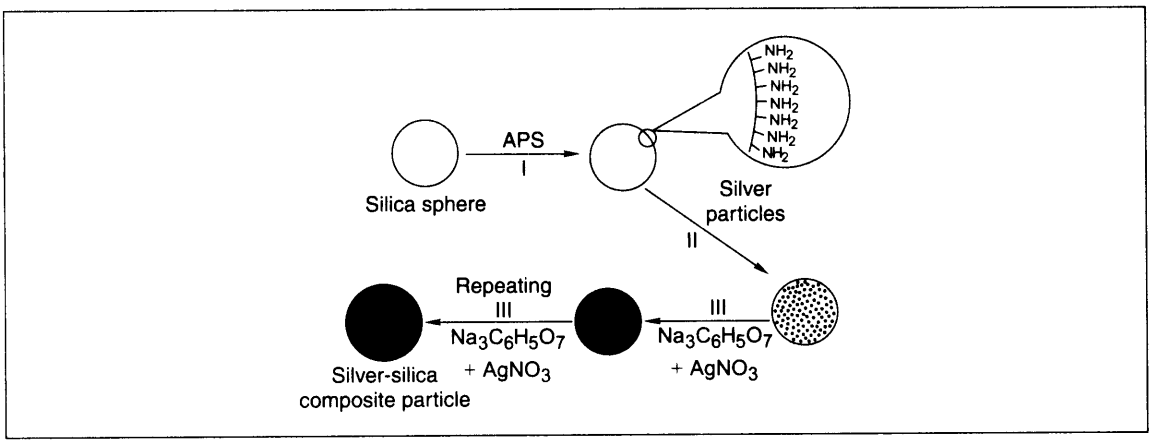

Fig. 10.4: *Fabrication procedure of a silver nanoshell on the silica sphere. Reprinted with permission from Jiang and Liu (Ref. 14). Copyright (2003) American Chemical Society.*

10.2.3 Nanoshells from Liposomes

Another method followed for the synthesis of silica nanoshells involves the use of liposomes as the templates.

It was found that liposomes which are covered with silica are nonporous in nature. Hence, the exact properties of the lipid system are retained. This is important as liposomes are very sensitive to parameters such as pH and ionic strength, and also to the presence of organic solvents in the reaction mixture. Hence this kind of a system can find use in the case of drug delivery mainly because liposomes are biological systems and are also biodegradable.

Synthesis of Liposomes Covered with Silica

Unilamellar liposomes are prepared according the procedure of Bangham (Ref. 15). A suitable amount of L-α-dipalmitoylophosphatdylcholine (which forms the liposome) was dissolved in chloroform. Solvent was removed, a phosphate buffer solution was added and a 10 mg ml^{-1} lipid suspension was made. This contains multi lamellar vesicles. This suspension was then extruded above the transition temperature of

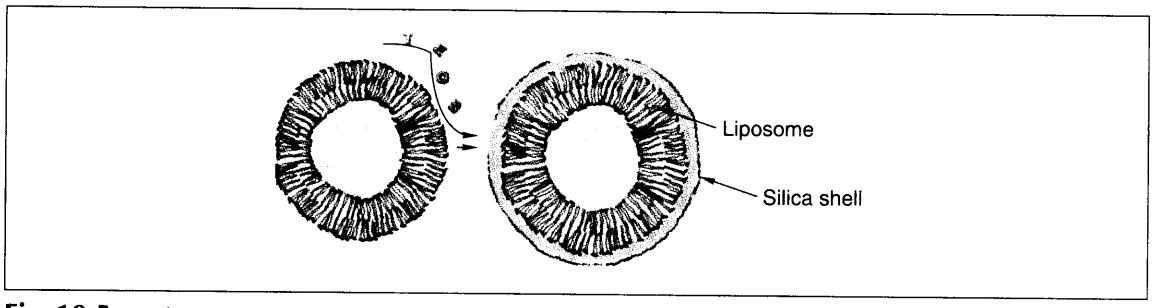

Fig. 10.5: *Schematic of liposome covered with silica. Taken from the Graphical Content of Begu, et al. (Ref. 15). Reproduced by permission of the Royal Society of Chemistry.*

the lipids (41 °C) using an extruder having polycarbonate membranes. The mean size of the vescicles was 108 nm, from quasi-elastic light scattering (QELS) measurements. QELS allows one to study the dynamics of a system in real-time (see chapter 9). The silica shell is grown by adding tetraethylorthosilane (TEOS) to the diluted suspension of liposomes at room temperature with stirring, followed by the addition of NaF (4% molar ratio with respect to TEOS). The reaction mixture was again stirred for 48 h and dried at 40 °C to obtain silica covered liposomes (Ref. 16).

10.3 Properties

10.3.1 Reactions Inside the Silica Nanoshell

Colloidal Alloy Formation Inside Silica Shells

$$AuCl_4^- + 3Ag\ (core) \rightarrow Au\ (core) + 3AgCl\ (core) + Cl^-$$

Reactions like colloidal alloy formation are possible inside the silica shell. It is found that the silver core of the core-shell silica particle can be converted to gold core via oxidation with $AuCl_4^-$. Generally this process is expected to be very fast. But since a shell is present outside and the silver surface is passivated by the precipitated AgCl, the reaction is bound to be slow. The AgCl precipitated in this case is very thin, which is why the shell does not beak or expand. It is found that there is a definite rate dependence on the rate of diffusion of the gold ions through shell, clear from the fact that the reaction is very fast in the case of bare silver particles compared to that of core shell particles.

These processes are taking place because the silica shell is porous in nature and also catalytically active, even though the core is separated by a shell. Thus the shell acts as a selective membrane which controls the rate of the chemical reactions with the metal cores. In some cases, almost complete inhibition of the reactions happens while in some others, the rate is retarded. The rate can be controlled by varying the thickness of the silica shell.

Formation of Carbon Onions Inside Silica Nanoshells

Nanoshells can be formed from $Au@SiO_2$ by leaching gold using carbon tetrachloride. It is found that the amorphous carbon produced in the leaching process gives rise to carbon onions inside the shell.

This is an important reaction since this is the first report of formation of carbon onions at room temperature in a solution. Figure 10.6 shows a high resolution image of silica shell containing a carbon onion. It gives important information regarding the nature of the shell. The silica shell stretches itself so that it can accommodate carbon onions formed inside implying the plastic nature of the shell. The cavity left behind after the removal of gold is smaller than the dimension of the leached out metal implying that catalytic destruction of the halocarbon occurs and more carbon per metal ion is generated (Ref. 17).

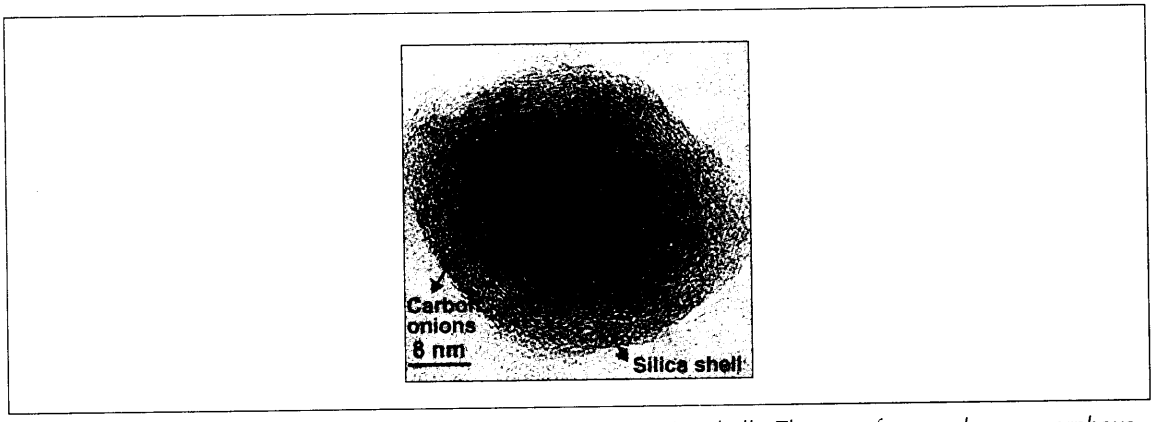

Fig. 10.6: *High resolution TEM images of carbon onion containing shells. The outer few nm shows amorphous contrast and is the silica shell, inside this the typical concentric ring structure of a carbon onion is seen, in this case more than 20 concentric graphitic planes are visible. Reprinted from Rosemary, et al. (Ref. 17), Copyright (2004), with permission from Elsevier.*

10.3.2 Incorporation of Molecules Inside the Nanoshells

One of the main advantages of nanoshells is that they can be used as carriers of molecules. This allows nanoscopic containers to be used for controlling the environment of the molecule. This helps protect the molecule from unwanted chemical reactions and the cavity also provides a rigid environment for adsorbed molecules. Colloidal dispersions of silica shells are optically transparent, providing an opportunity to study the behavior of the molecules incorporated without excessive light scattering problems. Imhof, *et al.* have studied the incorporation of fluorescein isothiocyanate inside silica spheres where the objective was to increase the photostability of the dye molecule (Ref. 18). The results of this study seemed to suggest an inhomogeneous distribution of the molecules inside the shell. Studies have also been carried out on the excited state reactions of the photochemically important molecule, ruthenium tris (bipyridyl) dye inside silica shells, wherein the excited Ru(II) shows a significant enhancement of the phosphorescence yield

and lifetime. Moreover, the dye reacts with molecules such as methylviologen. Bosma, *et al.* (Ref. 19) have synthesized colloidal poly(methyl)methacrylate (PMMA) particles wherein fluorescent dyes are incorporated into the polymer network. In these studies, there has been a significant focus on the photochemistry and spectroscopy of the adsorbed molecules, possibly to the neglect of other interesting properties of the incorporated molecules. Since these molecules are isolated, they may show different properties in contrast to the free ones when confined within a shell.

Since most of these nanoshells are used as containers for molecules, they can also be used for drug delivery as well as for studying the photochemistry of these molecules.

Incorporation of Dye Molecules Inside Silica Nanoshells

Most of such molecules have been incorporated inside silica shells. This is because the formation of silica-covered core-shell particles provides an easy method for the incorporation of these molecules. The formation of a silica shell includes the usage of aminopropylsilane as a precursor for the shell formation. Molecules which have amino or thiocyanato functional groups can also be used along with aminopropylsilane, while the silica shell formation takes place. In order to incorporate any molecule, the first step is to functionalize it (the molecule) to have an amino or thiocyanto group. The next step is to add the functionalized molecule together with aminopropylsilane, do further polymerization using tetramethyl orthosilicate and allow further shell growth in ethanolic medium (Ref. 3).

The subsequent removal of the core can be done by any of the methods discussed above using NaCN, NH_3 or CCl_4.

Fluorescein Isothiocyante@SiO_2

Fluorescein isothiocyante is a very important dye molecule, with applications in the field of protein labeling. But one disadvantage of this dye is that it undergoes photobleaching very fast. Hence, it is important to make this dye inside a shell which can be studied by spectroscopic techniques as well as used for different applications. The disadvantage of this system is that self-quenching occurs in it because of which there is a decrease in the quantum yield of the encapsulated dye. It was found that the incorporation of this dye on the shell surface decreases the porosity of the nanoshell. It takes more time for mineralization using cyanide ion when the shell has the dye.

10.3.3 Modification of Silica Shell for Immunoassays

Binding of immunoreagents to different particles is important from the point of view of many applications like site-specific drug delivery to the targeted portions of the body. The success of targeted drug delivery depends upon two facts: (1) attachment of antibody to the silica surface, and (2) the ability of the antibodies to bind their specific antigen while they are attached to the shell. In the case of the first criterion, the molecule which has a silanol group at one end and an organic group at the other has been found to be useful. In most of the cases, APS is used for this purpose. Since APS doesn't have any functional group to

make covalent bond with the molecules, another molecule, N-5-azido-2-nitrobenzoyloxysuccinimide (ANB-NOS), which can form a strong covalent bond with the antibody, is often used. About 10 per cent of the bound antibodies on the APS and 12 per cent on the ANB-NOS surface were found to be active (Ref. 20).

10.4 Characterization

Nanoshells can be characterized in terms of many spectroscopic techniques, especially transmission electron microscopy, atomic force microscopy, etc.

Transmission Electron Microscopy

Transmission electron microscopy is the main technique used for the characterization of nanoshells as we can see the nano structures. As shown in Fig. 10.7, we can clearly see approximately 15 nm-sized silica nanoshells.

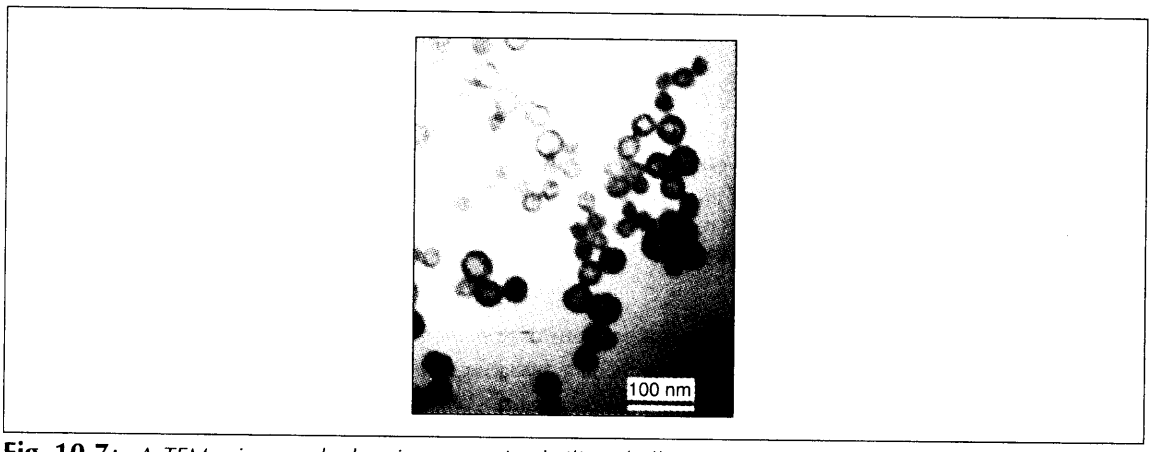

Fig. 10.7: *A TEM micrograph showing nano-sized silica shells with an average inside diameter of ~15 nm containing 195 Cascade Blue dye per particle. Reprinted from Ostafin et al. (Ref. 4), Copyright (2003), with permission from Elsevier.*

Optical Spectroscopy

There are many methods by which one can use optical spectroscopy to characterize nanoshells. In the case of silica nanoshells formed by the leaching of gold or other nanometal core, it is possible to monitor the disappearance of the plasmon peak characteristic of it (Fig. 10.8). In the case of shells incorporated with molecules, it is possible to get the absorption characteristics of that molecule from absorption

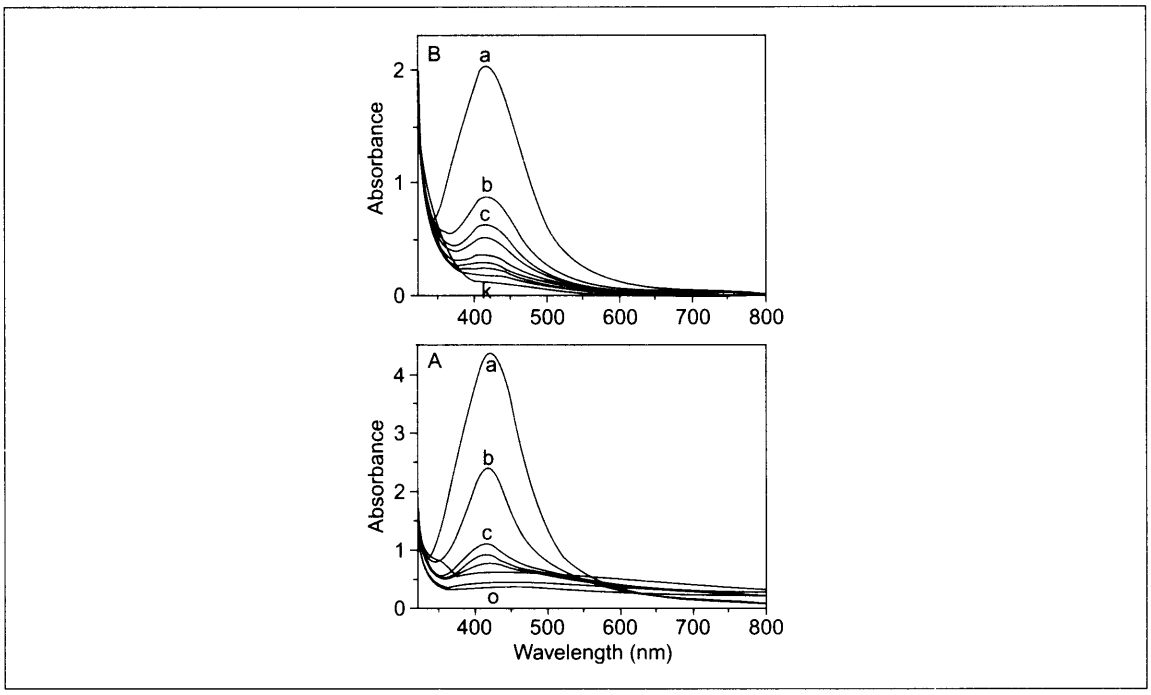

Fig. 10.8: *Time-dependent UV–visible spectra of the reaction of $Ag@ZrO_2$ with (A) CCl_4 and (B) benzyl chloride indicating the selective leaching of the metal core. Trace a corresponds to the parent material. In (A) the traces were recorded after every 30 minutes and in (B) after every 10 minutes (after addition of CCl_4 and benzyl chloride, respectively). From Nair et. al. (Ref. 6). Reproduced by permission of the Royal Society of Chemistry.*

spectroscopy. For metal nanoshells, the formation is monitored principally using the absorption spectroscopy. For the different applications of metal nanoshells, it is possible to tune its surface plasmon resonance by changing the layers of the metal shell.

Fluorescence Spectroscopy

Apart from absorption spectroscopy, fluorescence spectroscopy is also used to characterize nanoshells. Here the emission spectrum of the incorporated molecule can be used for its characterization (Ref. 3).

Cyclic Voltammetry

Cyclic voltammetric studies provide valuable information on the molecules present inside the nanoshell, thus probing the shell indirectly. Apart from the usual characterization, it also provides information regarding the environment of the molecule inside the nanoshell. It is a very useful tool in cases where one is looking at the reactions taking place inside the nanoshell. For example, ciprofloxacin-incorporated silica nanoshell

shows two irreversible cathodic reduction peaks at –0.75 V and –1.18 V (Ref. 18). In the case of pure ciprofloxacin molecules, however, the peak potentials are at –0.81 and –1.25 V, respectively, with a shift of 60 mV towards the cathodic region with respect to ciprofloxacin@SiO_2. This may be due to the presence of the SiO_2 shell outside the ciprofloxacin molecule which retards the electrochemical reduction.

Infrared Spectroscopy

Infrared spectroscopy provides information about the kind of linkages present in nanoshells. In the case of silica nanoshells, the Si-O-Si linkage can be characterized by using stretching modes which appear at 801 and 1100 cm^{-1}. Zirconia shell shows two features at 534 and 725 cm^{-1} which are analogous to the 530 cm^{-1} main feature and 725 cm^{-1} shoulder seen for cubic zirconia (Ref. 6).

10.5 Applications

Ion Selective Films

Strong ion sieving propertied of nanoshell films can be used for applications. Dopamine can be detected electrochemically by carbon fiber electrode, but the major problem in this is the interference from ascorbic acid, which also falls in this electrochemical window. The layer-by-layer assembly of (TiO_2 nanoshells/ poly acrylic acid) acts as an excellent detection tool for dopamine without any interference from ascorbic acid as shown in Fig. 10.9.

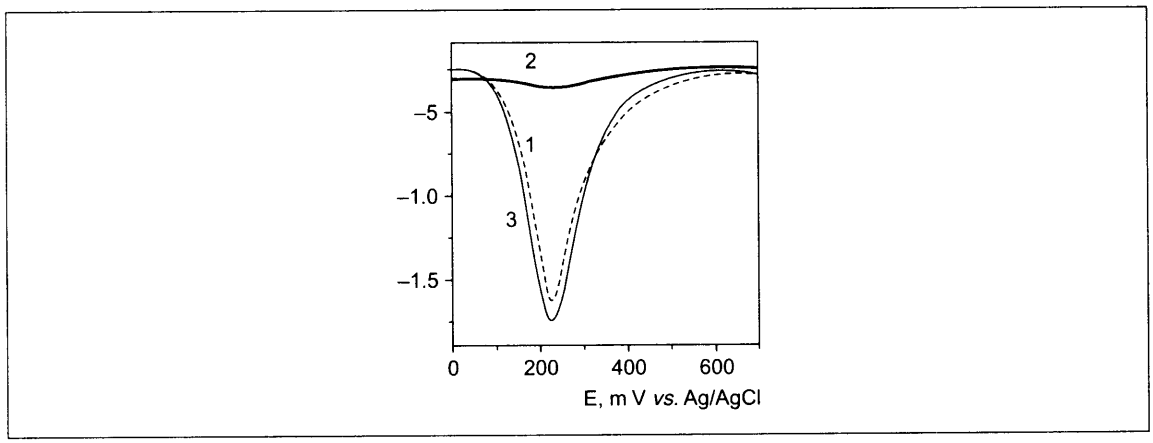

Fig. 10.9: *Electrochemical dopamine sensing using an LbL of TiO_2 nanoshells. Reprinted from Ref. 8. Copyright (2002) Wiley-VCH.*

At pH = 7, the TiO_2 nanoshells are negatively charged and therefore, the diffuse part of the electrical double layer is composed primarily of cations, an ideal condition necessary for the selective detection of

positively charged dopamine over negatively charged ascorbic acid. The ratio between the dopamine and ascorbic acid signals changes from 1:3 for a native glassy carbon electrode surface to 9:1 for a nanoshell modified surface, which gives an overall 27-fold enhancement of the selectivity between these substances. The signal from the mixture of ascorbic acid and dopamine (trace 1 in the figure) is virtually equal to that from 1 mM dopamine (trace 3). The ascorbic acid peak current (trace 2) was negligible under these conditions.

Gold Nanoshells for Blood Immunoassay and Cancer Detection and Therapy

For conventional blood immunoassays, optical tests are performed at visible wavelengths. Since it is necessary to separate out several unwanted biomaterials which absorb visible light, the whole procedure can take long time, of the order of several hours or days. In the immunoassay procedure proposed by Halas and West (Ref. 1), nanoshells are conjugated with antibodies that act as recognition sites for a specific analyte. The analyte causes the formation of dimers (Fig. 10.10), which modify the plasmon-related absorption feature in a known way. A fast absorption measurement can determine the presence of the molecule, avoiding the purification step.

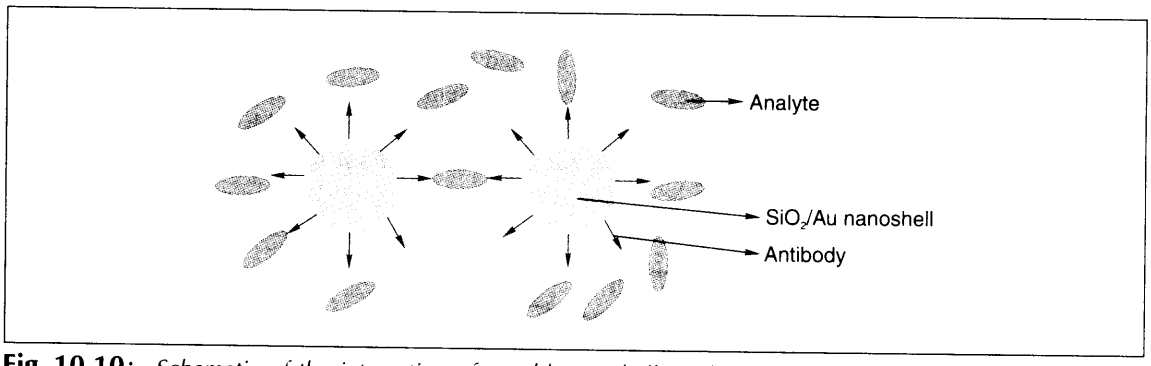

Fig. 10.10: *Schematic of the interaction of a gold nanoshell modified using an antibody with an analyte. Adapted from Ref. 22. Used with permission from the author, Copyright (2003) Nature Publishing Group.*

Since these nanoshells have a large optical scattering cross section, they can be used as potential contrasting agents for photonics-based imaging modalities. Among the methods, reflectance confocal microscopy (RCM) and optical coherence tomography (OCT), which facilitate early cancer detection are important. Optical properties of the nanoshells can be tuned in such a way that they can be used for both imaging and therapy. The colloidal regime allows controlling both scattering and absorption properties simultaneously by changing size. Selective accumulation of the nanoshell can be used to image the tumor by using the high permeability and retention properties of the cancer cells.

Figure 10.11 (Plate 6) shows SKBr3 breast cancer cells imaged by using targeted HER2 nanoshells (Ref. 10). HER2 is an acronym and refers to human epidermal growth factor receptor, a protein. HER2 receptors are over-expressed in the case of a cancer cell. Among the three figures in the first row, the one

with nanoshells shows a better image. After the therapy, it is also found that the cells treated with nanoshells are dead. This effect was not observed in the case of non-cancer cells. This is also found to have applications in the case of silver staining also were better imaging was possible. The cytotoxicity of the nanoshells was checked by treating cancer cells with the nanoshells and taking the image without NIR radiation. It was found that there was no death of cells due to the nanoshells alone.

Even though these kinds of gold nanoshells are found to have applications in many biological fields, no one really knows what will happen to the material itself after treatment with the tumor cells. The fact that these are non-biodegradable and also catalytically active which may create problems for the biological systems.

Gold Nanoshells for Enhancing the Raman Scattering

Raman scattering is a phenomenon which is used to study different surfaces. But this technique has a very weak sensitivity. However, roughened surfaces can be used for enhancing the Raman signal (Ref. 23). Interactions of light with individual nanoshells allowed a 10 billion-fold increase in the Raman effect.

Review Questions

1. What are nanoshells?
2. What are the principal kinds of nanoshells? How to make them?
3. What makes gold nanoshells attractive in biology? What are their applications?
4. What are the major breakthroughs in this area which make the application of nanoshells promising?
5. What are the essential features of nanoshells useful in biology?
6. How would one investigate the porosity of the shells?
7. Why nanoshells are made over dielectric materials and not over metallic particles?

References

1. Hirsch, L.R., J.B. Jackson, A. Lee, N.J. Halas, J.L. West, *Anal. Chem.*, **75** (2003), p. 2377.
2. Graf, C., A.V. Blaaderen, *Langmuir*, **18** (2002), p. 524.
3. Makarova, O.V., A.E. Ostafin, H. Miyoshi, J.R. Jr. Norris, D. Meisel, *J. Phys. Chem. B*, **103** (1999), p. 9080.
4. Ostafin, E., M. Siegel, Q. Wang, H. Mizukami, *Micropor. Mesopor. Mater*, **57** (2003), p. 47.
5. Stöber, W., A. Fink, E. Bohn, *J. Colloid Interface Sci.*, **20** (1968), p. 62.

6. Nair, A.S., R.T. Tom, V. Suryanarayanan, T. Pradeep, *J. Mat. Chem.*, **13** (2003), p. 297.
7. Eswaranand, V., T. Pradeep, *J. Mat. Chem.*, **12** (2002), p. 2421.
8. Koktysh, D.S., X. Liang, B. Yun, I.P. Santos, R.L. Matts, M. Giersig, C.S. Rodriguez, L.M.L. Marzan, N.A. Kotov, *Adv. Funct. Mater.*, **12** (2002), p. 255.
9. Sun, Y., Y. Xia, *Anal. Chem.*, **74** (2002), p. 5297.
10. Christopher, L., L. Amanda, N. Halas, J. West, R. Drezek, *Nano. Lett.*, **5** (2005), 709.
11. Duff, D.G., A. Baiker, *Langmuir*, **9** (1993), p. 2301.
12. Hao, E., S. Li, R.C. Bailey, S. Zou, G.C. Schatz, J.T. Hupp, *J. Phys. Chem. B*, **108** (2004), 1224.
13. Xia, H.L., F.Q. Tang, *J. Phys. Chem. B*, **107** (2003), p. 9175.
14. Jiang, Z.J., C. Liu, *J. Phys. Chem. B*, **107** (2003), p. 12411.
15. Bangham, A.D., *J. Mol. Biol.*, **13** (1965), p. 238.
16. Begu, S., S. Girod, D.A. Lerner, N. Jardiller, C.T. Peteilh, J.M. Devoisselle, *J. Mater. Chem.*, **14** (2004), 1316.
17. Rosemary, M.J., I. MacLaren, T. Pradeep, *Carbon*, **42** (2004), p. 2352.
18. Imhof, J.A., M. Megens, J.J. Engelberts, D.T.N.D. Lang, R. Sprik, W.L. Vos, *J. Phys. Chem. B*, **103** (1999), p. 1408.
19. Bosma, G., C. Pathmamanoharan, E.H.A. de Hoog, W.K. Kegel, A.V. Blaaderen, H.N.W. Lekkerkerker, *J. Colloid Interface Sci.*, **245** (2002), p. 292.
20. Wong, C., J.P. Burgess, A.E. Ostafin, *Journal of Young Investigators*, issue 1, volume 6, (2002).
21. Rosemary, M.J., V. Suryanarayanan, P.G. Reddy, I. MacLaren, S. Baskaran, and T. Pradeep, *Proc. Indian Acad. Sci.*, **115** (2003), p. 703.
22. Brongersma, M.l., *Nature Materials*, **2** (2003), p. 296.
23. Jackson, J.B., S.L. Westcott, L.R. Hirsch, J.L. West, N.J. Halas, *Appl. Phys. Lett.*, **82** (2003), p. 257.

Additional Reading

1. Nalwa, H.S. (ed.) (2002), *Nanostructured Materials and Nanotechnology*, Academic Press, New York, 2002.
2. New, R.R.C. (ed.) (1990), *Liposomes: A Practical Approach*, Oxford University Press, Cambridge, 1990.

PART

FOUR

Evolving Interfaces of Nano

Contents:

- Nanobiology
- Nanosensors
- Nanomedicines
- Molecular Nanomachines
- Nanotribology

Chapter 11

NANOBIOLOGY

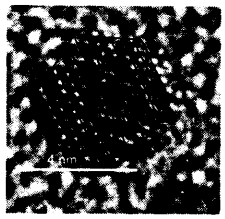

Biological functions take place in nanometer-sized objects. Therefore inorganic nanoparticles can be integrated into biological molecules such that one can understand, control and manipulate biological processes. This has been made possible now through the utilization of several properties of nanosystems, many of which have been discussed in earlier chapters. Here the objective is to appreciate the science of bio-nano hybrid systems with selected examples.

Learning Objectives

- What is nanobiology?
- How can one use nanomaterials for biological applications? What are the examples?
- What are the applications of nanomaterials in biology?
- What are the promising areas for the immediate application of nanomaterials in biology?
- What are the outstanding issues in nanobiology?

11.1 Introduction

With the evolution of science, all scientific phenomena have been investigated in progressively microscopic dimensions. Thus we see that science has progressed from big to small. Optical microscopy helped the scientist to look at phenomena in the regime of the micrometer. Later on, the invention of electron microscope helped the scientist to examine phenomena in the regime of nanometer. Due to the electronic confinement of nano objects, their chemical and optical properties are different from those of larger objects. As we look at life forms in smaller and smaller dimensions, we end up with biological objects which are involved in fundamental life processes. The key molecules in biology such as DNA, enzymes, receptors, antigens, antibodies and oxygen carriers can be included in the dimension of nanometers. Thus it is clear that all fundamental processes in biology are taking place in the dimension of 1–100 nm. Molecular self-organization around nanoparticles, utilizing the tools of surface science, can be of use in the development of probes for understanding fundamental life processes. The synergy of surface science and molecular biology has given birth to a new subject called 'nanobiology', which symbolizes a path-breaking

evolution in the progress of biology. This new subject is capable of unveiling many fundamental secrets of life forms.

The science of nanobiology has progressed significantly and can be branched into several disciplines of life science such as cellular biology, genomics, proteomics, oncology, immunology, diagnosis, targeted drug delivery, etc. The idea of creating the hybrid systems of inorganic nanoparticles with biological moieties has helped solve several technical difficulties in medical and biosciences. Using nanomaterials, instead of conventional materials, in life science applications has increased efficiency while decreasing cost. Thus the hybridization of nano-bio-technologies has laid the ground for many novel methodologies, which are capable of solving several technical difficulties in bio-analysis. The ideas and innovations of nanobiology can be extended to the frontiers of biotechnology. In this chapter we discuss the following four major aspects of nanobiology:

1. Interaction between biomolecules and nanoparticle surfaces
2. Biological imaging using nanoparticles
3. Analytical applications of nanobiology
4. Medical diagnosis and targeted drug delivery
5. Biosynthesis of nanomaterials

11.2 Interaction Between Biomolecules and Nanoparticle Surfaces

One of the objectives of nanotechnology is the packing of nanoparticles in ordered arrays with the ability to tailor the size and inter-particle distance. While the assembly of nanoparticles from solution into hexagonally close-packed monolayers and superlattice structures on solid surfaces has been fairly successful (see Chapter 8), the controlled assembly of nanoparticles in solution had hitherto remained a relatively unexplored area. The construction of three-dimensional arrays of nanoparticles in the aqueous phase can be achieved by bioconjugation, the phenomenon in which intermolecular interactions lead to assembly. The interaction of nanoparticles functionalized with conjugate biomolecules, can lead to the formation of desired superstructures in the aqueous phase. The first steps in this direction leading to the construction hybrid bio-nano assemblies, were taken by the groups of Mirkin (Ref. 1) and Alivisatos (Ref. 2), who demonstrated that DNA-modified nanoparticles could be assembled into superstructures by the hybridization of complementary base sequences of the surface-bound DNA molecules. From a fundamental point of view, Mirkin, *et al.* have used this strategy to critically study the role of inter-particle separation (Ref. 1) and aggregate size on the optical properties of DNA-modified colloidal gold solution. Other interactions such as the biotin-avidin molecular recognition process, hydrogen bonding between suitable terminal functional groups bound to the nanoparticle surface, electrostatic assembly on DNA templates, and control over electrostatic interactions stabilizing nanoparticles in the aqueous phase have been used to construct the nanoparticle assembly in solution (Ref. 3). Sastry, *et al.* (Ref. 4) described the surface modification of aqueous silver colloidal particles with the amino acid, cysteine and the cross-linking of the colloidal particles in solution. Capping of the silver particles with cysteine was accomplished by a

thiolate bond between the amino acid and the nanoparticle surface. The silver colloidal particles were stabilized electrostatically by ionizing the carboxylic acid groups of cysteine. The amino acid, cysteine (H_2N–$CH(CH_2SH)$–CO_2H) plays an important role in defining the tertiary structure of proteins through disulfide (cystine) bridges (Ref. 5).

11.2.1 Influence of Electrostatic Interactions in the Binding of Proteins with Nanoparticles

It has been suggested that each gold nanoparticle has an Au(0) core and an Au(I) surface, as a result of the preferential adsorption of Au(I) ion on the surface at the time of formation of the nanoparticle. Citrate ions co-ordinate to the Au(I) atoms on the surface, resulting in an overall negative charge for each particle. Nanoparticles are capable of binding with oppositely charged species in aqueous solutions through electrostatic interactions based on the ionic characteristics of their surfaces (Ref. 6). Amphiprotic species, such as peptides and proteins, have unique isoelectric points (p*I*). When the pH of a protein sample solution is below the value of the p*I* of the protein, the protein molecules have a net positive charge. This means that by increasing the pH from 0 to 14, the molecule will get more and more negatively charged by the consequent removal of protons. At a particular pH, the molecule will have a net charge zero. This point is called the isoelectric point (p*I*). Therefore, below the p*I* value, the molecule is positively charged. Negatively charged gold nanoparticles tend to attract positively charged protein molecules to their surfaces through electrostatic interactions. On the other hand, if the pH of a protein solution is above the value of the p*I* of this protein, the protein molecules are negatively charged and repel any negatively charged gold nanoparticles. With regard to the nature of interaction of the biomolecule and nanoparticle, it is clear that they are interacting through electrostatic attraction. Thus by considering the attraction between two opposite charges,

$$\text{Electrostatic force, } F = (kq_+q_-/r)$$

F is the force in Newton and $k = 8.9874 \times 10^9\ \text{Nm}^2\text{C}^{-2}$, r is the distance in meter (m), q_+ and q_- are the positive and negative charges in coulomb (C), respectively. For simplicity we can consider, r and q_- (the charge on the nanoparticle surface) are constant. Thus the electrostatic force between the biomolecule and nanoparticle,

$$F \alpha q_+$$

i.e. the electrostatic force is proportional to the net charge on the biomolecule (q_+).

From the above equation, it is clear that the p*I* is the key factor in the binding of the biomolecule on the nanoparticle. Above the p*I* value, there is no attraction between the biomolecule and the nanoparticle because the biomolecule becomes negatively charged. The selective binding of proteins on the nanoparticle surface as a function of the pH is illustrated by matrix-assisted laser desorption ionization mass spectrometry (MALDI-TOF MS). The p*I* values of the proteins, cytochrome *c* and myoglobin are 10.6 and 7, respectively (Ref. 7).

The absence of the adsorption of proteins, cytochrome *c* and myoglobin on the gold nanoparticle surface above their p*I* value is reported by Teng, *et al.* (Ref. 8). In Fig. 11.1, aqueous solutions of cytochrome

c and myoglobin have been employed to demonstrate this. From a solution at pH 6, both cytochrome *c* and myoglobin were detected in MALDI-TOF MS analysis (Fig. 11.1(a)). At pH 8, only cytochrome *c* was detected in the MALDI-TOF mass spectrum (Fig. 11.1(b)), and signals for neither analyte are observed in the MALDI-TOF mass spectrum at a pH 12 (Fig. 11.1(c)) (Ref. 8). These results demonstrate that isoelectric points play an important role in the binding of nanoparticles with proteins. Thus, gold nanoparticles can be used to bind specific proteins selectively by adjusting the pH of their sample solutions.

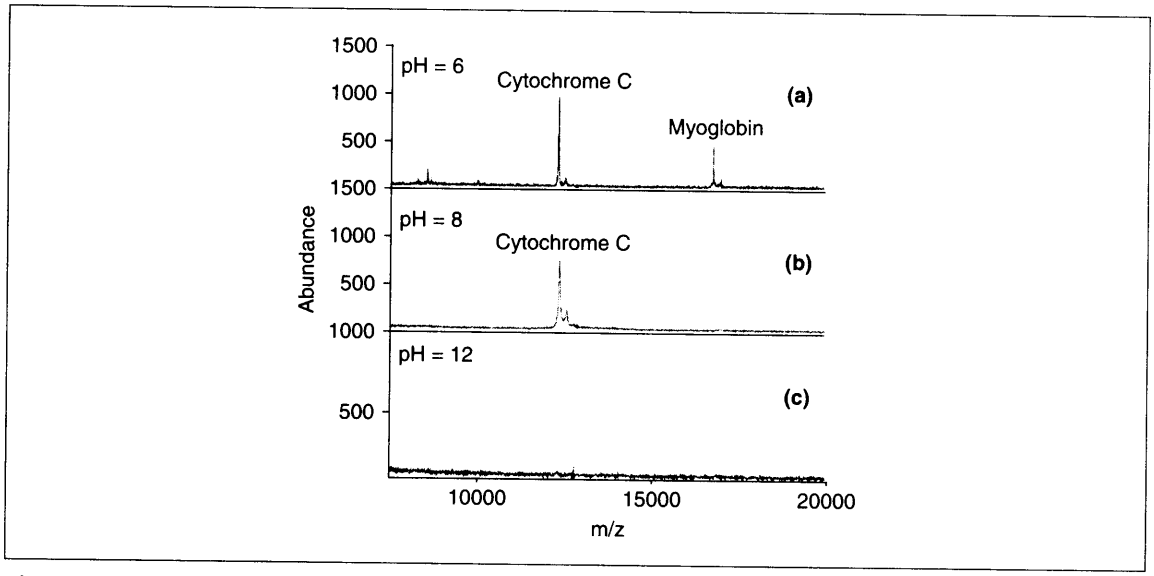

Fig. 11.1: *MALDI-TOF mass spectra obtained from a mixture of cytochrome c and myoglobin at: (a) pH 6, (b) pH 8 and (c) pH 12. Reprinted with permission from Teng, et al. (Ref. 8). Copyright (2004) American Chemical Society.*

11.2.2 The Electronic Effects of Biomolecule-Nanoparticle Interaction

When a biomolecule has interacted with the surface of a noble metal nanoparticle, its surface charge density is deformed by the electrostatic attraction. The extent of deformation of surface charge density depends on the following factors:

1. The size of the noble metal nanoparticle
2. Molecular diameter of the biomolecule
3. pH of the medium
4. Ionic strength of the medium

As a result of the interaction, the surface charge density of both the nanoparticle and the biomolecule get perturbed. This perturbation of the surface electron density is manifested in the change in the electronic

spectrum of both the nanoparticle and the biomolecule. The functional groups of the molecules which are close to the vicinity of the nanoparticle surface get perturbed more. The binding of the biomolecule can affect the surface plasmon resonance of the nanoparticle. Sometimes, this interaction can be manifested in the assemblies of nanoparticles and biomolecules. The surface electron density of the nanoparticle is spherically symmetric. The perturbation to charge density of the nanoparticle induced by the interaction with the biomolecule is isotropic. But in the case of noble metal nanorods, their charge density is anisotropic. Thus the interaction with the biomolecule can lead to anisotropic perturbation of electron density of the nanorods. The difference in the interaction of the biomolecule to the nanorod and nanoparticle is manifested in the UV-vis spectrum. The surface plasmon resonance (SPR) of noble metal nanoparticles is due to polarized oscillation of the electron cloud, induced by the electric vector of the electromagnetic wave according to Mie's theory. This phenomenon is highly sensitive to the dielectric constant of the micro-environment around the nanoparticle. Thus, such an interaction with a biomolecule can be manifested in the form of alterations in the SPR band. The molecular diameter of a biomolecule is a key factor which decides the biomolecule–nanoparticle interaction. Bigger molecules will form stable nano-bio conjugates. They will form thicker shells above the surface of the nanoparticle. Such shell formation can prevent the aggregation of nanoparticles. As an example we can consider the interaction between an antibiotic vancomycin and gold nanoparticle (Ref. 9).

The changes in the SPR band of the nanoparticle and the dimension of the interacting molecule are directly related. In Fig. 11.2, the dashed line represents the free nanoparticle. After the capping of vancomycin, the SPR band is broadened and shifted slightly from 520 to 528 nm. This indicates a change in the dielectric constant of the micro-environment around the gold nano-core. The formation of aggregated structures can be observed from the SPR features of Au@cysteine, including the shifting of the SPR band

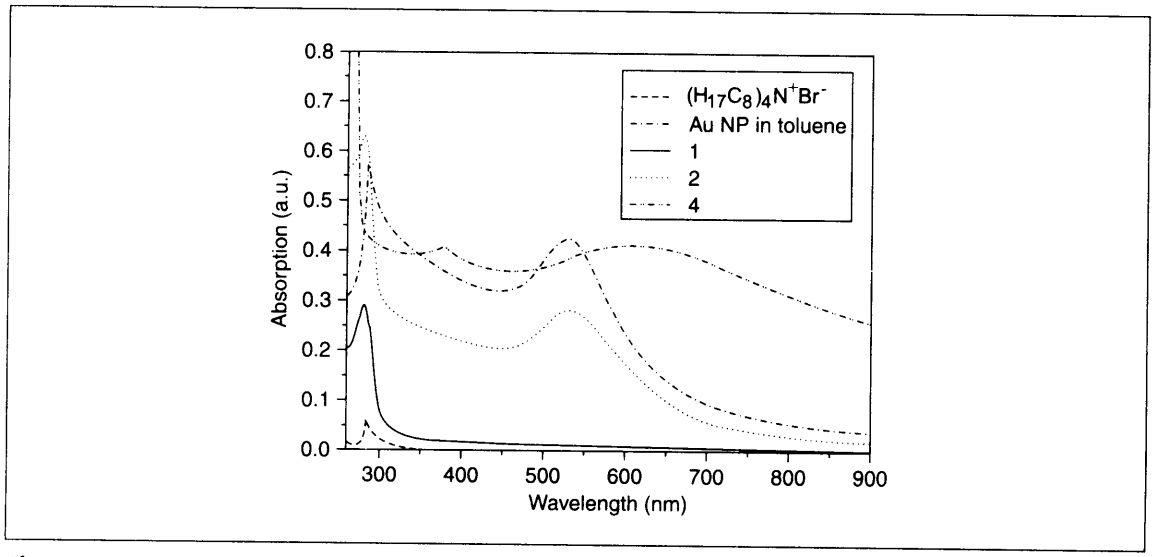

Fig. 11.2: *UV-vis spectrum of: (1) vancomycin, (2) Au@vancomycin and (4) Au@cysteine. Reprinted with permission from Gu, et al. (Ref. 9). Copyright (2003) American Chemical Society.*

to 631 nm as well as the increase in background intensity. A similar kind of an aggregation is reported for cystiene-capped silver nanoparticles (Ag@Cysteine) by Sastry, *et al.* (Ref. 4). The bare nanoparticles (AuNP) stabilized with tetra N-octyl ammonium bromide show the SPR band at 520 nm. After the vancomycin capping of the nanoparticle surface, the SPR feature has no significant shift. This indicates that due to the bigger molecular diameter of vancomycin, the nanoparticle aggregation is absent.

The TEM image Fig. 11.3(a), (b) clearly illustrates the difference between the interaction of a bigger and smaller biomolecule with the nanoparticle. In the TEM image, Au@cysteine shows the aggregated structure, while the Au@vancomycin shows well-separated particles. This indicates that there is a thicker shell of vancomycin around the gold core, which prevents the aggregation of the nanoparticle. As mentioned earlier, similar kinds of observations are reported in the case of cytochrome *c* capped nanoparticles also (Ref. 10). The absence of nanoparticle aggregation is due to electrostatic repulsion between the thicker cytochrome *c* shells of the neighboring nanoparticles. Also, the formation of aggregates or scaffolds in the bio-nano hybrid system, may bring two nanoparticles closer. So their electron clouds get perturbed. This kind of perturbation can be manifested in the form of a coupling between the SPR bands. In the case gold nanoparticle–biomolecule hybrid systems, this inter-plasmon coupling is isotropic. But in the case of gold nanorod–biomolecule hybrid systems, this inter-plasmon coupling is anisotropic. These kinds of electronic interactions are manifested in the form of a color change in both gold nanoparticles and nanorods after binding with biomolecules. This observation can be used for developing cheaper and efficient technologies for medical diagnosis, proteomics, genomics and biotechnology. In 2005, Thomas, *et al.* (Ref. 11) reported the inter-plasmon coupling of cystiene and glutathione-capped Au nanorods. Gold nanorods possess two plasmon absorption bands. In the case of both cysteine and glutathione, a dramatic decrease in the intensity of the longitudinal surface plasmon absorption band, with a concomitant formation of a new band was observed (Fig. 11.4(a), (b)). The appearance of a new red shifted band at 850 nm in the presence of cysteine/glutathione results from the coupling of the plasmon absorption of Au nanorods assisted through self-assembly. The longitudinal alignment of nanorods after the binding of cysteine and glutathione has resulted in the anisotropic coupling of the SPR band.

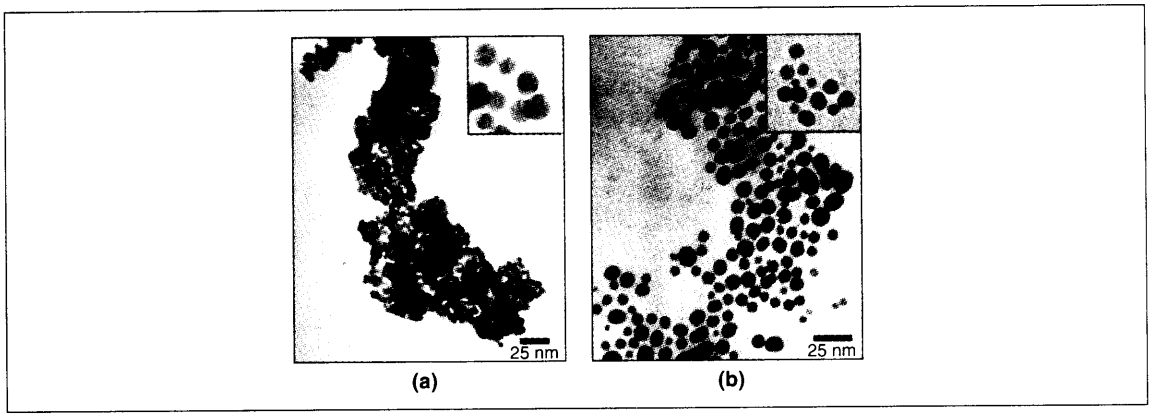

Fig. 11.3: *TEM image of cysteine (a) and vancomycin (b) capped gold nanoparticles, in the aggregated state after cryodrying at concentrations of 6.7 and 50 μg/mL. Reprinted with permission from Gu, et al. (Ref. 9). Copyright (2003) American Chemical Society.*

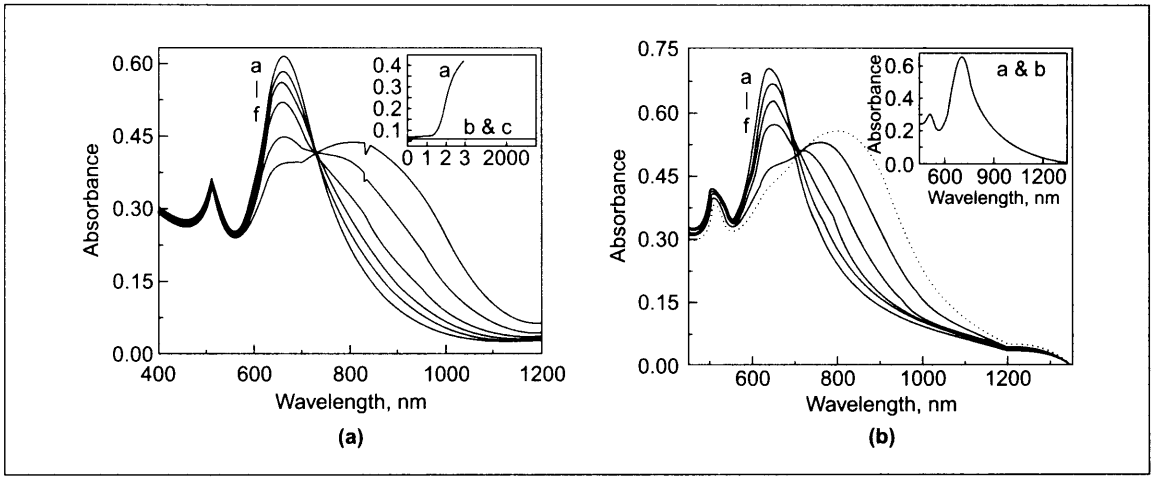

Fig. 11.4: *(A, B) Absorption spectral changes of Au nanorods (0.12 nM) in acetonitrile/water (4:1) on addition of (A) cysteine at: (a) 0 (b) 1.75 (c) 2.0 (d) 2.25 (e) 2.5, and (f) 3 μM, or (B) glutathione at: (a) 0, (b) 7, (c) 9, (d) 11, (e) 13, and (f) 14 μM. Figure 11.3(a) (inset): Changes in optical density at different concentrations of: (a) cysteine, (b) tyrosine, and (c) leucine. Figure 11.3(b) (inset): Effect of addition of 1-hexylmercaptan at (a) 0, and (b) 10 μM. Reprinted with permission from Thomas, et al. (Ref. 11). Copyright (2005) American Chemical Society.*

11.3 Different Types of Inorganic Materials Used for the Synthesis of Hybrid Nano-bio Assemblies

11.3.1 Noble Metal Materials

Normally nano materials made of silver and gold are used for biological applications. There are various types of noble metal nanomaterials such as noble metal nanoparticles, nanorods, metal nanoshells, nanocages, etc. Nanoshells (Chapter 10) constitute a novel class of optically tunable nanoparticles that consist of a dielectric core surrounded by a thin gold shell. Antibodies can be immobilized to the gold surface of nanoshells (Ref. 12). The gold surfaces of nanoshells are considered to be biocompatible and polymers such as polyethylene glycol (PEG) may be attached to nanoshell surfaces to further enhance biocompatibility and improve circulation in the bloodstream (Ref. 13). Silver (Ref. 14) and gold (Ref. 15) nanoparticles are used as intracellular SERS (surface-enhanced Raman scattering) probes. The advantages of noble metal nanoparticles are that they offer and/or function as:

1. Ideal immuno labels for transmission electron microscopy
2. Efficient contrast agents for optical microscopy

3. Powerful surface-enhanced Raman scattering (SERS) probes
4. Inert to physiological conditions
5. Most biocompatible nanomaterials
6. Ideal systems for immobilizing biomolecules.

11.3.2 Semiconductor Nanocrystals (Quantum Dots)

Quantum dots are small (<10 nm) inorganic nanocrystals that possess unique luminescent properties; their fluorescence emission is stable and can be tuned by varying the particle size or composition. Quantum dots are generally composed of atoms from groups IIB–VI or III–V of the periodic table and are defined as particles with physical dimensions smaller than the exciton Bohr radius (Ref. 16). This size leads to a quantum confinement effect, which endows nanocrystals with unique optical and electronic properties. Semiconductor nanocrystals can be capped with inert oxides or sulphides and can be attached to a biomolecule with a specific function. The salient features of semiconductor nanocrystals are as follows:

1. Size-tunable emission (from the UV to the IR) of quantum dots
2. Narrow spectral line widths
3. High luminescence
4. Continuous absorption profiles
5. Stability against photobleaching
6. Ideal immuno-labels for *in vitro* and *in vivo* fluorescent imaging

11.3.3 Magnetic Nanoparticles

The phenomenon of magnetism has received significant attention in life sciences and medical sciences. Intracellular ferrimagnetic nanocrystals of greigite (Fe_3S_4) magnetite (Fe_3O_4) have been found in magnetotactic bacteria (Ref. 17). These ferrimagnetic nanocrystals are aligned in a linear fashion in the intracellular part called 'magnetosome', which helps the bacteria in its alignment and motion parallel to the geomagnetic field. A variety of remarkable applications in biology such as in the field of biosensors, magnetic resonance imaging, drug delivery and magnetic fluid hyperthermia can be attained by the synergy of magnetic nanocrystals and biomolecules. Magnetic nanocrystals are size-compatible, competent enough to inter-relate with biological entities, detectable in an applied magnetic field and capable of conveying energy from an alternating magnetic field. Magnetic nanomaterials have a variety of applications in the following spheres:

1. Proteomics
2. Molecular cell biology
3. Medical science

4. Analytical biochemistry
5. Clinical diagnostics
6. Microbiology
7. Immunology
8. Biotechnology
9. Targeted drug delivery

11.4 Applications of Nano in Biology

Accurate and sensitive detection of water-soluble analytes such as toxins, carbohydrates, ionic species, and various biomolecules including DNA, proteins and peptides is a highly sought after scientific goal with implications in healthcare and industrial applications (Ref. 18). The interaction of a target molecule with a protein receptor in a biological recognition process is often associated with a change in the protein conformation as a response to the binding event. Many scientists are focusing on the design and development of recognition-based sensing assemblies that can account for such changes via signal transduction in a medium of interest (Ref. 19). The above drive leads us to the key issue concerning the fabrication of nano-bio hybrid systems. First, we have to think about inorganic nanoparticles in aqueous medium. These nanoparticles have either a positive or a negative charge on their surface depending on the synthetic methodology adopted for their preparation. A majority of biomolecules have electrostatic charge due to the presence of acidic and basic functional groups. Thus electrostatic self-assembly of biomolecules around the nanoparticle can be used to fabricate nano-bio hybrid systems. Another protocol used for the fabrication of assemblies is the immobilization of biomolecules above the surface of inorganic nanoparticles by using covalent bonding with the aid of an anchor molecule, see Scheme 11.1 (Plate 7). Both the methodologies can be used according to the requirement of the desired application. The tactics used in the construction of nanoprobes for a specific purpose can be adopted from the logic of bio-conjugation. This means that we are utilizing the principle of molecular interactions in the construction of nanoprobes. Immobilization of the molecular conjugate of the target molecule on the nanoparticle surface is the most efficient protocol. For example, antibody–nanoparticle hybrid systems can be used for the detection of antigens and vice versa. Such nanoprobes are now available in the market. The kind of nanoprobes used for optical microscopy depends on the nature of the technique. For instance, semiconductor quantum dots are used for confocal fluorescence microscopy of biological samples while noble metal nanoparticles are used for transmission electron microscopy of biological samples. Among the metal nanoparticles, gold nanoparticles are widely used due to their unique properties such as strong optical absorption, chemical inertness and ease of surface functionalization.

Inorganic nanoparticles such as noble metal nanoparticles, magnetic metal oxide nanoparticles and semiconductor nanocrystals are used for bio-conjugation. They are further utilized in different analytical applications. In normal protocols, an antibody of biologically important molecule is immobilized on the surface of the nanoparticle which, in turn, is used for applications such as molecular detection, targeted

drug delivery and biological imaging. Sensing studies utilizing Fluorescence Resonance Energy Transfer (FRET) between a fluorescent donor molecule bound to the target and an acceptor attached to a receptor protein, have been widely used to study receptor–ligand interactions and changes in protein conformation upon binding to a target analyte. It has also been used to study changes in the solution conditions (e.g., temperature, pH conditions, etc.). FRET is extremely sensitive to the separation distance between the donor and acceptor, and is ideal for probing such biological phenomena. For example, Clapp, *et al.* (Ref. 20) used luminescent CdSe–ZnS core-shell quantum dots (QDs) as energy donors in FRET assays. The interface of biological systems and inorganic nanomaterials has recently attracted widespread interest in biology and medicine. Nanoparticles are believed to have potential as novel intravascular probes for both diagnostic (e.g., imaging) and therapeutic purposes (e.g., drug delivery) (Ref. 21).

11.4.1 Biological Imaging Using Semiconductor Nanocrystals

In vivo targeting by using semiconductor quantum dots has proved to be highly feasible, as found out by Akerman, *et al.* (Ref. 22). It was found that ZnS-capped CdSe quantum dots coated with a lung-targeting peptide accumulate in the lungs of mice after injection, whereas two other peptides specifically direct quantum dots to blood vessels or lymphatic vessels in tumors. It was also seen that on adding polyethylene glycol to the quantum dot, coating prevents the non-selective accumulation of quantum dots in reticuloendothelial tissues. These results encourage the construction of more complex nanostructures with capabilities such as disease sensing and drug delivery. ZnS-capped CdSe quantum dots emitting in the green and the red (550 nm and 625 nm fluorescence maxima, respectively) were coated with peptides by using a thiol-exchange reaction. These peptide-coated quantum dots were injected into the tail vein of a mouse and allowed to circulate for a given time. Then it was frozen, sectioned and examined under an inverted fluorescent microscope or confocal microscope. The use of peptides to target drug carrying nanostructures such as those composed of dendrimers or stabilized drug nanocrystals is also possible (Ref. 22).

11.4.2 Immuno Fluorescent Biomarker Imaging

A critical requirement in molecular cell biology is the localization of specific biomolecules in cells and tissues. Immuno-fluorescent labeling is the standard approach, but fluorescence-based imaging is limited in spatial resolution by the wavelength of light. Hence, the application of transmission electron microscopy (TEM) in conjunction with immuno-labeling has proved to be advantageous for high-resolution structural studies (Ref. 23). The prevalent strategy for immuno-localization via TEM is to employ antibodies conjugated with colloidal gold of various dimensions (Ref. 24). The recent development of luminescent semiconductor nanocrystals, also termed as quantum dots (QDs), for immuno detection raises the possibility of their use as probes (Ref. 25). For instance, we can consider target selective staining by using CdSe@ZnS@PEG core shell quantum dots (see Chapter 9 for a discussion on core-shell nanoparticles). This quantum dot is red emitting and its solubility can be increased by capping it with PEG (polyethylene glycol). We can

denote these quantum dots as QD-PEG and QD-PSMA for the one without and with antibody anchoring, respectively.

Target-specific fluorescent imaging is shown in Fig. 11.5 (Plate 7). The methodology adopted in fluorescent imaging is the same as that explained in Scheme 11.1 (Plate 7). The anchor molecule used here is an antibody of prostrate selective membrane antigen (PSMA-Ab) (Ref. 26). The target molecule is antigen present in the cell membrane. This antigen is present only on the cell membrane of a prostrate cancer cell (C4-2). The mechanism of target-specific fluorescent cellular imaging entails bio-conjugate formation by the hybridization of the antibody on the nanoparticle surface with the antigen present of the cell wall of the cancer cell. Fluorescent staining happens only in the case of (a). This is due to the presence of the antigen containing cancer cells (C4-2) and antibody-capped nanoparticles (QD-PSMA). In the case of (b), the quantum dots are unable to attach on the cancer cell wall surface because they are not anchored with the antibody. In case (c), the quantum dots are unable to attach on the cell wall surface even though they are anchored with the antibody because of the absence of the target antigen on the cell wall of non-cancerous PC-3 cells. The above-mentioned cases illustrate the target specificity of immuno-fluorescent imaging and unveil the potential of semiconductor nanocrystal-based labels for medical diagnosis. The next example illustrates the imaging of the nucleus of a cell by using fluorescence microscopy and transmission electron microscopy. The nuclear promyelocytic leukemia (PML) protein was chosen as the target biomolecule (Ref. 27). The localization of PML protein in discrete sub-nuclear bodies has been well characterized with both fluorescence and electron microscopy. The inorganic nanoparticles used for fluorescence microscopy and transmission electron microscopy are antibody-anchored CdSe 10–15 nm nanocrystals and Au 10 nm nanoparticles, respectively.

Figure 11.6 (Plate 8) clearly explains the potential of inorganic nanoparticles for target selective imaging of intracellular parts. From this figure it is clear that both fluorescence and transmission electron microscopies are used for imaging the neucleus of the HEp-2 PML I cells. The mechanism of the imaging is the same as showed in Scheme 11.1. It also illustrates the potential of immuno-targeted gold nanoparticles (immunogold) for high resolution target selective imaging of intracellular parts with the aid of transmission electron microscopy. The schematic representation of target-selective binding of immunogold labels on cancerous cells is shown in Scheme 11.2 (Plate 8).

11.4.3 Immunogold Labeling

The term 'immunogold' indicates an immuno-targeted gold nanoparticle, which is functionalized with an antibody of a specific biomolecule of interest. In this protocol, gold nanoparticles are used as labels for imaging cell lines and tissues. Immunoglobulin G-capped gold nanaoparticles are used to image pathogenic organisms like *Staphylococcus aureus*, *Staphylococcus pyrogenes* and *Staphylococcus saprophyticus*. Ig G can bind specifically to the pathogens created by the bacteria (Ref. 27). Thus Ig G-capped gold nanoparticles are used to label the bacteria specifically.

Figure 11.7 illustrates a TEM image of the selective interaction of Immunoglobulin G-capped gold nanoparticles to the bacterium, *Staphylococcus saprophyticus*. From Fig. 11.7, it is shown that targeted gold nanoparticles can be used for the immuno-targeted imaging of bacteria. Figure 11.7(a) represents the

selective binding of Ig G-capped gold nanoparticles. There is no labeling when citrate capped (Fig. 11.7(b)) and BSA-capped (Fig. 11.7(c)) gold nanoparticles are used. Gold nanoparticles have a good optical absorption in the visible region. Thus they can also be used for optical microscopy. Many companies are selling immunogold probes in the market.

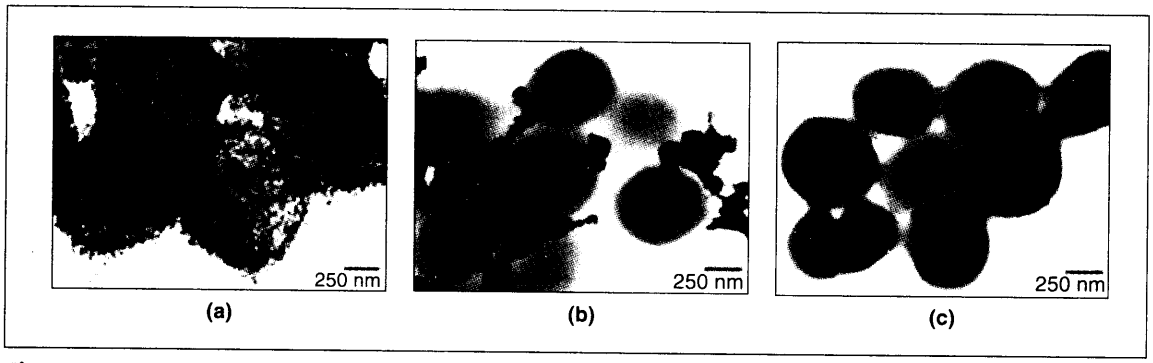

Fig. 11.7: *TEM images of Staphylococcus saprophyticus obtained after incubating these bacteria with: (a) Au-IgG nanoparticles, (b) unmodified gold nanoparticles and (c) Au-BSA nanoparticles. Reprinted with permission from Ho, et al. (Ref. 27). Copyright (2004) American Chemical Society.*

11.4.4 Diagnostic Applications of Immuno-targeted Nanoparticles

One of the major applications of immunogold labeling is that it facilitates the early detection of cancer. Gold nanoparticle-antibody bioconjugates are used for the vital imaging of cervical cancer cell suspensions as well as for fresh cervical biopsies. The principle applied for imaging the pre-cancerous tissues by reflectance imaging is based on the attachment of gold nanoparticles to probe molecules with high affinity for specific cellular biomarkers. Gold nanoparticle-antibody bioconjugates can be used as vital reflectance agents for the *in vivo* imaging of cancer affected parts for laser scanning confocal reflectance microscopy (Ref. 28). In cervical cancer cells, the epidermal growth factor receptor (EGFR) is over-expressed. The target selective imaging of cervical cancer cells (SiHa) was carried out by using 70 nm-sized gold nanoparticles anchored with monoclonal antibodies against EGFR. The mechanism of nanoparticle staining is similar to that cited in previous examples. This methodology, can deliver a cheaper technology for the early detection of cancer for the people in the Third World countries.

Anti-epidermal growth factor receptor antibody-conjugated gold nanoparticles (anti-EGFR/gold conjugates) were used to image the suspended SiHa cell lines as well as the biopsy of the cervical tissue. The scanning reflectance microscopic image shows efficient staining of SiHa cells by gold nanoparticles. The cross-sectional images (Figs 11.8 (c) and (d), (Plate 9)) show that the nanoparticles are staining only the outer surface of the cell. The target selectivity is clear from the absence of staining for the BSA-capped gold nanoparticles (Figs 11.8 (e) and (f), Plate 9).

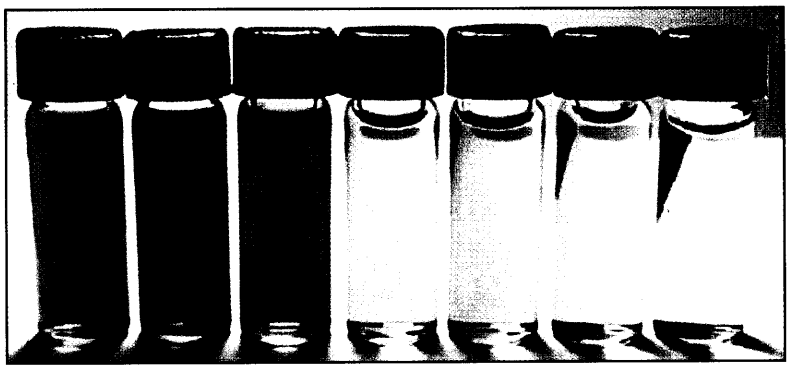

Fig. 10.2: *Nanoshells designed to absorb various wavelengths of light (the six vials on the right), including infrared (vial at far right) compared to gold colloid (far left). Used with permission from www.ece.rice.edu/people/faculty/halas.*

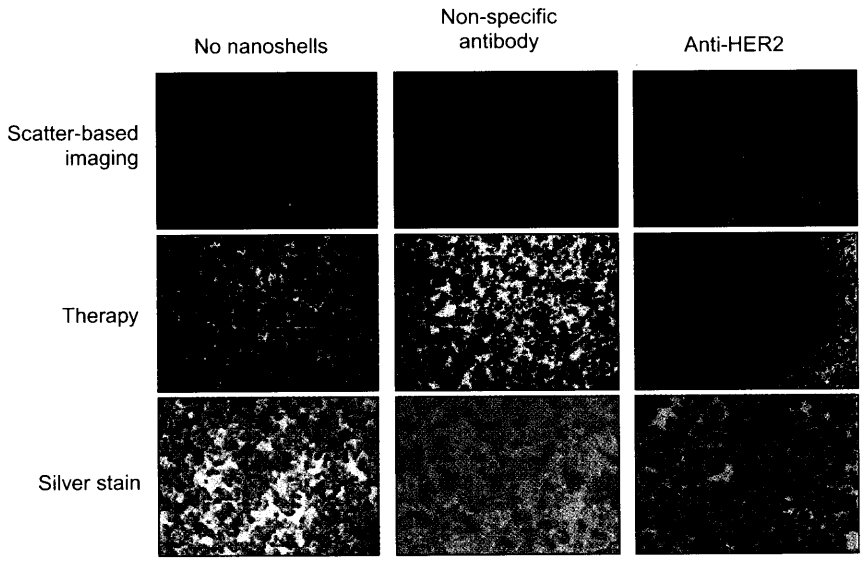

Fig. 10.11: *Combined imaging and therapy of SKBr3 breast cancer cells using HER2-targeted nanoshells. Scatter-based darkfield imaging of HER2 expression (top row), cell viability assessed via calcein staining (middle row), and silver stain assessment of nanoshell binding (bottom row). Cytotoxicity was observed only in cells treated with a NIR-emitting laser following exposure and imaging of cells targeted with anti-HER2 nanoshells. Increased contrast (top row, right column) and cytotoxicity (dark spot) are seen in cells treated with nanoshells as compared to others, called controls (left and middle columns). It is important to note that all experiments of this kind are done with appropriate controls. Reprinted with permission from Christopher, et al. (Ref. 10), Copyright (2005), American Chemical Society.*

Plate 7

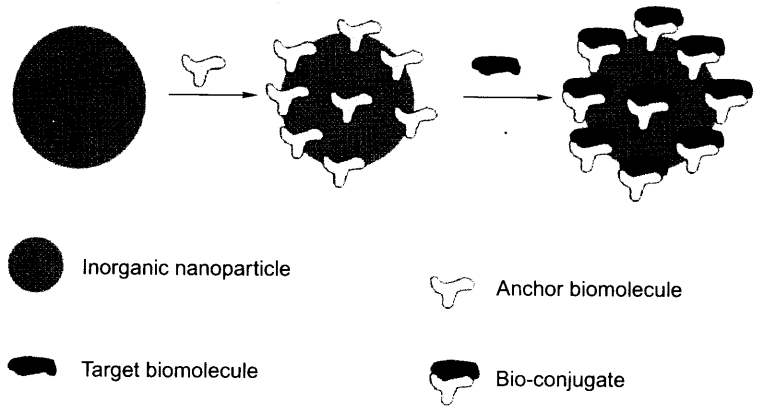

Scheme 11.1: *This scheme represents hybridization of conjugate biomolecules on inorganic nanoparticle surfaces.*

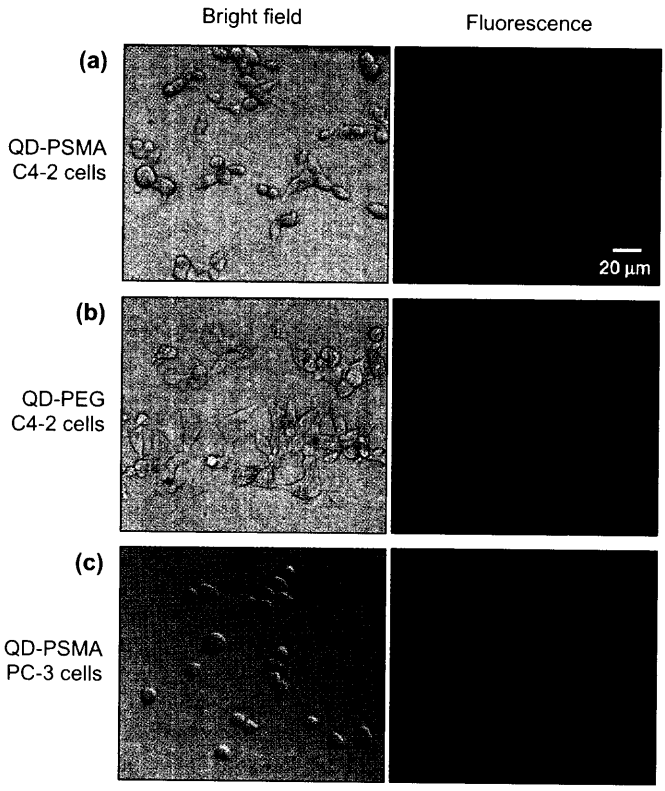

Fig. 11.5: *Interaction of CdSe@ZnS@PEG (QD-PEG) quantum dots with cancerous cells. C4-2 represents prostrate cancer cells; PC-3 represents non-cancerous cells. QD-PSMA is functionalized with the antibody of prostrate selective membrane antigen (PSMA-Ab). The negative staining of (b) and (c) can be explained by antigen-antibody interaction. From (Ref. 26).*

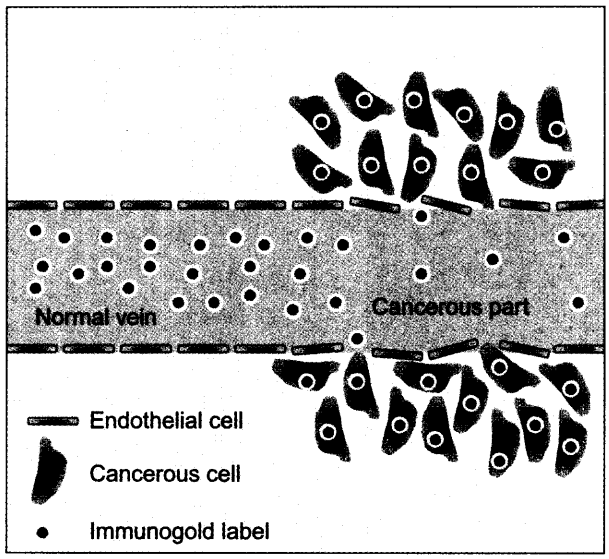

Scheme 11.2: *The scheme represents the mechanism of site-specific immunogold labeling.*

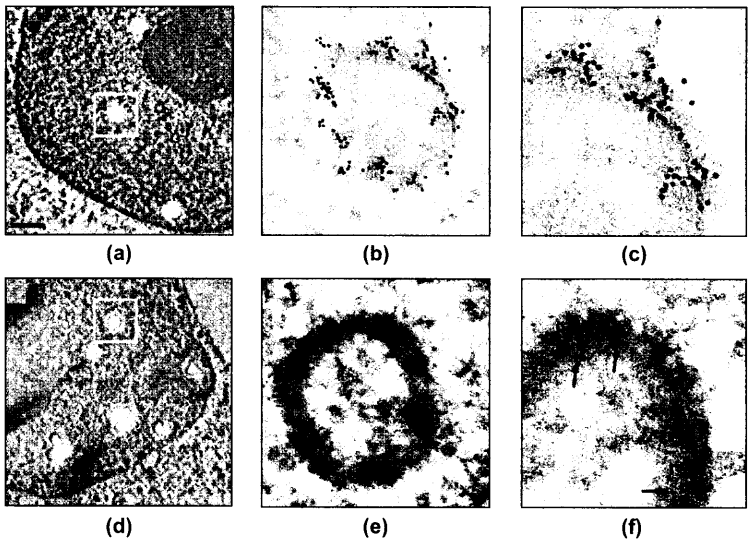

Fig. 11.6: *Target selective fluorescent and TEM imaging of PML bodies on cell nucleus using 10 nm gold and 10–15 nm CdSe nanocrystals. Figures (a) and (d) are fluorescence image of HEp-2 PML I cells labeled with 10 nm gold and CdSe particles, respectively. On gold-labeled sections, a Cy3 dye labeled secondary antibody was used, after incubation with gold, for generation of the fluorescence signal. (b) and (e) are the TEM images of the marked areas given in Figs (a) and (d), respectively. (c) and (f) are the enlarged views of (b) and (e), respectively. The dimension of the bar corresponds to 1000 nm, 100 nm and 50 nm for the set of Figs (a, d), (b, e) and (c, f), respectively. Sections were stained with uranyl acetate. The arrows in (f) mark CdSe nanocrystals. Reprinted with permission from Ho, et al. (Ref. 27). Copyright (2004) American Chemical Society.*

5. Good performance
6. Cost-effectiveness.

From the above examples, it can be safely concluded that nanobiology can lead to better drug delivery systems, and better technologies for bioimaging and synthetic viruses for gene delivery.

11.5 Nanoprobes for Analytical Applications—A New Methodology in Medical Diagnosis and Biotechnology

Several probes have been used during the past decades to understand the mechanisms of biological processes. The probes are normally molecular in nature, which are either incorporated with a fluorescent tag or labeled with a radioactive isotope. In order to understand the biological activity of a target molecule, the same is labeled with either a fluorescent tag or radioactive isotope and injected into the biological system for tracing the pathway of the molecule of interest. As a result of the malignancies or infections in the biological systems, some of the proteins are over-expressed. These over-expressed proteins are called 'biomarkers' for each malignancy or disorder. The antibody of the biomarker is used as a molecular probe with appropriate labels. As described earlier, the inorganic nanoparticles exhibit size compatibility and have excellent optical features in the visible region. The trend of using nanoparticles for probing biological processes is very recent. The nanoparticles exhibiting different properties such as light scattering, fluorescence or magnetism are used for particular applications. Ferrimagnetic Au-Fe_3O_4 nanocomposite particles are used as pre-concentration probes for peptides at extremely low concentrations (10^{-8}–10^{-7}M), which are formed by the digestion of cytochrome *c* by enzymes (Ref. 8). The mass spectrometric analysis of the enzyme digests of proteins is a methodology in proteomics for the elucidation of amino acid sequence. But the chances of obtaining the mass signature of these peptides in MALDI-TOF MS analysis are slim due to the large concentration of ionic impurities in broth obtained after enzyme digestion. The digest contains several impurities such as phosphate, chloride, sodium dodecyl sulphate and urea. These impurities are able to suppress the molecular ion peak in MALDI-TOF MS analysis. The electrostatic adsorption of each peptide on Au-Fe_3O_4 seed is driven by the surface positive charge of the peptide. This positive charge density depends on the pH of the medium and the intrinsic p*I* value of each peptide, as discussed earlier (Ref. 8). These seeds are incubated overnight in the digest and separated with the aid of applied magnetic field. The ionic impurities and urea are removed by washing with water. The MALDI-TOF MS analysis shows mass signatures of each peptide component. Another report describes the utility of magnetic nanoparticles for the detection of pathogenic bacteria in biological fluids by the selective adhesion of immunoglobulin G (IgG)-capped Fe_3O_4 nanoparticles on the cell wall of the bacterium (Ref. 27). The MALDI-TOF MS analysis of the residue obtained by magnetic separation shows the mass signatures of the pathogens secreted by the bacteria. This protocol shows the efficient detection from urine samples of pathogens at very low concentrations. The detection protocol of pathogens using Ig G-capped magnetite (Fe_3O_4) nanoparticles can be used in the clinical detection of many diseases in their early stages (Ref. 27).

The surface enhancement of Raman signals by noble metal nanoparticles has been known for several years. The use of noble metal nanoparticles as surface-enhanced Raman scattering (SERS) probes in biological applications was first investigated by the research group of Mirkin (Ref. 29). Their salient features are given below.

1. Metal nanostructures are useful for fabricating sensitive optical probes, based on enhanced spectroscopic signals.
2. The remarkable effect is connected with the confined optical fields is SERS.
3. SERS enhanced features can attain larger intensity, which produces signals to a level comparable to or even better than fluorescence.
4. In contrast to fluorescence, which creates comparatively broad bands, Raman scattering creates a distinctive spectrum composed of a number of narrow spectral lines, ensuing in well-noticeable spectra.
5. SERS probes offer elevated spectral selectivity, and are resistant towards photo-bleaching.

Metal nanostructures capped with Raman active molecules can be used as intracellular SERS probes. Silver nanoparticles capped with 4–mercapto benzoic acid were used as SERS probes for sensing the pH of the cytoplasm of Chinese hamster ovary cells (Ref. 30). Gold nanoparticle capped with indocyanine green is used as an intracellular SERS probe for rat prostrate carcinoma cell line (Ref. 15).

The SERS probe for immunoassay is fabricated by the integration of a noble metal nanoparticle, a Raman active dye and a target selective biomolecule. The target selective biomolecule is anchored to the nanoparticle through the dye molecule by covalent bonding. The analyte molecule is adsorbed on the gold coated glass plate functionalized with dithiobis (succinimide undecanoate) (DSU). The succinimide moiety of DSU reacts with the analyte molecule forming an amide linkage with the mercapo undecanoyl group on the gold coated glass plate. Thus the covalently fixed analyte molecule is marked by the bioconjugate formation as shown in Scheme 11.3 (Plate 9). The Raman dyes used for SERS experiments are bifunctional, which include disulphides for chemisorption to the nanoparticle surface and succinimides for forming amide linkage with monoclonal antibodies. In this way probe fabrication will confine the dye molecules in the optical field of the noble metal nanoparticles and confinement of the analyte for the enhancement of Raman modes occurs. Thus the hybridization of the monoclonal antibody tail of SERS probe with the analyte molecule on the Au coated glass substrate will result in the adhesion of probe on the substrate. The substrate is washed and analyzed for the SERS intensity from the dye. There are earlier reports similar to the antigen antibody hybridization protocol; a DNA strand with a known sequence can be used instead of a monoclonal antibody in the SERS probe, in order to detect target DNA (Ref. 29). The detection of extremely small quantities of biomarker is seldom achieved by using the normal methodologies of immunoassays.

Prostate-Specific Antigen (PSA), a 33-kDa glycoprotein, a biomarker for prostate cancer, is present in blood plasma, in concentrations ranging between 4 and 10 ng/mL for a healthy adult male. As a result of an increase in the occurrence of prostrate cancer, the chances of the complex formation of PSA and α-antichymotrypsin are elevated. This phenomenon decreases the amount of free PSA in cancer patients. Thus the concentration of free PSA is important for the determination of the extent of prostrate cancer.

A protocol has been developed recently for using SERS-based immunoassay using Au nanoparticle probe for femto molar detection of PSA (Ref. 31). 5, 5′-dithiobis (succinimidyl-2-nitrobenzoate) (DSNB) was used as the bifunctional Raman dye to connect Au (32 nm) nanoparticle and the monoclonal antibody of PSA. The immobilization of PSA was done on an Au-coated glass surface which is functionalized with dithiobis (succinimide undecanoate) (DSU). The PSA solution in human serum was taken in a concentration between 1 μg/mL (30 nM) and 1 pg/mL (30 fM) and was used for fixing on the DSU fuctionalized Au-coated glass plate. After the fixation of PSA at different concentrations on the substrate, it was allowed to hybridize with SERS probes as shown in Scheme 11.3. The SERS probe consists of a self-assembled monolayer of 5-merapto 2-nitro benzamide attached to a monocolonal antibody. The antibody was anchored to the 5-meracapto 2-nitro benzoyl group with a peptide linkage, which was formed by the condensation of the amino group of the antibody and the succinimidyl 2-nitro benzoate group. The Raman scattering intensity of the symmetric stretching of the nitro group of the 5-meracapto 2-nitro benzoyl moiety at 1338 cm^{-1} was taken as the maker signal for the immunoassay. In Fig. 11.10(a), the spectra were acquired using 60-s integration of SERS-based immunoassay. As mentioned above, the Raman features of the DSNB-labeled nanoparticles at 1338 cm^{-1} demonstrate a gradual enhancement as a function of the concentration of PSA. The concentration level shown in Fig. 11.10 is critical for prostate cancer diagnosis (Ref. 32). The trace labeled blank represents the Raman spectrum of the sample in the absence of PSA on the substrate. Additional information can be obtained from the dose-response curve shown in Fig. 11.10(b). This curve was created by plotting the intensity of the symmetric stretching of the nitro group at 1338 cm^{-1} versus logarithm of the concentration of PSA in pg/mL used for analysis. This report demonstrates the potential of the gold nanoparticle-based SERS probe for the early detection of prostrate cancer in a quantitative fashion. This also unveils the utility of nanoparticle-based SERS probes in a variety of applications in the fields of medical diagnosis and biotechnology.

11.6 Current Status of Nanobiotechnology

An overlap of nanotechnology, biotechnology and bio-informatics has resulted in the advent of a new technology called 'nanobiotechnology' (see Scheme 11.4). It is defined as a field that applies the principles of nanotechnology and bio-informatics to probe and modify biological systems or to apply the principles of life sciences and surface sciences to develop novel devices and systems for biocatalysis. During the past decade, this technology has reached a level, which enabled it to develop probes for understanding the intracellular and intercellular biological process, novel targeted labels for biological systems, and efficient nanoparticle-based immunoassays for the detection of biomarkers at extremely low concentrations and pre-concentration probes for selectively adsorbing the analyte from crude samples.

As compared to other branches of nanotechnology, nanobiotechnology has a high potential for catering to societal needs. The application of this technology in medical diagnosis and therapy is well known. There are reports highlighting the use of nanoceramic materials based supports for enzyme catalysis. This demonstrates the potential of nanomaterials as supports for several processes in industrial biotechnology. The application of nanomaterials for protein separation and analysis is also well-known. Many companies

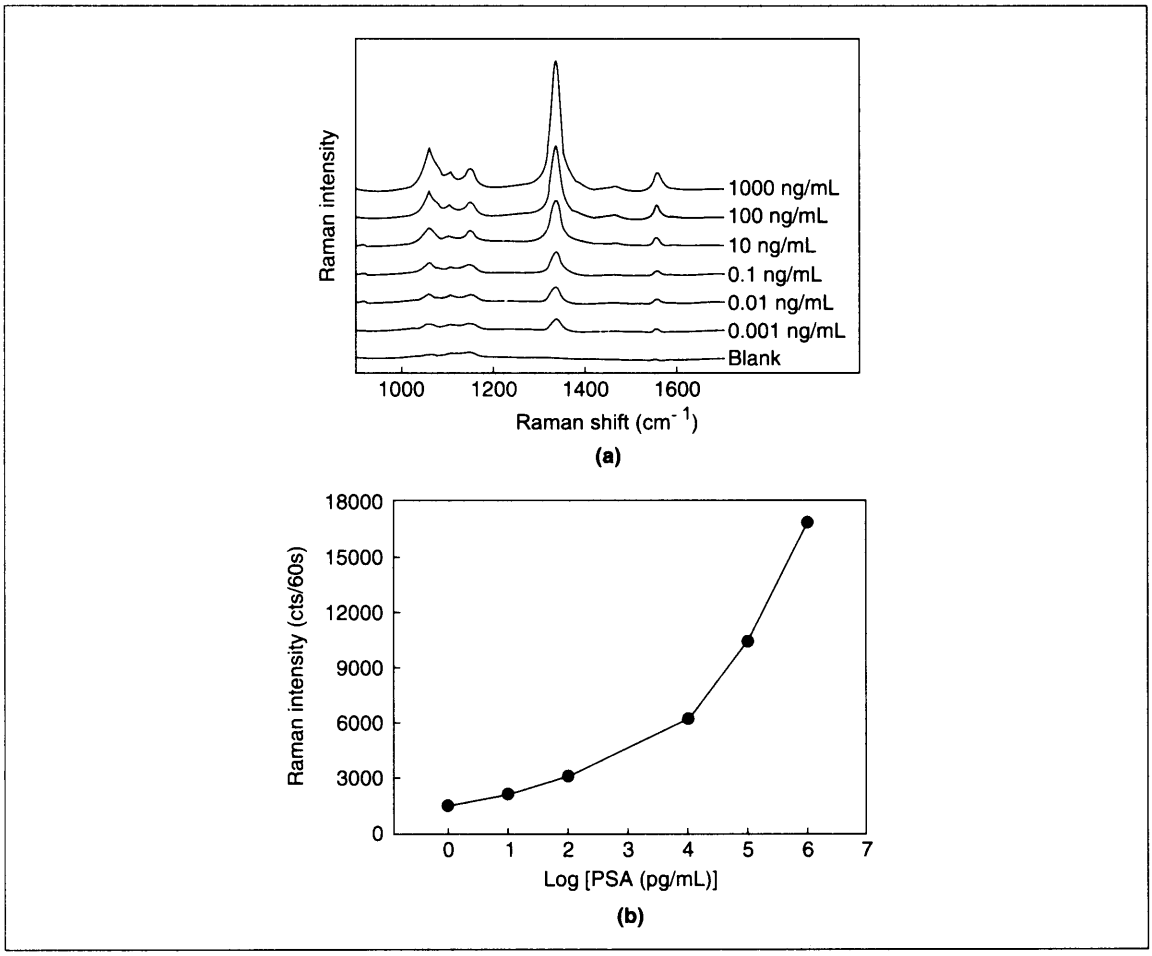

Fig. 11.10: *Demonstration of a SERS-based free PSA immunoassay. (a) SERS spectra, offset for clarity, acquired at various PSA concentrations. (b) Dose–response curve for free PSA in human serum. Reprinted with permission from Grubisha, et al. (Ref. 31). Copyright (2003) American Chemical Society.*

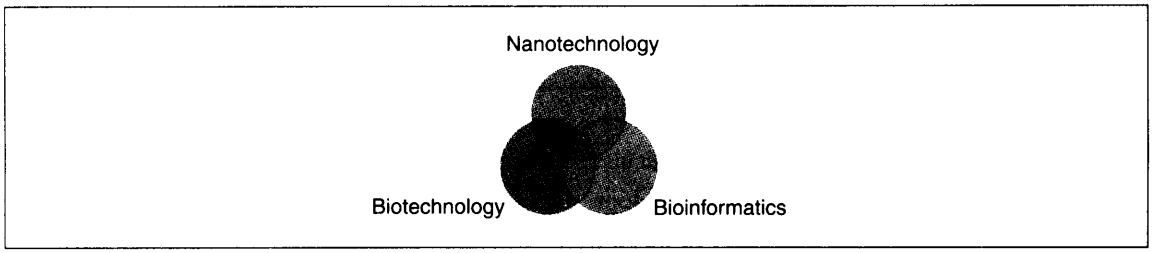

Scheme 11.4: *Schematic representation of the evolution of nanobiotechnology.*

are marketing nanoparticle-based labels in the market. A few of them are SPI-Mark™, Nanoink Inc, Nanoprobes, Biocompare Inc. and Tedpella Inc. Plenty of nanoprobes are available in the market for various applications in life sciences. Thus nanobiotechnology can be used in common applications such as clinical assay and medical diagnosis, and can provide cheaper and efficient solutions.

11.7 Future Perspectives of Nanobiology

Nanobiology can provide better methodologies for medical diagnosis and therapy. It can also provide better tools for biochemical analysis.

The future directions of nanobiology will be seen in the following areas:

- *Proteomics*: The methodology based on magnetic nanoparticles can be used for protein purification and separation. The magnetic nanoparticles can act as pre-concentration probes for MALDI TOF analysis. These techniques can be selectively used to adsorb each peptide formed by the enzyme digestion of a particular protein.
- *Medical sciences*: Nanoparticle-based targeted imaging of tissues and cell lines can be utilized for the early detection and screening of diseases. Also antibody-capped nanoparticles can be used for the selective destruction of tumors.
- *Biotechnology*: Nanoceramics can be used as inert supports for enzyme catalysis. Thus enzymes supported on nanometer-sized inert metal oxides have potential applications in industry. Magnetically triggered drug delivery and gene delivery vesicles are also promising areas. The development of nanoparticle-based SERS and fluorescent probes for immunoassays and DNA finger printing is a novel methodology in biochemical analysis.
- *Microbiology*: Nanobiology can be used to efficiently understand the pharmacological responses of different micro-organisms. The mechanism of drug resistance, drug action and drug uptake by the micro-organism can be probed by nanoparticle-based spectroscopic techniques. The selective imaging of intracellular parts is another salient application of nanoprobes. The SERS probes can deliver chemically selective vibrational information of intracellular parts. Finally nanobiology can offer target selective probes to examine fundamental issues such as cell division and membrane transport.

Review Questions

1. How do we probe the nature of molecular interactions between nanoparticles and biomolecules?
2. What makes the fusion of nanotechnology and biology possible?
3. What are the specific properties of metal nanoparticles in understanding biology?

4. What are the analytical applications of nanoprobes in biology? How single molecule detection become possible?
5. How can biomolecules be used for nanomaterial assembly?

References

1. Mirkin, C.A.; R.L. Letsinger, R.C. Mucic and J.J. Storhoff, *Nature*, **382** (1996), pp. 607–608.
2. Alivisatos, A.P.; K.P. Johnsson, X.G. Peng, T.E. Wilson, C.G. Loweth, M.P. Bruchez and P.G. Schultz, *Nature*, **382** (1996), pp. 609–611.
3. Rosi, N.L. and C.A. Mirkin, *Chem. Rev.*, **105** (2005), pp. 1547–62.
4. Mandal, S., A. Gole, N. Lala, R. Gonnade, V. Ganvir and M. Sastry, *Langmuir*, **17** (2001), pp. 6262–8.
5. Brennan, L., D.L. Turner, P. Fareleira and H. Santos, *J. Mol. Biol.*, **308** (2001), pp. 353–65.
6. Storhoff J.J., A.A. Lazarides, R.C. Mucic, C.A. Mirkin, R.L. Letsinger and G.C. Schatz, *J. Am. Chem. Soc.*, **122** (2000), pp. 4640–50.
7. Pan, P., H.P. Gunawardena, Y. Xia and S.A. McLuckey, *Anal. Chem.*, **76** (2004), pp. 1165–74.
8. Teng, C.H., K.C. Ho, Y.S. Lin and Y.C. Chen, *Anal. Chem.*, **76** (2004), pp. 4337–42.
9. Gu, H., P.L. Ho, E. Tong, L. Wang and B. Xu, *Nano Lett.*, **3** (2003), pp. 1261–3.
10. Jiang, X., J. Jiang, Y. Jin, E. Wang and S. Dong, *Biomacromolecules*, **6** (2005), pp. 46–53.
11. Sudeep, P.K., S.T.S. Joseph and K.G. Thomas, *J. Am. Chem. Soc.*, **127** (2005), pp. 6516–7.
12. Chen A.M. and M.D. Scott, *Bio Drugs*, **15** (2001), pp. 833–47.
13. Talley, C.E., L. Jusinski, C.W. Hollars, S.M. Lane and T. Huser, *Anal. Chem.*, **76** (2004), pp. 7064–8.
14. Kneipp, J., H. Kneipp, W.L. Rice and K. Kneipp, *Anal. Chem.*, **77** (2005), pp. 2381–5.
15. Chan W.C., D.J. Maxwell, X. Gao, R.E. Bailey, M. Han and S. Nie, *Curr. Opin. Biotechnol.*, **13** (2002), pp. 40–6.
16. Dunin-Borkowski, R.E., M.R. McCartney, R.B. Frankel, D.A. Bazylinski, M. Posfai and P.R. Buseck, *Science*, **282** (1998), pp. 1868–70.
17. Iqbal, S.S., M.W. Mayo, J.G. Bruno, B.V. Bronk, C.A. Batt and J.P. Chambers, *Biosens. Bioelectron.*, **15** (2000), pp. 549–78.
18. Looger L.L., M.A. Dwyer, J.J. Smith and H.W. Hellinga, *Nature*, **423** (2003), pp. 185–90.
19. Clapp, A.R., I.L. Medintz, M.J. Mauro, B.R. Fisher, M.G. Bawendi and H. Mattoussi, *J. Am. Chem. Soc.*, **126** (2004), pp. 301–10.
20. Niemeyer, C.M., *Angew. Chem.*, **40** (2001), pp. 4128–58.
21. Akerman, M.E., W.C.W. Chan, P. Laakkonen, S.N. Bhatia and E. Ruoslahti, *PNAS*, **99** (2002), pp. 12617–21.

22. Boisvert F.M., M.J. Hendzel and D.P. Bazett-Jones, *J. Cell Biol.*, **148** (2000), pp. 283–92.
23. Jensen H.L. and B. Norrild, *Histochem. J.*, **31** (1999), pp. 525–33.
24. Chan C.W. and S. Nie, *Science*, **281** (1999), pp. 2016–18.
25. Gao, X., Y. Cui, R.M. Levenson, L.W.K. Chung and S. Nie, *Nature Biotechnology*, **22** (2004), pp. 969–76.
26. Nisman, R., G. Dellaire, Y. Ren, R. Li and D.P. Bazett-Jones, *J. Histochem. Cytochem.*, **52** (2004), pp. 13–18.
27. Ho, K.C., P.J. Tsai, Y.S. Lin and Y.C. Chen, *Anal. Chem.*, **76** (2004), pp. 7162–68.
28. Sokolov, K., M. Follen, J. Aaron, I. Pavlova, A. Malpica, R. Lotan and R. Richards-Kortum, *Cancer Research*, **63** (2003), pp. 1999–2004.
29. Cao, Y.W.C., R.C. Jin and C.A. Mirkin, *Science*, **297** (2002), pp. 1536–40.
30. Talley, C.E.; L. Jusinski, C.W. Hollars, S.M. Lane and T. Huser, *Anal. Chem.*, **76** (2004), pp. 7064–68.
31. Grubisha, D.S., R.J. Lipert, H.Y. Park, J. Driskell and M.D. Porter, *Anal. Chem.*, **75** (2003), pp. 5936–43.
32. Polascik, T.J., J.E. Oesterling, and A.W. Partin, *J. Urol.*, **162** (1999), pp. 293–306.

Additional Reading

1. Jones, Richard A.L., *Soft Machines: Nanotechnology and Life*, (2004) Oxford University Press.
2. Goodsell, D.S., *Bionanotechnology: Lessons from Nature*, (2004), John Wiley and Sons Inc.
3. Robert A. and Jr Freitas, *Nanomedicine, Vol. IIA: Biocompatibility*, (2003), Landes Bioscience.
4. Caruso, Frank, *Colloids and Colloid Assemblies: Synthesis, Modification, Organization and Utilization of Colloid Particles*, (2004), Wiley-VCH.
5. Prasad, Paras N., *Introduction to Biophotonics*, (2003), Wiley-Interscience.

Chapter 12

NANOSENSORS

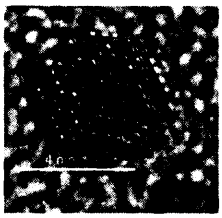

Sensors can be developed by using the properties of matter at nano dimensions. In such devices, the functional units will be nano entities though the material itself may not be nano in dimension. The properties of nanomaterials such as the large surface to volume ratio and photophysical properties will be used in generating a signal when analyte molecules interact with it. Several such sensors have been developed. Our objective here is to categorize these systems and put them in the perspective of materials discussed so far.

Learning Objectives

- What are nanosensors?
- What are the typical things one can sense with nanodevices?
- What are the properties used for sensing?
- What is the status of current research in this area?
- How useful can a smart dust be?

12.1 Introduction

One unifying property for all life forms is their ability to sense, perceive and react to situations. This characteristic is exhibited, albeit to different extents, by the most developed living organisms down to the lowest organisms. What is surprising, however, is that man, having proclaimed himself as the most advanced and developed of all species, looks at other 'lower' species for their exceptional ability to sense and react to their surroundings. They provide him with ideas and inspirations on how to develop and acquire an improved sense of perception. Since science has still not allowed man to tamper with and modify his own self to the extent he would like to, he attempts to develop external sensors and devices to obtain a better knowledge of his surroundings. This understanding equips him with the ability to react and eventually assume better control of his surroundings. Therefore, in his never-ending quest for controlling his locality, he tries to constantly innovate and invent devices equipped with better sensory perceptions than what has been bestowed on him naturally.

A careful analysis would reveal that the development of sensory devices has been vital for ushering in various technological advancements that have revolutionized civilizations. After all, every experiment, entails a measurement, which involves sensing something. In the modern day world, our ability to point to the exact location of a person owes its existence to a satellite that can sense the time delay between the signals it receives from various other satellites and translate it into distance on a three-dimensional space. Perhaps, it would be difficult to believe that this complex concept is also employed by a bat to sense its environment!

12.2 What is a Sensor?

In the context of this book, the term 'sensor' can be referred to any device that uses an active chemical species or component that generates a signal in presence of an analyte molecule. The signal, in turn, is used either directly or after suitable amplification to trigger a suitable detector.

Thus, the three essential components of a sensor device are:

1. *The responding element*, which recognizes the presence of the analyte species and generates a signal. This is the principal component which 'sees' the molecule, ion or process. In general, a sensor element has to satisfy certain requirements like:
   (a) It should be capable of detailing the analyte in a qualitative and quantitative manner.
   (b) It should be able to detect even very small amounts of the analyte.
   (c) The signal it generates should be reproducible. This implies that the sensor should not have a strong affinity for the analyte, in which case the sensor will be passivated with the analyte after some time, leading to an irreproducible response. The affinity should be optimal so that the analyte is disengaged from the sensor after a short interaction time period, during which the sensor transfers its response to the next stage.
   (d) The sensor should be very selective and specific in its response towards a target molecule.
2. *An amplifier*, which receives the signal of the sensor as an input and amplifies it to a level that is acceptable for processing by the detector, and
3. *A detector*, which receives the output of the amplifier as an input and converts it, in a pre-programmed manner, to a parameter which represents either the analyte species or its concentration or both. In most cases, the detector is equipped with a feedback control through which it signals to the sensor that the input has been received and processed. This acts as a trigger for the sensor to release the analyte molecule. This process causes an induction time period during which the sensor is not available for response. Therefore, the induction period should be as small as possible. An overall schematic of a sensor device is represented in Scheme 12.1.

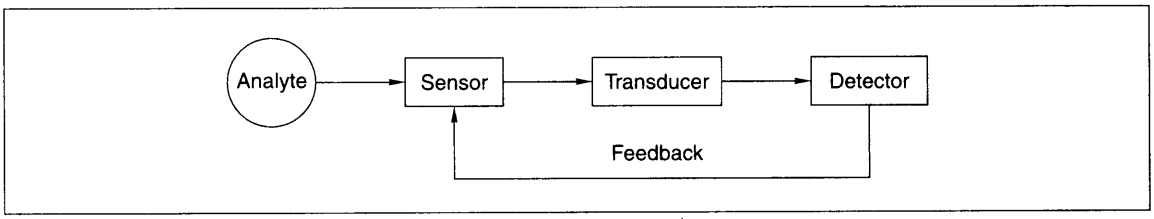

Scheme 12.1: *Schematic of the design of a sensor.*

12.3 Nanosensors—What Makes Them Possible?

So where do nanomaterials, and the properties that arise thereof, stand in the realm of things? As has been discussed in all the previous chapters, the size regime of nanomaterials gives rise to an entire gamut of physical and chemical properties, which are being currently explored by numerous research groups worldwide. The main properties of nanomaterials that are utilized for conceiving and designing a viable sensor are as follows:

1. Properties derived from the high surface to volume ratio
2. Optical properties
3. Electrical and electrochemical properties
4. Physical properties.

Apart from these broadly classified attributes, some specific properties also find application in the development of sensors. Such properties will be briefly discussed as and when required.

12.4 Order from Chaos—Nanoscale Organization for Sensors

A translation of liquid state properties to solid state is of utmost importance in the development of sensors and devices. One of the major hurdles in achieving this is that this transfer has to be done without altering the liquid-phase properties. In this process, assembling of the particles and an enhanced ordering have to be achieved to enable uniform and isotropic detection protocol. A variety of substrates are employed for carrying the nanoparticles, with the most common among them being metals like Au, Pt, etc. and conducting glass substrates. Metallic surfaces are utilized for the spectroscopic probing of the molecules using Surface Enhanced Raman Spectroscopy (SERS) that gives information about the alignment and the nature of interaction existing between the molecule and metal. On the other hand, transparent conducting glass substrates lend themselves to a variety of electrical and microscopic (as well as spectroscopic) probing, besides being technologically more attractive. Many methods are used to achieve the assembly and further ordering of the nanoparticles. The most important and relevant techniques are discussed here, with examples.

12.4.1 Self-assembly

This is one of the most widely used and simplest methods of organizing nanoparticles onto substrates. Normally, this method is adopted for attaching the nanoparticles (usually metallic) on surfaces like conducting glass or metal films. The substrate is first cleaned and activated suitably, with the process depending on the nature of the substrate and the nanoparticles. The surface is made either hydrophobic or hydrophilic as is necessitated by the type of the nanoparticle. In the case of metallic substrates, the cleaned surface might be sufficiently active for the attachment of the nanoparticles. Otherwise, the activated surface is functionalized with anchor molecules to facilitate the binding of the nanoparticles. These anchor molecules are characterized by the presence of certain functional groups to which the nanoparticles will adhere. A silane containing thiol (Ref. 1) or an amino functional group, capable of forming a covalent link, is best suited for the adhesion of gold nanoparticles. The type and extent of functionalization is controlled by the nature of application for which it is fabricated. For example, for electrochemical studies, a thick polymeric layer of alkoxysilane will hinder the transport of ions and electrons between the nanoparticles and the substrate. A representative schematic of the procedure is shown in Scheme 12.2.

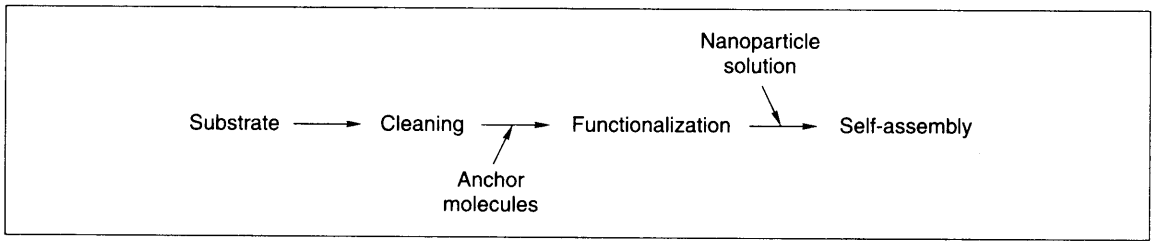

Scheme 12.2: *Schematic representation of self-assembly.*

The assembly thus achieved is referred to as a 'self-assembled layer' (SAL). More specifically, if a single monolayer adsorption is achieved, it is known as a 'self-assembled monolayer' (SAM). This is more relevant with respect to the organization of molecules on a metal or nanoparticle surface. It is thus known as there is no external driving force other than the mutual affinity between the nanoparticles and the functional groups on the substrate. This plays a crucial role in deciding the specificity of the nanoparticles that goes on to form the SAL or SAM. To know more about self-assembled monolayers, see Chapter 5.

12.4.2 Template Method

One of the main disadvantages of the self-assembly method is its sensitivity in terms of external parameters. It is almost impossible to obtain two similarly arranged surfaces, with the adhesion and the organization depending on various factors like solvent, concentration, temperature, type of substrate, and so on. In fact, even on a given surface, there is a high possibility of the existence of a coverage gradient, leading to inconsistency in results.

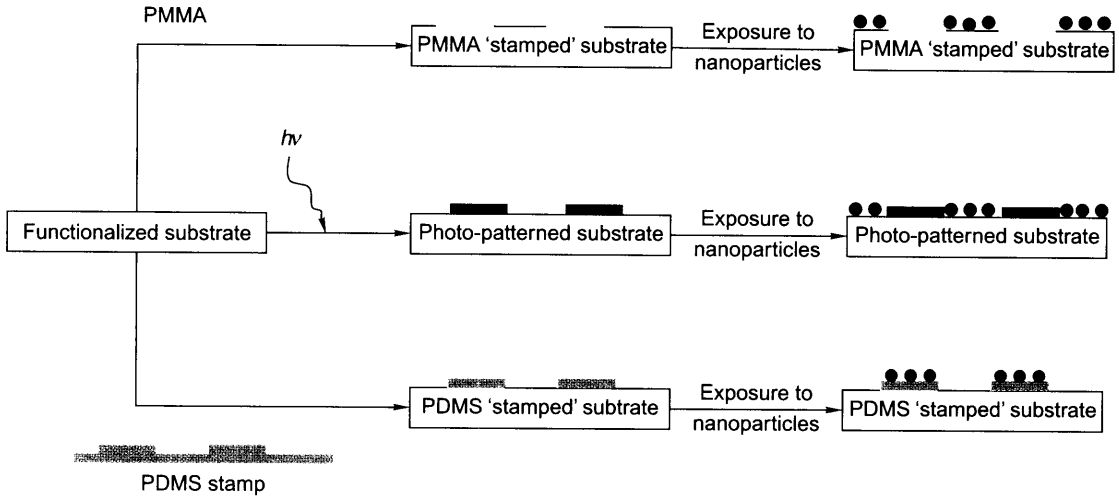

Scheme 12.3: *Some of the methods of template-assisted organization of nanoparticles.*

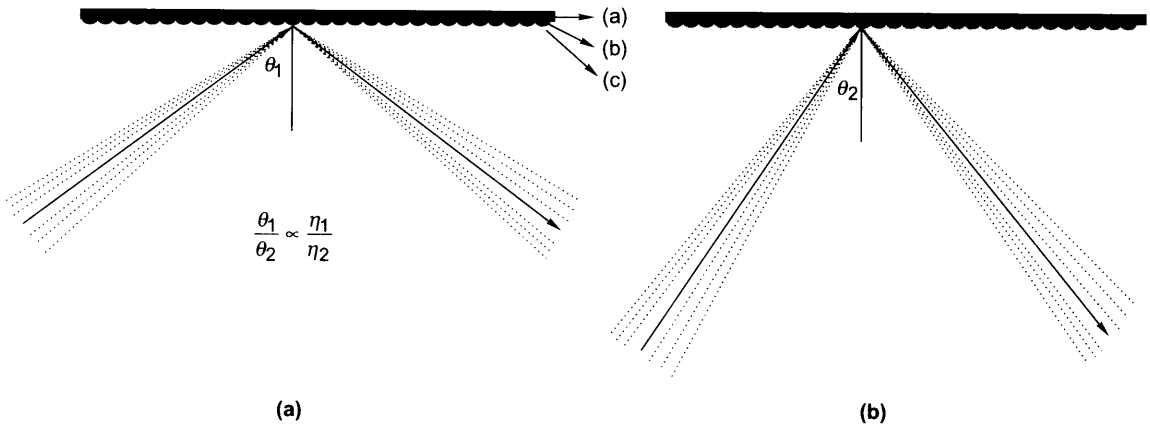

Scheme 12.4: *Schematic of SPRS: (a) Opaque substrate, (b) nanoparticle and (c) plasmon electric field in parent (a) and the modified (b) surfaces.*

Plate 11

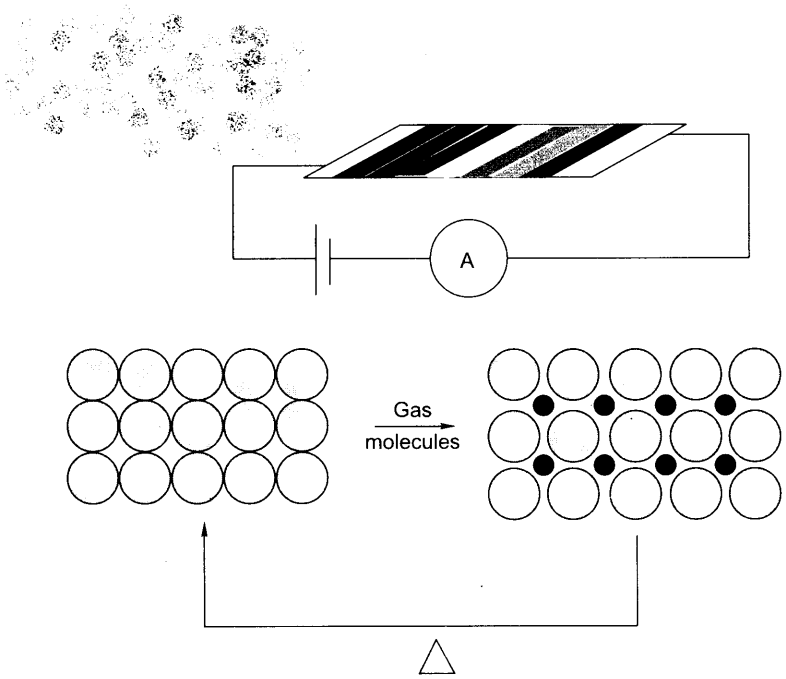

Scheme 12.5: *The working of an electronic nose. The diffused colors represent different gases while the solid colors represent the various nanoparticles that are sensitive to the specific gas molecules. The gases thus adsorbed on the films might be removed by suitably heating the array, thus making repeated use of the system possible.*

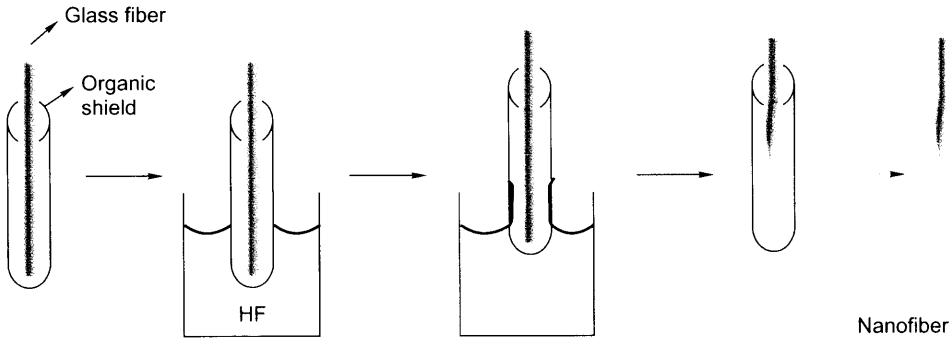

Scheme 12.7: *Cartoon representation of fabrication protocol of a nanofiber as a probe for biological sensing and imaging. As the optical fiber is withdrawn from the HF solution, surface tension causes the HF to initially rise along the organic cladding. Slow draining of HF from there causes a nanotip to be formed, after which the organic cladding is removed by treating with a suitable solvent.*